Report No. 177 / UILU ENG-98-4005

Surface Durability of Dry Coaxial Splines

by

Frank Leonard Bohm

B.S., University of Illinois at Urbana-Champaign, 1986

THESIS

Submitted in partial fulfillment of the requirements
for the degree of Master of Science in Mechanical Engineering
in the Graduate College of the
University of Illinois at Urbana-Champaign, 1998

Urbana, Illinois

SURFACE DURABILITY OF DRY COAXIAL SPLINES

Frank Leonard Bohm, M.S.
Mechanical Engineering
University of Illinois at Urbana-Champaign, 1998
Professor D. F. Socie, Advisor

The prediction of coaxial spline tooth wear requires knowledge of the tooth loading and relative movement characteristics, as well as the mechanisms for fretting wear, fretting corrosion, fretting fatigue, and reciprocating wear. This paper presents the proposed mechanisms and theories of many researchers, along with their empirical findings. Also presented is a model developed for the purpose of this analysis that can be used to determine the number of teeth in contact, contact stresses, sliding amplitudes, and pressure velocity products for a given coaxial spline configuration. These results can then be analyzed in terms of relevant wear theories to predict life and performance characteristics. While the model was initially developed to predict and improve the performance of coaxial splines in applications involving clutches, it can also be used to predict the interactions of splined couplings.

Table of Contents

I. Introduction

A. Applications Involving Coaxial Splines

Coaxial splines are used to transmit power in a wide range of applications, from vehicular to industrial. In the automotive industry, for example, they are found in the transmissions coupling to the engine, in drive shafts, and on both sides of the differential that drives torque to the rear wheels. The use of coaxial splines in machinery is endless, as they allow high torsion power transmission in conjunction with a desired axial movement of one of the two members. Some of the most challenging applications in terms of reducing spline fretting are on the quill shafts of drive accessories such as generators and hydraulic pumps [1].

The type of application that is the focus of this paper is that of electromagnetic clutches. In these clutches, a coaxial spline is used to allow an armature, the outer member, to freely move axially such that it does not drag against a mating clutch surface while disengaged. Once engaged, the clutch torque is driven through the spline. It was found that in some of these clutch applications the spline would wear quite rapidly. In others the wear would be gradual, in still others, the spline would not wear at all. One design, common among industrial clutches, is to have teeth of the splined hub made of plastic, while the teeth of the mating part, the clutch armature, are of low carbon steel. This combination has been used in various applications for years. Whereas in some applications there is a high probability that a clutch would exhibit excessive spline wear, in other applications there are no problems, suggesting an application specific cause for wear.

This led to a hypothesis that there are three primary factors that combine to cause extreme wear: (1) high temperature; (2) a continuous drag torque while the clutch is engaged; and (3) offset spline shafts. Each of these possible causes were independently evaluated in the laboratory. Those evaluations revealed that, acting alone, not one of the three causes

would produce the excessive wear. It was only when these factors were combined that the failure occurred quickly and repeatedly. These findings served to help validate the hypothesis.

B. Treatments to Reduce Spline Wear

When gear couplings exhibit premature failures, one of the first improvements considered is the lubrication of the gear surfaces. In fact, in lubricated gear couplings, some misalignment has been found beneficial. If there in no misalignment between the teeth, there is no relative motion between the teeth, the lubricant is squeezed out, and the coefficient of friction becomes static [2]. In the case of clutches, however, lubricant is not an option, as any lubricant contaminating the clutch face would reduce the torque and effectiveness of the clutch. Therefore, solutions to the problems involving clutches are limited to dry splines.

Lee [1] suggests several treatments that reduce spline wear in metal on metal systems. One treatment is plating one of the spline members with a soft, low-shear-strength material like silver. Although expensive, it has been shown to be effective. A more economical coating which has been shown to reduce fretting wear is molybdenum disulphide. The opposite approach is to apply a hard, wear-resistant coating on the teeth. Chromium and electroless nickel can be plated on one spline .0002 inches thick to protect the underlying material. Another technique is to change the core material of the teeth. Rather than a metal on metal system, a polymer on metal or metal on metal system can reduce the wear. The last recommended treatment by Lee is to reduce the relative movements as much as possible through the design of the components. Although fretting is somewhat random, it can usually be sufficiently reduced by employing these treatments. The materials used in the system are important to predict the failure mechanisms and the expected life.

These treatments are not always feasible, however, forcing engineers to find alternatives. Fisher and Wilson [3] patented a vibration-proof coupling which eliminates fretting

corrosion. The invention is a splined coupling that uses a collar to clamp the external member onto the internal splined shaft. While this can be expected to eliminate fretting corrosion by eliminating relative movement, axial movement is also eliminated, limiting the functionality of this design. Ying and Cooper [4] also patented a coupling which would prevent fretting corrosion. This invention works on the same principal as Fisher and Wilson's, except the inner member expands outward to prevent the motion. It has the same limitations regarding axial play as the Fisher and Wilson invention.

C. Combining Technologies to Predict Coaxial Spline Performance

There are three technologies involved in this evaluation. They are gear design, fretting, and wear. Gear design is an older, primarily empirical form of engineering. Much of what has been learned has been through experience with real applications. Therefore, the majority of the publications involve lubricated steel gear reducers. The information available with respect to fretting is somewhat more theoretical but still highly empirical. Researchers hypothesize as to the causes of fretting, then develop theoretical models and adjust them through constants to match actual results. The information concerning wear is of a similar nature, but the volume of research with respect to the wear is less extensive than that of fretting. Relating the findings from these three technologies serves to provide an understanding of the mechanisms that cause dry coaxial spline teeth surfaces to wear, as well as to help identify potential solutions.

As demonstrated later in the paper, there is a fourth technology required in this evaluation, that of mechanics. Failure models that consider the interactions between various loading conditions have not been found in the literature. Therefore, a model was developed and presented which determines the loads, sliding speeds, and other parameters involved in the spline teeth interface.

II. Gear Tooth Wear

A. Types of Wear

Gear tooth wear is one of the oldest phenomena studied by engineers. AGMA 210, "The American Gear Manufacturers Association Standard For Surface Durability (Pitting) of Spur Gear Teeth" was first approved in 1961 [5]. Dudley [6], in 1954, published the first editions of the *Handbook of Practical Gear Design*, which today is still one of the better gear design references. This handbook, along with the vast majority of the literature on gear design, evaluates the most common application of gears, that of power transmission. Emphasis is placed on pairs of lubricated external tooth gears, and design rules for the loading and durability of gears are based on gear speed reducers and lubricant temperatures.

Gear tooth failure occurs through a variety of means. These are identified in Figure 2.1 as wear, pitting, fracture, and scoring [7]. According to Dudley, gears typically fail first by wear, then by fracture.

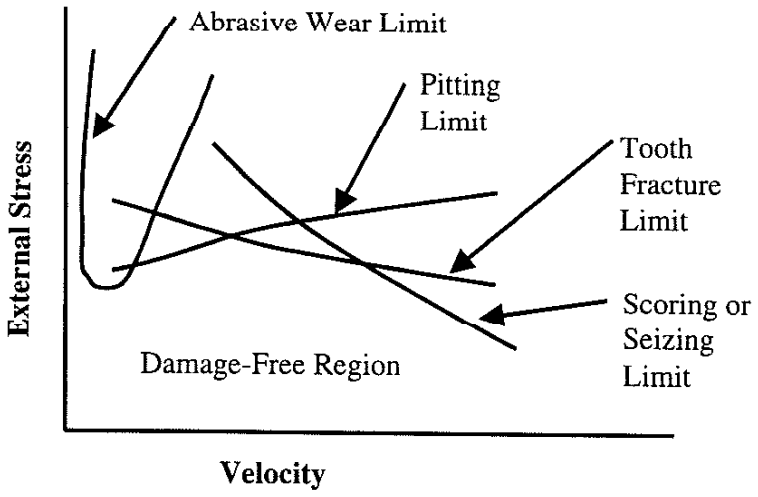

Figure 2.1: Relationship between gear stress and speed to surface damage.

In this section, gear tooth wear by scoring, pitting, galling, fretting and abrasion will be discussed, as well as tooth fracture.

1. Scoring

Scoring, which is denoted in the far right region of Figure 2.1, is usually considered to be a lubrication failure and is most likely to occur at medium and high speeds.

There have been many models used to predict scoring of gears. In 1937, Blok presented the flash temperature criteria. This is based on a constant equal to the load times velocity to the power x. The value of x has since been debated to range from -1 to 2 [8]. Today, the most famous model is the critical temperature model. Others are the critical power intensity model, critical power model [9], flash temperature index model [10], Meng's criteria, Almen's criteria, Borsoff and Godet's scoring factor, and Rozeanu's stability criterion [8]. Most of these scoring criteria contain two parameters, load and velocity. Ku [9], however, found in the analysis of several sets of aircraft gears which failed due to scoring that the major problems were misalignment and dynamic tooth loading.

For a set of new gears, scoring is the first performance barrier that must be overcome [9]. With soft gear materials, run-in has been found to reduce scoring. Run-in is the light loading of the teeth early in their life. This produces light wear on the teeth surfaces, which lowers contact stresses. In light of this, if the gear accuracy is not sufficient, scoring is more likely to occur [6]. Although expensive, it has also been found that plating the teeth with copper or silver can eliminate scoring [6]. This, perhaps, allows run-in to occur faster.

Alman and coworkers [11] identify that scuffing or scoring is a result of the tearing of the tooth material due to insufficient lubricant. The indentations created on the surface are from small amounts of material welding under high pressures and friction-induced heat. Sliding a small cylinder against the flat side of a disk can be used as a standard wear test. Comparisons of the disk test data, however, to gear data have been unsuccessful to date.

This may be due to the fact that the disk data is collected is under steady-state conditions, whereas the actual gear applications are not steady state. Although the exact mechanism of scoring is not yet understood, gear design engineers generally agree that it is thermal in nature [9].

2. Pitting

Dudley [6] considers pitting to be a fatigue failure. This wearing of the tooth profile is a result of concentrated loads at the pitch line and higher local coefficients of friction, which produce surface rupture. Typical observations are that the gear which acts as the driver is more likely to experience pitting in a transmission [12]. Wilde [13] uses the relation between the teeth action and stresses to predict the location of pitting.

The contact point on the driver moves outward, increasing speed. The driven tooth has the opposite action as the driver. This causes the area indicated in Figure 2.2 with an x to be in tension, and it is therefore most likely to pit.

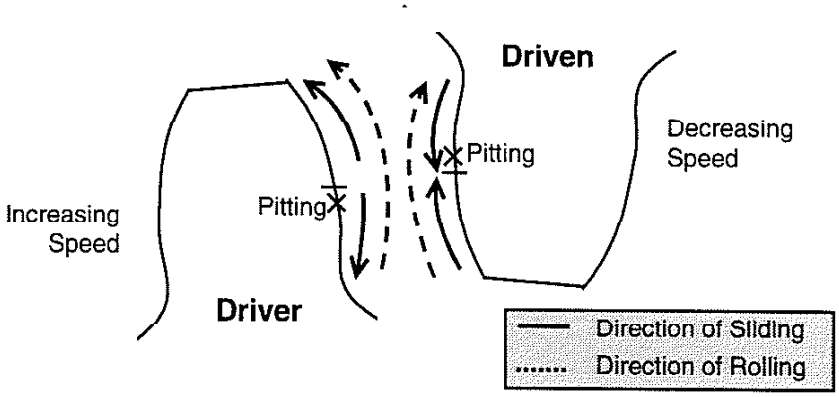

Figure 2.2: Surface action and stresses.

Reversing the rotation of the gear can retard or stop pitting. This is due to the fact that tensile stresses accelerate pitting, while compressive surface stresses serve to retard the effect. Additionally, it has been found that if the tensile stresses fall below a critical value, pitting stops entirely [12]. This critical limit is a function of the tooth's material

and can be reduced by strain hardening the surface [14]. This, however, is in contradiction to some of the early literature, which disclaim the existence of such an endurance limit [6].

Pitting is also dependent on the number of cycles encountered. Gay [15] reports that pitting rarely occurs after 10 million cycles. Initially, while surface cracks may appear, actual pitting requires a minimum of 20,000 cycles before it begins. Others, such as Yoshida, Ohue, and Karasuno [16], say that it can take 500,000 or more cycles to produce even a crack, and that this is independent of the lubricant used in the application. It is generally agreed, however, that the number of cycles before pitting begins is a function of the tooth's stress.

One interesting theory, proposed by Lipson [12], is that if a lubricant is present, its hydrodynamic wedging in the crack actually causes the pitting and, therefore, pitting cannot take place without oil. Another hypothesis proposes that any conditions which increase the tooth stress can cause pitting. Misalignment and deflection under load can both serve as stress risers [15].

In 1975, Bartz and Kruger [17] claimed that the cracks initiate at or below the surface, depending on the substrate material. While cracks can occur at stress risers, processing scars, or when strain hardening of the surface exceeds the elastic limit, it is the shear stresses alone that control the cracks. The maximum amount of shear stresses is predicted to occur at .78 times the contact radius below the surface and have a magnitude of .3 times the maximum Hertzian pressure, p_0, as shown in the cylinder-plate system in Figure 2.3 [14].

After particles fall away, pitting may stop as the load is spread over a larger area of the tooth, reducing the stress level. Tooth fracture, however, remains a concern under these conditions [15]. In 1982, Bartz and Kruger [14] continued the debate of where cracks are first produced. They proposed the cracks produced by pitting are 45 degrees to the

surface and shell shaped. The pits have rounded corners and shear edges. In the early stages of wear, their shape can be confused with indentations caused by foreign material [15].

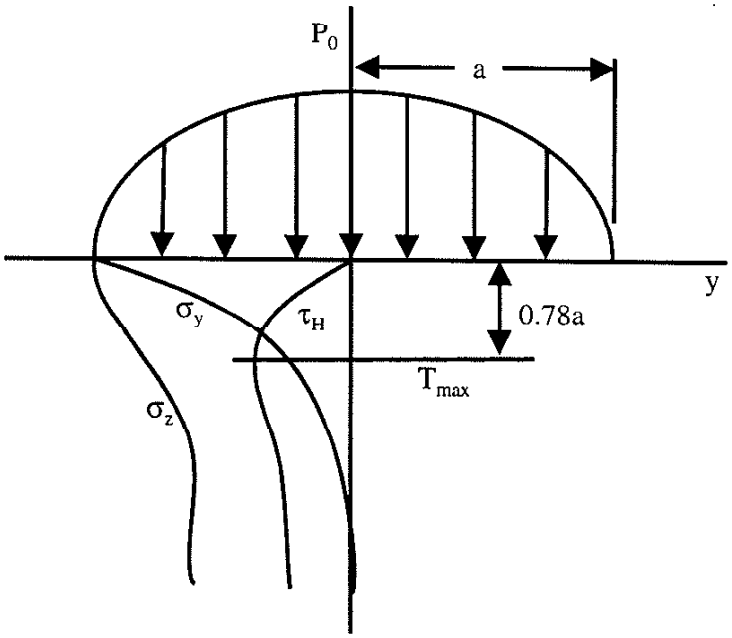

Figure 2.3: Stresses in a cylinder plate system.

One common method of reducing pitting is to use different materials. If the gears are unhardened or made of soft materials, pitting can occur at run-in. Once the surface peaks are removed and the contact area is sufficiently large to transmit the load, pitting stops [17]. Eighty to ninety percent of face contact is usually required before design loads can be accommodated [18]. The carbon content and hardness of the carborized case, along with the oxidized grain boundaries, have a significant effect on pitting resistance, while the grade of steel, heat treatment method, retained austenite, and excess carbides have been found to have little effect [13].

In the case of powder metal, induction hardened gears have been found to fail due to pitting and spalling. Powder metal has less surface durability than steel, leading to its surface degradation, because of the porous nature of the material [16].

3. Galling

Galling is another form of surface deformation. It occurs at slow speeds in sliding systems that operate intermittently. Identification of galling is made by visual inspection and is subjective. The surface deformations galling produces should be seen without the aid of a microscope. Typically, the contact pressure has to exceed a threshold value for galling to occur [19].

4. Fretting, Abrasion, and Tooth Fracture

Notice that in Figure 2.1 there is no mention of failure by fretting. Fretting, the surface wear produced by low amplitude sliding, has not always been considered a failure mode for gears. Wilde [13] is one of the few references which suggests the existence of fretting fatigue failures in gear teeth. It appears that the relationship between gear teeth and fretting was first discovered in the late 1970's.

Abrasive wear occurs on gear teeth as a result of debris between the two surfaces [13]. It can also occur when the speed is sufficiently slow and the load high enough to cause the surfaces to make contact and their asperities to plastically deform.

Tooth fracture, the ultimate failure, happens when the load is large enough to cause a crack to grow across the tooth. Although tooth fracture is a form of gear tooth failure, this study focuses on those failures resulting from surface wear.

B. Other Parameters

1. Geometry

In a typical gear reducer, variations from tooth to tooth in a gear's geometry have been identified as a source of concern. These variations can cause torque fluctuations in the drive, increasing the tooth's load. Coupled with inertia, dynamic loads can increase five to six times those transmitted. Variations from the ideal gear train, including manufactured tooth form, deflections, tolerances from assembly, and changing contact

interfaces from thermal expansion, can influence both strength and lubrication-related failures [9].

Thermal expansion is of particular interest in coaxial splined couplings, as it effects the fit of the spline. If the two materials have different thermal expansion rates, a close fit between mating splines may become tight at high temperatures. This can produce excessive stresses on the components. In the case of plastic gears, humidity, as well as temperature, may cause the gears to swell.

The manufacturing processes can significantly impact the gear tooth's geometry. If the gear is produced with powder metallurgy, the tolerance of the teeth should meet an AGMA quality number of 6 to 8, as sintered [20]. The higher the quality number the better the gear fit. The majority of industrial applications fall in the quality range of 10 to 13 [10]. For this reason, it is recommended that if gears from powder metallurgy are used, secondary processing should be considered. In Chapter 7, evaluations will be made with involute splined teeth. There, the ANSI class determines the quality of fit. The classes range from 4 to 7. The smaller the ANSI class, the tighter the fit.

Changes in tooth deflection, the tooth form, machining marks, and other imperfections can disrupt the evaluation of alloys and heat treatment changes [11]. Therefore, when testing potential application improvements, these items should be controlled. One of the most difficult imperfections to handle in gear evaluations is misalignment. It is both difficult to measure and control [9].

2. Tooth Contact

The tooth's contact area shape is an important aspect in the evaluation of its stresses, since contact stress is a direct function of the area of contact. The classical Hertz method of calculating the contact area will be described in Section C. The contact shape is not always rectangular; it can be elliptical [9]. One method of determining not just the shape of the contact area, but whether contact is being made on all of the teeth, is to coat the

gears with red lead paste. By loading the gear assembly with an auxiliary brake and rotating it at a slow speed, the contact areas can be identified [21]. Another method is to do the following: (1) flash plate the pinion with a chemically reducible element like copper; (2) assemble the gears without lubricant; (3) rotate the gears with a light load, then statically load them with torque; (4) fill the gear box with a reducing gas such as H_2S, hydrogen sulfide; and (5) purge the gear box with fresh air and inspect the gears. The plated surfaces will tarnish dark, except at the areas of contact [21].

The manufacturing tolerances of gear teeth in reducers can cause axial parallelism problems, resulting in the loading of the ends of the teeth. A common treatment of improper parallelism in the application of biaxial gear shafts is to crown the teeth [10]. A crown relieves the axial ends of the teeth so that angular misalignment creates contact toward the center of the tooth, rather than on the edge.

3. Tooth Deflection

Whether in a gear reducer with parallel shafts or with coaxial splines, when one of the gear teeth deflects under load, the ability to predict the loads on the surrounding teeth is significantly reduced. The contact stresses for gear teeth with a deflected neighboring tooth are quite different from stresses calculated through classical gear design. Yet whenever a load is applied to a gear tooth, there is movement. This is the hypothesis that will be a major contributor to the coaxial spline tooth durability analysis and will be the focus of this paper.

The evaluation of gear tooth deflection was empirically evaluated for sets of gear teeth in the 1930's. The exact results presented by Walker [22] and [23] are of little use in coaxial splines. As they are presented, the reduction ratio of the gears is key to the results. Walker's general solution [23], however, found tooth deflection to be proportional to load divided by the Young's modulus. Walker also found the tooth deflection to be independent of pitch. For a constant number of teeth and pressure angle, the deflection of the tooth is constant for a given load, regardless of changes in pitch [23].

This concept that deflection is independent of pitch was evaluated in a machine in which the gear was rigidly mounted. A dead weight was applied to the tooth being tested and the deflection measured. Additional weights were then added and further deflection measurements made. One disadvantage of this method is that the deflections measured with this device included both the tooth deflection and surface deformations [23]. Taking this drawback into account, this simple test method may be sufficient to verify predictions of other geometry and material changes.

Deflections in the system can contribute to the relative tooth deflection. They include the gear bodies, shafts, and support bearings, as well as the housing. Even an approach to solving this problem was not identified until the past few decades [9]. In that time, computational capabilities have increased substantially, possibly allowing the analysis of deflections through finite element analysis. Another method to consider would be similar to Walker's tooth measurement method. It would involve the measurement of the actual deflection in the entire system.

For the evaluations made later in this paper, these system deflections will be assumed zero. If they were considered, they could easily be included by adding them to the spline offsets.

4. Lubrication

Although this paper focuses on dry applications, the majority of the work done has been with lubricated gears. Therefore, the significance and impact of lubrication will be considered and applied where possible. When lubricants are used, their main function is to prevent the oxidation of the gear tooth surface. If the surfaces are extremely smooth, however, oxidation will occur despite the application of lubricant [12].

When the lubricant film is insufficient, there is also a possibility for scratching, scoring, scuffing, corrosion, fretting corrosion, hot flow burning, wear [24], mixed friction and

abrasion due to direct contact [7]. If operating at low speed, the gears may seize [7]. These symptoms, however, may not be solely the result of a poor lubricant film. They can also be due to operating conditions, such as load and speed. Lubricant characteristics that could effect the effectiveness of the film include viscosity, quality, and purity [24].

Wilde [13] suggests that the way to avoid abrasive wear is to provide an oil film sufficient to prevent metal-to-metal contact, since it is the metal-to-metal contact which produces debris. He points out that if the debris and foreign particles remain smaller than 30 micrometers, abrasive wear normally does not occur. Gay [15], however, claims that typical asperities on the teeth can be sufficiently large enough to bridge the oil film.

Fowle [18] suggests that dry gears, which are the focus of this work, are covered by absorbed gasses and an oxide film. They act as the primary lubricant. If these are removed through severe rubbing, the coefficient of friction and resulting wear rates increase substantially.

5. Heat

Heat, with the exception of lubrication limitations, is generally not an issue in the design of steel gears. This is not true in the case of plastic gears, however. With plastic gears, high speed causes hysteresis heating, and the gear wear is in the form of melting. The design parameter used to predict this occurrence is the PV limit of the plastic. The PV value is the product of the contact pressure and the velocity. If the PV value stays below the PV limit, the wear is minimized. The PV limit is discussed further in Chapter 6. Typical approaches to reducing this failure mode include reducing the stress, increasing the gear diameter, and increasing the root area [25].

6. Surface Finish

It is well known that polished surfaces have better fatigue lives than rough surfaces. This is related to the stress concentrations in the surface finish. In the case of gear life, the surface roughness is usually associated with the effectiveness of the lubricant. If a rough

surface is used against a smoother one, the smooth one will become slightly rougher while the rough surface would become quite smooth. Eventually, they will have the same surface finish [13].

There are many models and predictions on the effect of asperities. Generally, if the slope of the asperity is less than 1 degree, then the deformation is elastic and the oxide film remain intact, reducing wear [18]. When the asperity angle is greater than one degree, the deformation is plastic and the oxide layer breaks, exposing bare metal and allowing adhesion to occur [18].

7. Debris

At any speed, debris increases wear [6]. The production of debris, as well as its properties, is important in predicting gear tooth wear. As welding occurs between the gear teeth, the joint work hardens, and there is a fracture in the weaker parent material. Material then breaks free and becomes a particle. This can lead to a form of plowing. If the two gears have significantly different hardness, the harder wear particles can embed themselves into the softer material and cause greater wear on the harder surface [18]. In a study by Stoew, [26] particles need to be larger than 20 micrometers for this type of wear to occur.

Foreign particles can produce plowing wear as well. Any hard, sharp edged particles like sand or grinding dust which get caught between the gear teeth can produce excessive wear in the same manner as the wear particles [18].

C. Predictions Of Tooth Stresses

For gear sets which have offset shafts, such as reducers, the maximum compressive and shear stresses are found by the Hertzian stresses for cylinders on cylinders. They can be calculated according to Equations (2.1) through (2.5) [6]. These stresses, however, according to Dudley [6], are only valid at the pitch line.

$$S_c = \frac{4F}{L\pi B} \tag{2.1}$$

$$S_s = .295 S_c \tag{2.2}$$

$$B = \sqrt{\frac{16F(K_1 + K_2)R_1R_2}{L(R_1 + R_2)}} \tag{2.3}$$

$$K_1 = \frac{1-\nu_1^2}{\pi E_1} \qquad K_2 = \frac{1-\nu_2^2}{\pi E_2} \tag{2.4, 2.5}$$

where

S_c = Maximum compressive stress,

S_s = Maximum shear stress,

F = Force,

L = Tooth length,

B = Bandwidth of contact,

K_i = Constant,

R_i = Radii of cylinder (subscript denotes member number),

ν_i = Poisson's ratio, and

E_i = Young's modulus.

Dudley [6] also identifies the depth of maximum shear stress as being .393 times the contact bandwidth, B. Additionally, it has been found that the more teeth on a pinion, the lower their strength requirement is. Fewer teeth provide less wear resistance. However, if the gears in the reducer have a one-to-one ratio, the Hertzian stresses increase by 25%.

The compressive stress evaluations presented are typically used for gear design, but are only valid for a pair of external teeth, such as those in a typical reducer. For coaxial gears, which have internal and external teeth, the previous method of Hertzian stress and

contact area calculation does not apply. A more appropriate model is the cylinder within a cylindrical socket. This necessitates a change in the above model in the calculation of the bandwidth of contact, B. The term (R_1+R_2) in the denominator should be (R_1-R_2) [27].

In typical gear reducers, a hunting pattern may exist. This is when one tooth on a gear eventually contacts all of the teeth on its mating gear. This allows the teeth to wear evenly and produce a consistent spacing between them [6]. In coaxial gears, this does not exist, and the subsequent wear advantages are not realized.

D. Testing

The AGMA standards, as well as publications such as Dudley's, are based on test results. Love reported that splined axle shafts that were tested with static reversed twist both at high loads and fatigue loads produced a wide variety of interesting fractures. Based on these empirical results, he concluded that conventional fatigue testing would not solve the problems seen in gear teeth [28].

E. Reducing Gear Tooth Wear

While gear teeth can experience wear through a variety of failure modes, it is possible to significantly reduce wear. One solution is hardening the surfaces of the teeth though carborizing, nitriding or hard chrome plating. In lubricated applications, nitriding is recommended for fine teeth [6]. Several coating such as molybdenum disulfide, MoS_2, are on the market that can also reduce gear tooth wear by reducing the coefficient of friction.

When the coefficient of friction or surface hardening are inadequate, there are other proprietary coatings available. One is WC/C by Balzers Tool Coating, Inc. in North Tonawanda, New York [7]. This coating is made of amorphous carbon with tungsten carbide inclusions and applied by PVD, physical vapor deposition, to only a few micrometers thick. This film has the lowest coefficient of friction of hard surfaces, .1 to

.2. WC/C coatings provide a 10% to 15% increase in load capacity in case hardened gears and a 30% to 40% increase for heat-treated gears. In one study, the oil was removed from a gear case. Whereas this would normally result in seizure, when WC/C coatings were applied, there was almost no wear, despite the absence of lubrication [7].

F. Summary

The gear tooth failures of interest for this study are scoring and pitting. Scoring is a lubrication failure whose criteria is proportional to the load times velocity. Pitting is considered a fatigue failure, which has a load limit. The maximum pitting stress is .3 times the Hertzian stress and occurs below the surface. The Hertzian stress calculations used by gear engineers is for cylinders on cylinders. This is valid provided the gear teeth are not internal and external. In determining stress, tooth deflection is a recognized factor and has been found to be independent to the pitch of the gear. The geometry of the gear can cause dynamic loads to increase by up to a factor of six.

Oxidation is a contributor to gear tooth wear, and the primary purpose of lubrication is to prevent oxidation. It has also been found that debris size effects wear. If the debris between the teeth is larger than 20 micrometers, wear will increase.

Testing of splined axle shafts can produce a variety of failures, indicating the difficulty of relating conventional fatigue data to real applications. Common methods of reducing gear tooth wear include hardening the surfaces to increase resistance or coating them with materials which will reduce their friction coefficient.

III. Fretting Wear and Corrosion

Independent of the research in gear design is the study of fretting and its effect on surface durability. There are three types of surface degradation that are related to fretting: fretting fatigue, fretting wear; and fretting corrosion. They are all the result of low amplitude reciprocating sliding motion between two surfaces. Fretting corrosion occurs due to environmental chemical interaction with the contact surfaces. Fretting wear, however, involves the removal of material from the contact surfaces.

In the most simplified approach, it is believed that there are three stages of wear in the fretting process [29]. The first stage is the development of adhesion particles. In the case of metals, this is followed by their oxidation, which then permits corrosive wear to occur. The last stage is the abrasive wear due to the harder particles acting on the parent material. In this chapter, fretting wear and fretting corrosion, which are related to each other, will be considered together.

A. History

Tomlinson [30] in 1927, was the first to systematically study fretting. He thought that molecular attraction caused fretting and that the cohesive forces between the molecules on the surface caused the surface to tear away and oxidize. Uhlig [31,32] hypothesized that there are both chemical and mechanical factors involved in fretting. He suggested the wear model in Equation (3.1).

$$W = \left(k_0 L^{1/2} - k_1 L\right)\frac{C}{f} + k_2 lLC \tag{3.1}$$

where

W = Weight loss,

L = Load,

C = Number of cycles,

f = Frequency,

l = Slip amplitude, and

k_0, k_1, and k_2 = constants.

Holiday and Hirst, in the 50's, were the first to use optical and electronic microscopy, along with electron diffraction to evaluate the fretting process. They wanted to relate fretting to the slip magnitude. They found that, depending on the amount of slip, the surfaces could weld together. They also found that fretting was not dependent on the formation of an oxide [33].

Godfrey and his co-workers also used microscopy to establish the mechanism and identify the nature of fretting fatigue. They found that contact produced adhesion and very fine particles that broke loose from the surface and then oxidized. They also determined that fretting occurred in less than one cycle and therefore concluded that fretting does not require alternating motion [34-38].

Also in the 50's, Feng and Rightmire suggested a four-stage process to fretting fatigue. The stages are: (1) initial; (2) transition; (3) declining; and (4) steady-state. These stages incorporate the breaking away of particles, oxidation, and adhesion. They believed the process changes from transient to steady-state once the oxide becomes sufficiently thick on the surface [39-42]. At about the same time, Waterhouse[43] considered the theories of others and concluded that fretting was like wear, where adhesion, welds, and the transfer of material occur. He proposed that, in some cases, oxides play an important role as well.

Since this research, the understanding of fretting mechanisms has evolved considerably. Besides the increased number of observations, current theories are much closer in agreement with each other. Although the theories are increasingly similar, there is still no single over-reaching theory regarding fretting wear and corrosion.

B. Fretting Wear

Fretting wear takes place when several wear mechanisms act together under small displacements to cause either wear or fatigue cracks. The end product in ferrous materials is nonmetallic reddish oxide particles. These particles are often referred to as "cocoa", "red-mud", or "blood" in industry [44].

1. Adhesion and Abrasion Theories

The adhesion theory and the abrasion theory both relate to fretting wear. The adhesion theory claims there are two types of contact conditions, a strong one which produces metal transfer and a weak one that produces loose wear particles. Either of these can occur, regardless of the oxide layer. The presence of an oxide film can, however, reduce the number of strong contacts [45].

The abrasion theory is based on plastic deformation of surface asperities. Their peaks shear off, and small particles gather in the spaces between the high spots. There the particles can oxidize. Those particles can then abrade the contact surface [41, 46].

2. Work of Adhesion

Sikorskii [47], in an attempt to predict fretting wear, predicted a value called the work of adhesion, W_{ab}, between two surfaces. This is shown in Equation (3.2).

$$W_{ab} = \gamma_a + \gamma_b - \gamma_{ab} \tag{3.2}$$

where

γ_a, γ_b = Surface energies per unit of area of each material and

γ_{ab} = Interface free energy.

Rabinowicz [48] demonstrated that high friction coefficients and adhesions occur between materials that have a high ratio of the work of adhesion to material hardness. He further found that if the two materials are identical, the work of adhesion is proportional

to the hardness raised to the 1/3 power. This explains why harder materials require more energy to join by adhesion than softer materials.

3. Asperity Deformation

With small slip amplitudes, wear will occur if there is plastic deformation of the asperities. If the stress is above the endurance stress of the material, particles will form and wear will occur.

If the slip amplitude, half of the total sliding distance during one cycle, is sufficiently small, there exists a stick region surrounded by a slip region in the area of contact. Within the stick region, surface damage is limited to the asperities, which are adhesively joined and become plastically sheared. The energy required to shear those asperities, though, is small compared to the elasticity energy of the bulk material [49]. Those that are not plastically sheared but joined may deflect either elastically or plastically. The prediction of their plastic deformation is quite complex. But for the elastic case, Midlin [50] derived the relationship of asperity deflection to force and asperity size as shown in Figure 3.1.

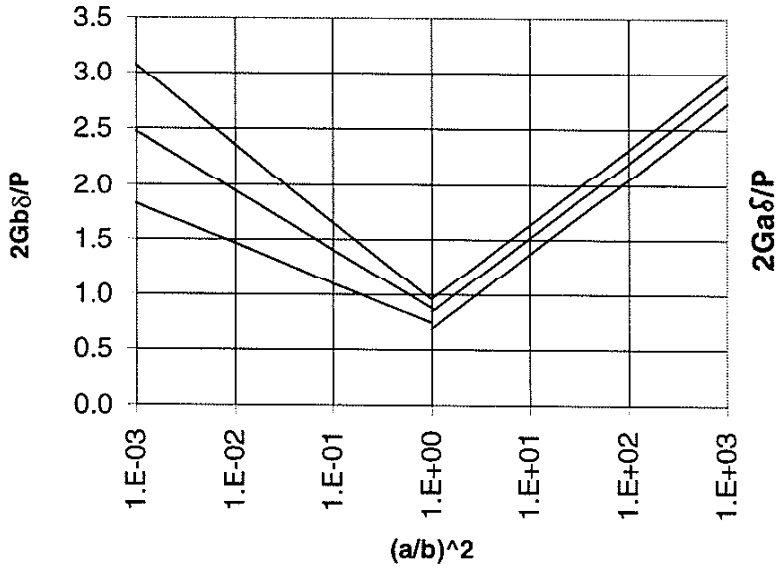

Figure 3.1: Elastic deformation of asperities.

The asperity ratio, a/b, is the ratio of the contact length and width of the asperity. Notice that the asperity ratio plays a key role in establishing the deflection of the asperity. The deflection is also proportional to the load divided by the Young's modulus. An analysis of Midlin's work through the use of curve fitting techniques produces the relations in Equations (3.3) and (3.4).

$$\delta_x = \frac{P_x}{2Gb}\left[.95-.17\nu-.52\nu^2+(.3\nu-.3)\mathrm{Ln}\left(\frac{a^2}{b^2}\right)\right], \quad \frac{a^2}{b^2} \le 1 \tag{3.3}$$

$$\delta_x = \frac{P_x}{2Ga}\left[.96-.42\nu-.24\nu^2+.29\mathrm{Ln}\left(\frac{a^2}{b^2}\right)\right], \quad \frac{a^2}{b^2} \ge 1 \tag{3.4}$$

where

δ_x = Asperity displacement,

P_x = Load,

a = Half the asperity contact surface width in the load direction, x,

b = Half the asperity contact surface width normal to the load direction,

G = Modulus of rigidity, and

ν = Poisson's ratio.

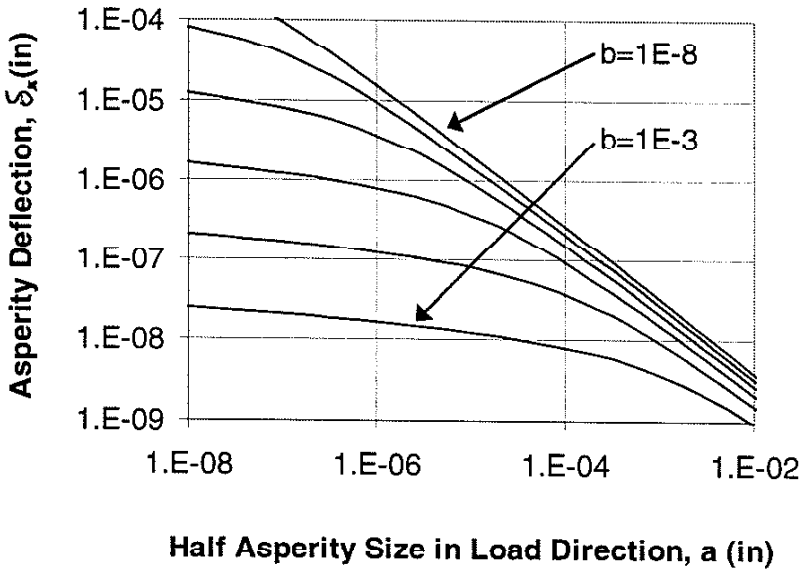

Figure 3.2: Elastic deflection of steel asperities.

Figure 3.2 shows the asperity deflections for steel with a .0001 pound load applied. Here it can be seen that for the asperities which are between .0001 and .010 inches, their elastic deflections according to Midlin are quite small, on the order of $100(10^{-9})$ inches. This evaluation could be used to predict how much elastic deformation occurs. If the displacement exceeds the elastic deformation, plastic deformation and wear is likely.

C. Fretting Corrosion

In the cyclic slip characteristics described above, adhesion, abrasion, and asperity deformation add to the mechanisms for fretting corrosion damage. Lispon [12] claims fretting corrosion is caused by the tearing and subsequent oxidation of the surface as soon as relative motion starts. In the fretting corrosion theory [31, 32], there are both mechanical and chemical phenomenon which cause the wear. The chemical portion occurs when a moving asperity produces tracks of clean metal surfaces which then oxidize or absorb gasses. This process is repeated with each contacting asperity. The mechanical portion of the process takes place when an asperity plows into the surface, producing welding and shearing action which dislodges particles [12]. The difference between fretting corrosion and wear is that, in fretting corrosion, the particles or surfaces in contact react to the environment [12].

D. Other Parameters

While there have been few models developed that will serve to predict fretting wear and corrosion, several parameters can be considered for their observed effects.

1. Sliding Amplitude

When the slip amplitude is less than 70 micrometers (.0028 inches), the surface wear is called fretting oxidation. Slip amplitudes greater than that tend to involve both mechanical and chemical wear mechanisms [51]. Amplitudes over 225 micrometers (.009 inches) are considered to wear by purely mechanical means [12].

Ohmea and Tsukizoe [51] claim that at larger amplitudes, over 300 micrometers (.012 inches), surface wear becomes more consistent with reciprocating wear. Bill [52], however, believes the transition from fretting wear to reciprocating sliding wear occurs at slip amplitudes as low as 70 micrometers. Ohmea and Tsukizoe [51] found that in experiments with the slip amplitude over 70 micrometers, the surfaces are found to be extremely rough with areas of adhesion and grooves.

Some have shown experimentally that the wear rate of fretting corrosion and slip amplitude have a relationship which is not always proportional [12]. Induction hardened steels have been found to wear to a depth, based on slip amplitude, after 10 million cycles by Nishioka and Kirakawa [53] as shown in Figure 3.3. Notice as the slip amplitude increases, the wear depth increases as well, but not proportionally.

Figure 3.4 is fretting wear data for a .25% carbon steel. It shows the effect on wear volume with changes in slip amplitude after 100,000 cycles and after 36 meters (120 feet) of slip [51].

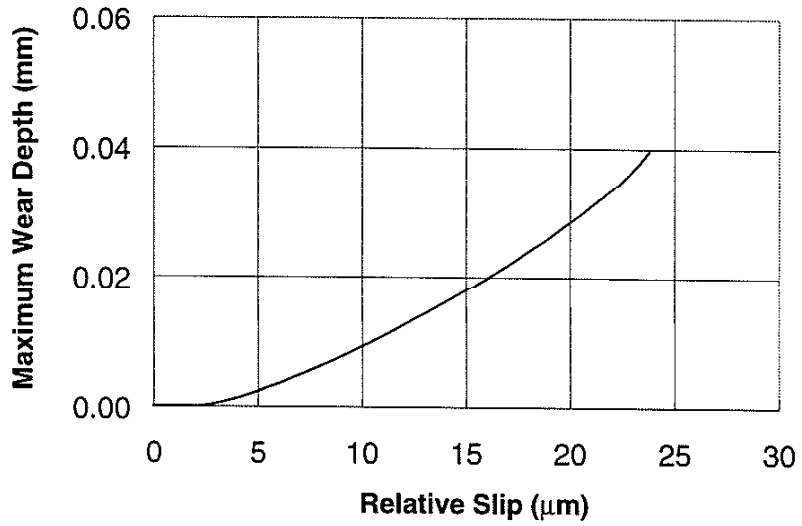

Figure 3.3: Wear depth of hardened steel.

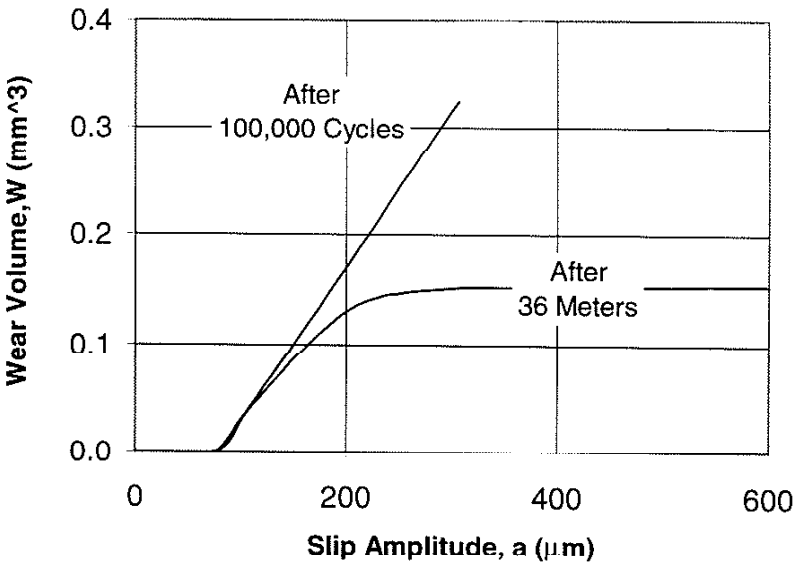

Figure 3.4: Wear volume after cycles and distance.

The data shows that the fretting wear volume after 100,000 cycles is nearly proportional to the amplitude, provided the amplitude is over 70 micrometers. Further, if the test is stopped after a known total sliding distance, the amount of material removed is not consistent unless the amplitude is over 300 micrometers [51].

Figure 3.5 shows Bill's [52] work with mild steel and suggests the transition point into fretting wear occurs at about 25 micrometers (.001 inches). It also demonstrates the nonlinear relationship of wear with amplitude.

The work of Nishioka and coworkers, Ohmae and coworkers, and Bill all show similar results. Up to a critical value, the fretting wear rate is nonexistent. After that value, the wear rate becomes nearly proportional with amplitude. Bill [52], suggests the critical value is a function of the surfaces' contact geometry.

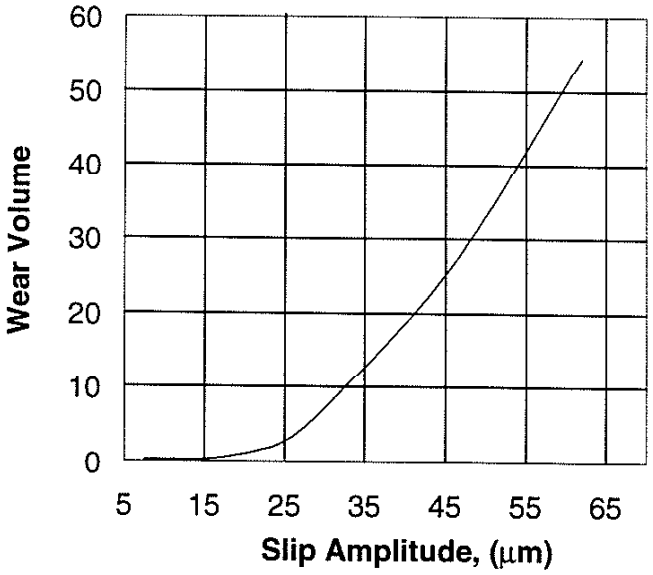

Figure 3.5: Wear volume versus amplitude.

Mason and White [54] developed a model which predicts when gross sliding occurs. It is based on spherical surfaces, involving a high shear strength material paired with a low shear strength material. The critical displacement, δ_x, which is the point up to which gross sliding does not occur, is defined by Equation (3.5).

$$\delta_x = \frac{\left(\frac{3N}{G}\right)^{2/3}(2-\nu)\mu}{8\sqrt[3]{r(1-\nu)}} \tag{3.5}$$

where

N = Normal load,

G = Shear elasticity of the softer material,

ν = Poisson's ratio of the softer material,

r = Radius of surfaces, and

μ = Coefficient of friction.

Notice that the critical displacement is linear with the coefficient of friction and increases, but not linearly, as the load increases. The coefficient of friction will be shown to be a function of the surface contact geometry in Chapter 7. For two, one-inch steel spheres, with a 100-pound load and coefficient of friction of .5, the total critical displacement is .0001 inches.

2. Humidity

The environment can also affect a material's ability to resist fretting wear and corrosion. With highly pure iron, humidity has a significant impact. Humidity promotes the formation of oxides, a key component in fretting wear and corrosion. Fretting peaks at about 10% relative humidity. Once humidity levels are above 10%, the fretting wear decreases. It then increases slightly as the humidity approaches 100% [52]. The engineer needs to be aware of the surrounding environment. It is important to take humidity levels into account, particularly as the lower, more damaging, levels typically prevail during the winter months.

If the material being considered in the design is plastic, humidity should also be considered, not because of corrosion, but because it can affect the size of the part [55]. This may change the stress levels in the part or allow relative movement, affecting the possibility of fretting.

3. Temperature

The rate of oxidation and corrosion have also been shown to increase with temperature [52]. When evaluated between −150 and +150 C, the greatest surface damage was found to occur at -150 C. Between −150 and 0 C, the amount of damage slowly decreases. From 0 to 50 C, the amount of damage quickly decreases, and then it gradually increases at temperatures above 70 C [12].

Some propose that the increased wear at lower temperatures in steel is related to the ductile-brittle transition temperature. Others attribute it to the effectiveness of the

lubricity from absorbed water. The actual cause has still not yet been proven [56]. Just as humidity affects some plastics, temperature can also change material properties. In addition to changing size through thermal expansion, some materials also experience variations in their elastic modulus and ultimate strength due to temperature. Size changes through thermal expansion would have the same effect as the humidity changes in the size of plastic. Higher temperatures also tend to decrease the Young's modulus and strength of material, and are therefore expected to decrease their wear resistance.

4. Cycle Frequency

One of the greater influences on oxidation, and therefore abrasion, fretting wear, and corrosion, is the cycle frequency. In mild steel, as the cycle rate increases from 0 to 30 hertz, the wear rate decreases. During the cycle, the oxide film thickness grows at a rate proportional to the period, until the period becomes so short that the film is completely worn away [57]. Therefore, at frequencies over 30 hertz, the oxides do not have time to form, and do not seem to affect fretting wear at higher frequencies [52]. There is disagreement as to the frequency where this occurs, as Hoeppner and Gates [57] claim it to be 1000 cpm, or 17 hertz. If the environmental conditions allow, the debris, as well as

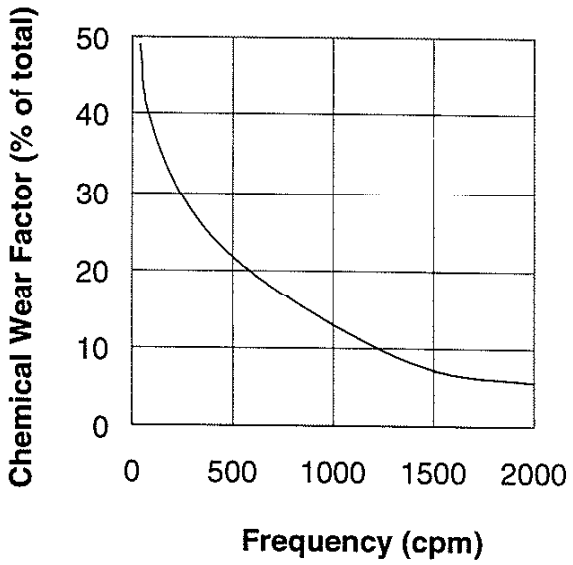

Figure 3.6: Chemical wear factor.

the surface, can oxidize and provide the mechanism for fretting corrosion at lower frequencies [57].

Lipson [12] provides relations between amount of wear and frequency in mild steel similar to that shown in Figure 3.6. Note the exponential increase in wear as the frequency decreases. At higher frequencies, Lispon claims the only wear mechanism that occurs is plowing.

5. Surface Finish

In fretting, the surface roughness affects the coefficient of friction, which is related to asperity deformation discussed earlier. Surface roughness is also related to the material hardness. Hoeppner and Gates [57] found that if the surface is rougher, minor movements can be accommodated without damage after the surface has work hardened. More importantly, a rough surface minimizes fretting wear by allowing the debris to escape [58]. If, however, the temperature is high, the debris is allowed to quickly oxidize and the benefit of roughness is reversed [57].

6. Debris

The debris material created in fretting wear may become an issue if it remains between the two surfaces. When surface cracks intersect, particles are released. Plastic deformation adds to the particles' elongation and extrusion. These particles can be trapped or crushed into smaller particles, just by the fretting action [49]. The oxide debris produced during fretting corrosion is the same as those produced during unidirectional sliding in the mild wear regime [59].

With the exception of the absorbed oxygen at its free surface and its internal areas of disorder, the initial debris produced by fretting is of virgin material. Once debris from other than virgin material is produced, the wear process may then be accelerated by work hardening the particles and oxidized debris. These can then act as abrasive lapping material. In order for abrasion, cutting, and scratching to take place, the particles

involved should be twenty percent harder than the surface being abraded [60]. As the slip amplitude decreases, so does the size of the debris particles [44]. Waterhouse [59] found that if hard particles like alumina or boron carbide are introduced to the friction interface, adhesion increases.

The actions of the debris may be affected by the size of the two contacting surfaces. Surfaces with large contact areas may have higher critical fretting wear amplitudes than surfaces with a smaller contact area because larger areas do not permit easy removal of the debris [52]. As will be shown in Chapter 4, the size of the contact area may effect the stick-slip area size, which in turn changes wear resistance.

7. Material

Evidence suggests that fretting wear is reduced by choosing materials with high hardness, high energy, and a high capability of work hardening [47, 48, 61]. Harder alloys have greater fatigue resistance because they are less susceptible to abrasive wear [57]. Campbell [62] believes that a harder material producing a soft oxide will resist wear quite well. A soft material, however, which produces a hard oxide particle will produce severe wear.

The surface hardness of the material can play an important role in reducing fretting. It can decrease the susceptibility to wear and crack initiation. Treatments which change the surface hardness, include nitriding, carborizing, and induction hardening. Methods such as drop forging, surface rolling and shot peening, can be beneficial as well, because they introduce a compressive residual stress into the surface[57].

Not only is the material of each surface important, but the two materials interacting with together should be considered as well. Typically, adhesion between surfaces is considerably higher if the two materials are similar or identical [59]. Mason and White [62] found that similar materials with different hardness and surface finish characteristics can make the best pair to resist fretting. Therefore, the selection of the most appropriate

pair of materials can help alleviate fretting problems. The considerations for making such a choice are generally empirical [57].

8. Cycles

For many materials there is a cycle threshold which is required for the start of steady state wear. This threshold is identified by microspalling pits, indicating the surface fatigue mechanism is operative [52]. Hurricks [63] separates the fretting corrosion process into three stages. In the first stage, adhesion begins and metal transfer occurs. Oxidized debris is produced during the second stage. In the third stage, steady-state wear is obtained.

The literature reveals two completely opposite observations regarding the early stages of fretting wear. When two surfaces are destined to wear by fretting, Bill [52] claims the initial wear is quite low. This may last one to ten thousand cycles, as indicated in Figure 3.7. In those early cycles, Bill suggests there is plastic deformation of the surfaces and adhesion wear takes place.

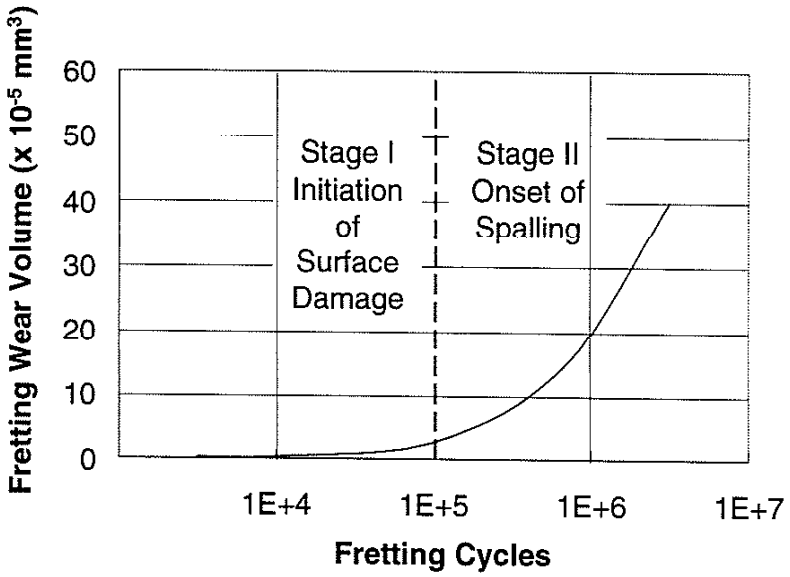

Figure 3.7: Fretting wear volume versus cycles.

Micropitting and corrosive damage are seen once the surfaces are in the high wear rate region. This region is also considered to be the onset of spalling [52]. The high wear region is thought to be the result of stripping the original oxide layer and embedding that material into the softer surface [42].

Waterhouse [59], however, says that the long-term effects of fretting are similar to mild wear, while the early stages are more like severe wear. Early in life, the surfaces become rough and there is significant macroscopic adhesion. It is in this period that fatigue cracks are likely to be initiated. In the later stages of its life, surfaces become smooth and adhesion drops closer to zero. At this time, the surfaces also start becoming separated by debris.

Bethune and Waterhouse[64] found that, in carbon steels, adhesion increases rapidly early in life and peaks at five thousand cycles. Adhesion then falls to about zero at around fifty thousand cycles. It is suggested that fatigue separation is responsible for the majority of the damage in the steady-state stage of fretting wear. Based on this information, the effect of cycles cannot be generalized. Their effect can be significantly different and need to be determined for each situation.

9. Load

Many references report that fretting wear increases proportionally, or nearly proportionally, to load [52]. Archard [65] tried to explain the nonproportional effect of load by suggesting the existence of a protective layer and a smooth surface that produces mild wear. At low speeds, low loads, and cool temperatures, the conditions are right for this protective film of oxides to be established on the surface. At higher loads, the surface is broken, after which the wear rate becomes more proportional.

E. Testing

The purpose of testing is to gain an understanding of the effects of changing variables. With respect to fretting, these variables include surface finish, treatments, and coatings,

shot peening, and base materials. Controlled test parameters to the application include pressure, sliding amplitude, frequency, and residual stresses. Some of the most difficult quantities to determine and reproduce in testing are the sliding amplitude and loading in the joint [66].

The most common fretting test is with a flat on flat specimen or a cylinder on a flat specimen. Because the coefficient of friction is an important quantity in the evaluation, a strain gage is often used to measure the tangential loads. The advantage of using a cylinder on a flat in testing is that the stress distribution can be calculated for the initial condition. Once wear occurs, however, these calculations are no longer valid [66]. During the test, the nature of the fretted surface is usually identified by a roughness measurement and weight loss [57]. Increasing the cycle rate can accelerate the test. This, however, can introduce effects of temperature rise and chemical reactions[66].

F. Reducing Fretting

Obviously, eliminating slip can prevent fretting. Coatings on the interface or lubricated surfaces can also be used. Campbell [62], however, claims there is not a liquid lubricant which can entirely prevent true fretting. For press fit assemblies, residual compressive stresses on the surface have been found to be most effective [12]. Shot peening is also used. It improves the surface finish, increases the hardness, and produces residual compressive stresses on the surface, all of which improve fretting resistance. Debris removal techniques and improved environmental protection also reduce fretting. Some believe that excluding the atmosphere reduces fretting as well. The ultimate solution is to remove the fretting surfaces from the design [67].

G. Summary

The difference between fretting wear and corrosion is the effect of the environment. Both can occur at low amplitude sliding. With fretting wear there is adhesion and abrasion of the surfaces. Fretting corrosion adds the oxidation of the surface. At sliding amplitudes

of less than about 70 micrometers, fretting oxidation occurs. At amplitudes up to about 225 micrometers, both fretting wear and corrosion can occur.

Fretting corrosion is at its greatest at 10% relative humidity and lower temperatures. The cycle rate for fretting corrosion needs to be less than 30 hertz as well.

Debris plays a complex role in fretting wear and corrosion, along with material and the combinations of materials. Fretting wear and corrosion change with time, and are situation dependent. The fretting wear rate has been found to be nearly proportional to the load.

IV. Fretting Fatigue

Fretting fatigue can occur when there is both cyclic friction stresses of the surface and cyclic stress due to external loading. This combination results in the initiation and propagation of fatigue cracks. These cracks can either cause a particle to separate from the surface, resulting in surface deterioration, or combine with the internal cyclic stress to grow and cause fracture. The reduction in the fatigue life of the part is indicated in Figure 4.1.

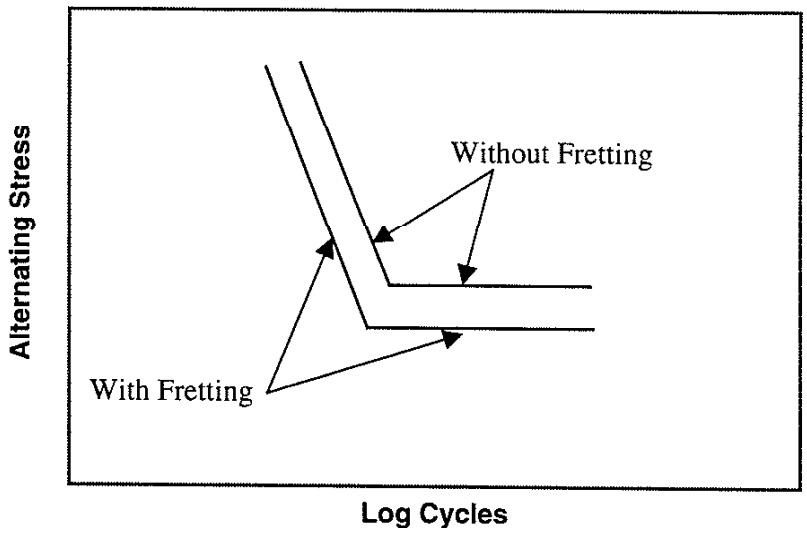

Figure 4.1: Effect of fretting on fatigue stress.

Waterhouse [68] explains the reduction of the horizontal lines is a result of crack initiation and the shift to the left is from an increase in the crack propagation. Endo and Goto [17] found that failure from fretting fatigue is most likely to occur after ten million cycles [69]. When a fatigue failure is a result of fretting fatigue, there are usually scars in the sliding direction at some of the surface asperities [70]. Later, it will be shown that for a given stress level, the reduction in fatigue life can be estimated.

The surface damage produced from fretting fatigue includes pits, third body oxides and debris, scratches or wear tracks, and metal transfer. This damage involves surface plasticity, fretting craters, subsurface cracks, and cracks of different geometry at various angles to the surface, including parallel to the surface [71].

A. History

Midlin [50] developed an early model of the effect of tangential loading on stresses in 1948. While it is in agreement with the observations of brittle materials and metals under plastic conditions, it was restricted to bulk dimensions and elastic contact. It did not consider plastic deformation either in asperities or the bulk material [49].

Stepanov [72] and Filimonov [73] recommended using a method of drawing fretting fatigue Wohler curves. Their calculations, however, did not correlate well with experimental data. Stress models of the fretting fatigue process by Waterhouse, [74] were more effective, as they determined that the initiation of the crack is controlled by the stress conditions existing within the area of contact. Inputs to their models include coefficients of friction, contact pressure, and the slip amplitude. Sato [75] used the concept of equivalent stress of Tresca. His results were in good agreement with experimental data. It is suggested by Dobromirski [76] that there are as many as 26 variables which can effect fretting fatigue.

B. Crack Nucleation and Growth

One of the criteria for fretting fatigue is the initiation of a crack. Fatigue cracks, often more than one, are thought to initiate at about the same time the surfaces obtain maximum adhesion [59]. There is disagreement, however, regarding where the cracks initiate. Hoeppner and Gates [57] claim they usually begin at the base of pits. Nishioka and coworkers [77], however, found that most cracks initiate without relationship to the pits on the surface. This suggests that there is no relationship between the pits and the initiation of cracks under fretting fatigue [77].

Waterhouse [59] suggests that fatigue crack initiation is related to the appearance of a slip region. The slip region is a result of the decrease in adhesion, and can be caused by loose debris between the surfaces. This is very difficult to model and predict. Vingsbo and Soderberg [49] agree, suggesting that it is a mix of slip and partial slip at the contact surface that promotes crack nucleation. Either way, once the cracks initiate, they may become connected until they are several millimeters long in the direction perpendicular to the sliding direction.

Once a crack grows sufficiently far from the surface, it can continue to grow perpendicular to the surface until the maximum tensile stress is reached and failure occurs [57]. It has been found, however, that once the crack has grown to a certain depth, the frictional stresses on the surface no longer affect the crack growth. Only the repeated bulk stresses have an effect. Therefore, there is the possibility that the crack may become nonpropagating [69].

This is illustrated in Figure 4.2. Note that the results are two straight lines describing the growth rate [69].

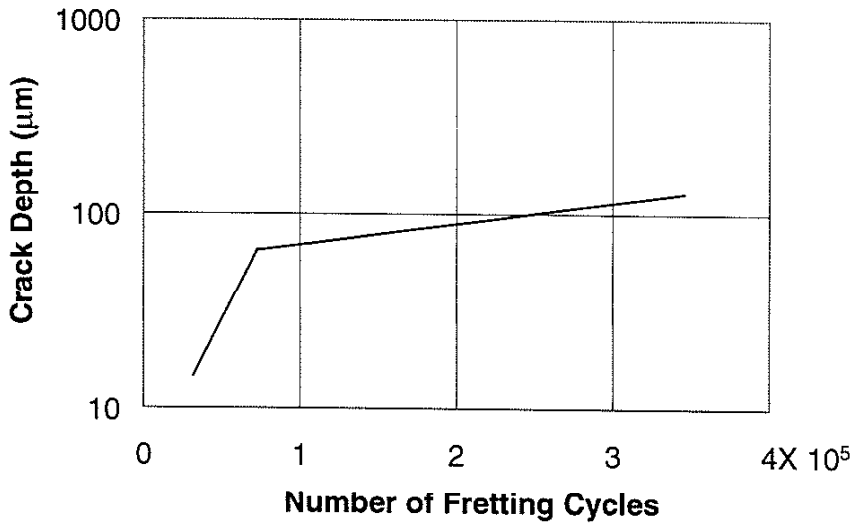

Figure 4.2: Change in crack growth.

Nishioka and Hirakawa [78] have graphed the relationships between fretting fatigue, alternating stress, and slip amplitude as depicted in Figure 4.3.

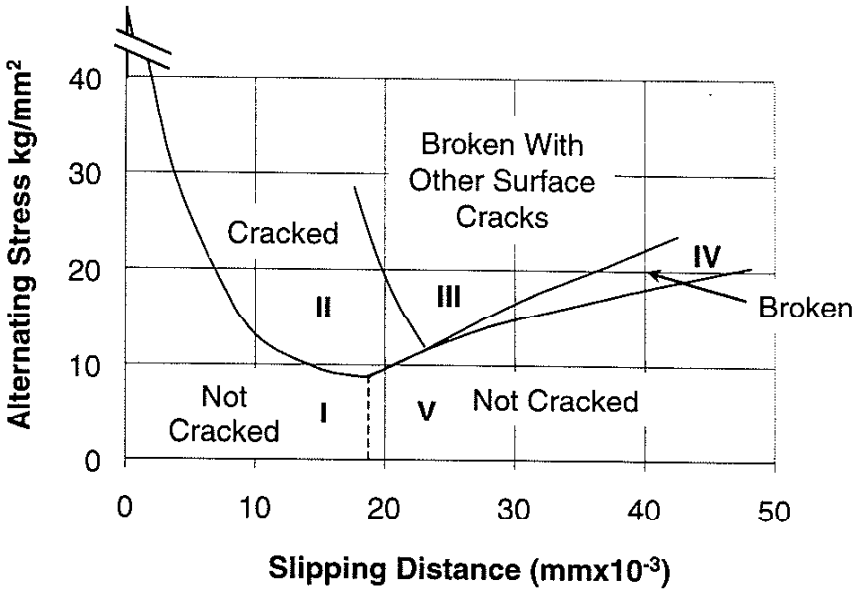

Figure 4.3: Regions of crack growth.

They found that cracks and failures form in five distinct regions in the graph. In the first region, that of low slip amplitudes and stresses, fretting wear and small pits occur, but no cracks are found. Region two, with higher stresses than region one, has small cracks and pits. The cracks in the second region do not grow large enough to cause fracture, due to the slip amplitude. In the third region, the alternating stress and slip are large enough that minute cracks form, one of which results in the complete fracture of the part. Applications in the fourth region fail similarly to those of region three, except that only one crack forms, causing the failure. The fifth region has a surface appearance similar to that of region one. No cracks are found in the fifth region. The wear produced by fretting in this region is considerable, however. The boundary between regions one and five is not as evident as the others, but is identified where the fretting wear becomes significant. As the wear resistance of materials increases, region five shifts to the left.

According to Nisshioka and Hirakawa [78], the critical stress necessary to initiate a fretting crack in region five exists, but does not cause failure. This is due to the fact that, while cracks may initiate in this region, their depth is of the same order as the maximum wear, 10 to 40 micrometers (.0004 to .0016 inches). Therefore, as the slip amplitude increases, the stress required to nucleate and grow cracks which are not worn away, increases. The discrepancy between theoretical and experimental results involving fretting fatigue is considered to be due to the wearing away of the surface cracks [53].

Nishioka and Hirakawa [77] have also developed a theoretical relationship for the angle between the normal of the contact face and the maximum principle stress, θ, as Equation (4.1).

$$\theta = \frac{1}{2}\tan^{-1}\left\{\frac{\sqrt{1-(x/a)^2}}{(x/a)-(\sigma_a/2\mu p_0)}\right\} \tag{4.1}$$

where

x = Tangential position,

a = Contact radius,

σ_a = Alternating bending stress amplitude,

μ = Coefficient of friction, and

p_0 = Maximum contact pressure.

The angle to the maximum stress is shown in Figure 4.4. Note that at the edge of the contact surface, $x = \pm a$, the crack direction is perpendicular to the surface. At locations closer to the center of the contact area, the angle of the crack is likely to be more than 25° from the normal to the surface. Figure 4.4 also shows the relative effect of the coefficient of friction on the crack angle, with higher coefficients decreasing the angle of the crack to the surface.

Waterhouse [59, 68], however, disagrees, claiming that the nucleation of fatigue cracks is at 45° to the surface in stage 1, as indicated in Figure 4.5, and is at the edge of the stick-slip region as discussed earlier.

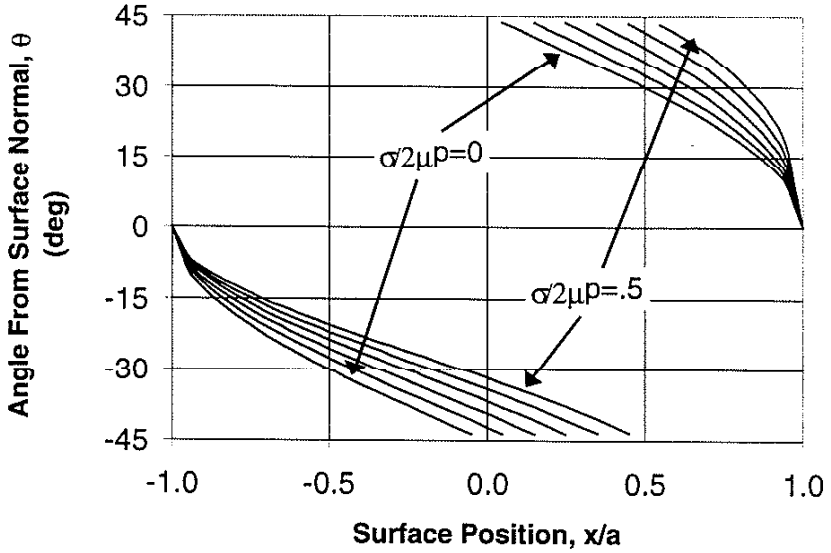

Figure 4.4: Angle to maximum principle stress.

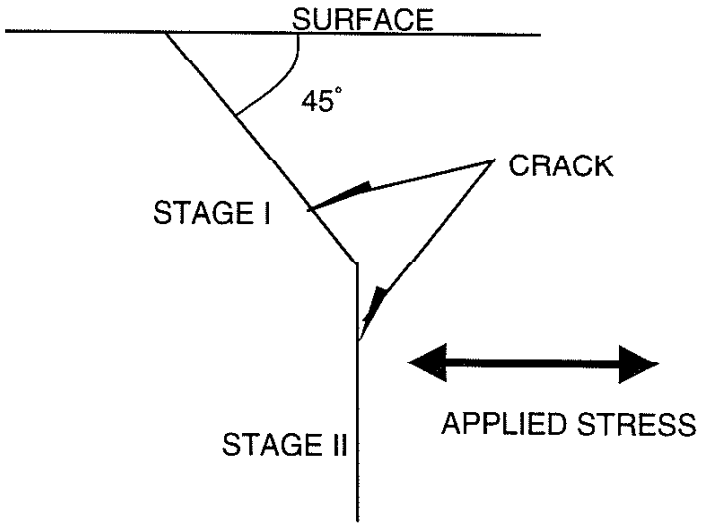

Figure 4.5: Crack propagation.

The length of the stage 1 crack depends on the environment and stress levels. The crack will become longer if it is in a corrosive environment with low alternating stresses. The surface near the crack will also have a pronounced lip on one fracture surface and a chip on the other as a result of the fretting action. Stage 2 of the crack growth is controlled by the stresses at the crack tip, and therefore grows perpendicular to the surface and normal to the principal stress [68].

Nishioka and Hirakawa also propose a stress concentration factor, K_t, in evaluating crack nucleation in Equation (4.2). It is a relationship of the ratio of alternating normal stress to alternating bending stress [77].

$$K_t = \left|\frac{\sigma_r}{2\sigma_a}\right| = \left|1 - 4\mu\left(\frac{x}{a}\right)\left(\frac{P}{\pi a\sigma_a}\right)\right| \tag{4.2}$$

where

σ_r = Alternating normal stress,

σ_a = Alternating bending stress amplitude,

μ = Coefficient of friction,

x = Tangential position,

a = Contact radius, and

P = Load.

The result is a maximum K_t at the edge of contact and is equal to $2P/\pi a\sigma_a$-1, if the coefficient of friction is .5. Nishioka and Hirakawa have shown K_t to be as high as eight. From this, it seems that the nucleation of fretting cracks at low alternating stresses might be due to the high stress concentrations at the surface. Even if these cracks initiate on the surface, they quickly grow into a region of lower stresses. This, the retardation of crack propagation, is the most significant difference between fretting fatigue and normal fatigue [77].

One approach to predicting the initiation of a crack is metallurgical in nature. McLean [79] suggests the minimum stress, σ_m, to produce sliding at the grain boundary is as in Equation (4.3).

$$\sigma_m = \left[\frac{12\gamma G^{1/2}}{\pi d}\right] \tag{4.3}$$

where

G = Shear modulus of the material,

d = Average grain diameter, and

γ = Surface energy.

For steel on steel in sliding and rolling contact and an ASTM grain size of 5, the resulting minimum stress is about 127 MPa. This, he predicts will result in a crack [80].

There are many theories and observations of the initiation and growth of cracks. Those presented here should give an appreciation for the mechanisms and their effect on the surface wear.

C. Stress

Crack growth and propagation is dependent on the stress levels in the part. In fretting fatigue, the tangential stress combines with the contact pressure to produce the crack damage. Newell and Hills [81] developed the stress relationship for a cylinder on a flat plate. The pressure distribution, p(x), derived from the Hertz equation for a cylinder on a plate made of the same material, is as shown in Equation (4.4).

$$p(x) = p_0\left\{1-\left(\frac{x}{a}\right)^2\right\}^{1/2} \tag{4.4}$$

where

p_0 = Maximum pressure,

x = Tangential position, and

a = half of contact diameter.

The maximum pressure, p_0, is given in Equation (4.5).

$$p_0 = \left\{ \frac{PE}{2\pi(1-\nu^2)R} \right\}^{1/2} \tag{4.5}$$

where

P = Normal force,

E = Young's modulus,

ν = Poisson's ratio, and

R = Radius.

Newell and Hills then used the Hertzian stress to create the tangential load, q(x), in Equations (4.6) and (4.7) where the bulk strain in one member produces an effective displacement, e, in the stick zone [81].

$$q(x) = -fp_0 \left\{ 1 - \left(\frac{x}{a} \right)^2 \right\}^{1/2} + q'(x) \qquad |x| \le a \tag{4.6}$$

where $q'(x) = 0 \qquad |x-e| \ge c \qquad |x| \le a$

$$q'(x) = \frac{cfp_0}{a} \left\{ 1 - \left(\frac{x-e}{c} \right)^2 \right\}^{1/2} \qquad |x-e| \le c \tag{4.7}$$

This solution is valid if Equation (4.8) is satisfied.

$$\frac{\sigma_{max}}{fp_0} \le 4 \left\{ 1 - \left(1 - \frac{Q}{fp} \right)^{1/2} \right\} \tag{4.8}$$

where

Q = Tangential force,

c = Radius for change from stick to slip contact,

p = Normal load,

f = Coefficient of friction,

p_0 = Maximum pressure,

x = Tangential surface position,

a = Contact radius, and

e = Displacement change in stick zone due to bulk strain in one member.

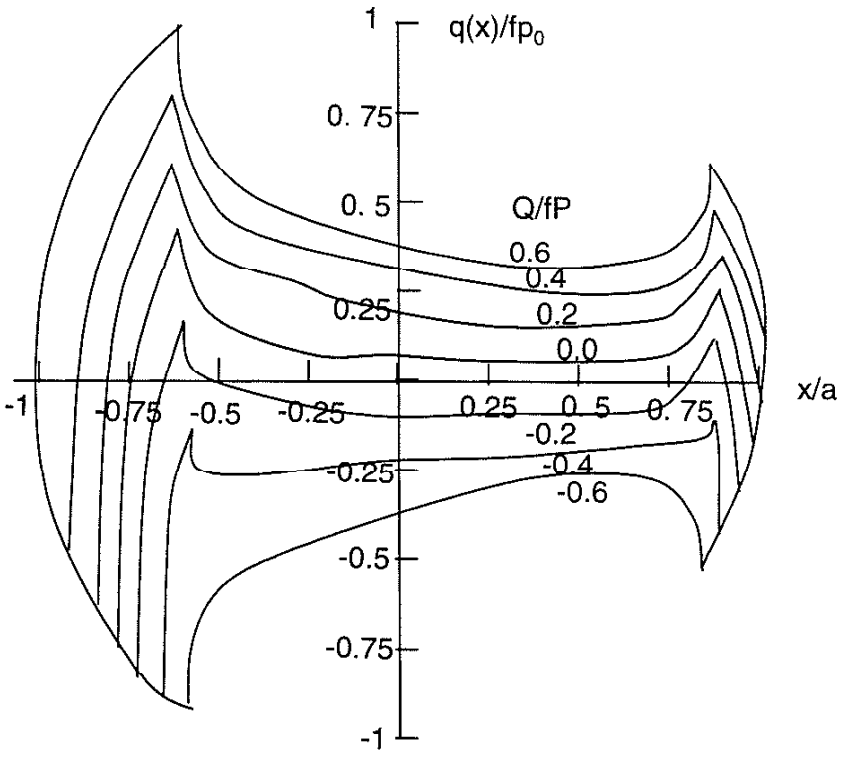

Figure 4.6: Newell and Hills stress distribution.

The plot of this model in Figure 4.6 shows that as the coefficient of friction increases, so do the tangential traction to normal pressure ratios. Those ratios are also larger for the lagging contact positions than the leading positions. They are at their peak at the edge of the stick slip region and decline faster when moving through the stick zone.

In the case of splined couplings, this model may not properly represent the application. Because the surrounding members of the gear teeth are significantly rigid, the tangential

force on the teeth surfaces is sufficient to ensure sliding if the sliding amplitude is large enough. If so, the radius defining the stick-slip region is zero, and the tangential tractions become the normal force multiplied by the coefficient of friction.

Szolwinski, et al., [82] has proposed a less complex model to determine the tangential stress which accounts for the bulk stress in the material. His results are comparable to those obtained using a finite element analysis. He determined the peak tangential stress at the trailing edge of contact, σ, as given in Equation (4.9).

$$\sigma = 2p_0\sqrt{\frac{\mu Q}{P}} + \sigma_0 \tag{4.9}$$

where

σ = Maximum stress,

p_0 = Maximum Hertzian contact pressure,

μ = Coefficient of friction,

Q = Tangential force,

P = Normal force, and

σ_0 = Applied bulk stress.

Again, in the case of coaxial splined couplings, the tangential force is so large that sliding must take place on the teeth. Therefore, the applied tangential force is the product of the normal force and coefficient of friction. This model then reduces to Equation (4.10).

$$\sigma = 2p_0\mu + \sigma_0 \tag{4.10}$$

Nishioka and Hirakawa [53] propose a model that predicts the alternating stress amplitude to initiate fatigue cracks as a function of the slip amplitude as Equation (4.11).

$$\sigma_{fw1} = \sigma_{w1} - 2\mu p_0\left(1 - \exp\left(-\frac{S}{k}\right)\right) \tag{4.11}$$

where

σ_{fw1} = Alternating stress amplitude,

σ_{wf} = Fatigue strength of the material,

μ = Coefficient of friction,

p_0 = Hertzian pressure,

S = Slip amplitude, and

k = Constant.

The decrease in the fatigue strength of the material is predicted to be linear with the coefficient of friction and an exponential function of the slip amplitude. All three of these methods that determine stress reduction result in the adjustment in the Goodman diagram as shown in Figure 4.1.

D. Stick-Slip Area

In fretting fatigue, the area where slip occurs is considered the location of crack initiation and growth. Nakazawa and coworkers [83] found that fretting fatigue life reaches a maximum when the contact pressure is low. The minimum life, however, is obtained at medium pressure, not at high pressure. This, they thought, is due to the slip area and stress concentrations in the fretted area. Figure 4.7 schematically shows this effect during fretting fatigue. On the outside of the contact region there is a slip region, and in

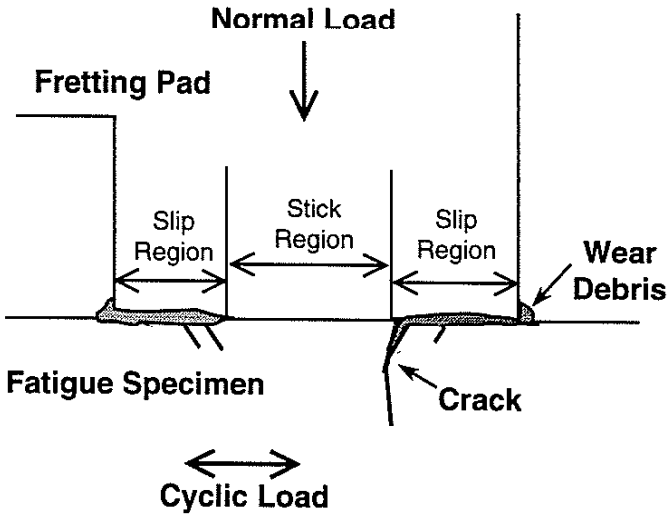

Figure 4.7: Fretting damage.

the middle, a stick region. The major cracks, which are responsible for failures, initiate at the boundary of the stick and slip region [83].

Naturally, if the pressure is high, the stick region is large and the formation of cracks is closer to the edge of contact. At lower pressures, however, the stick region is small, and cracks initiate near the middle of the contact area. This produces a minimum fretting fatigue life [83].

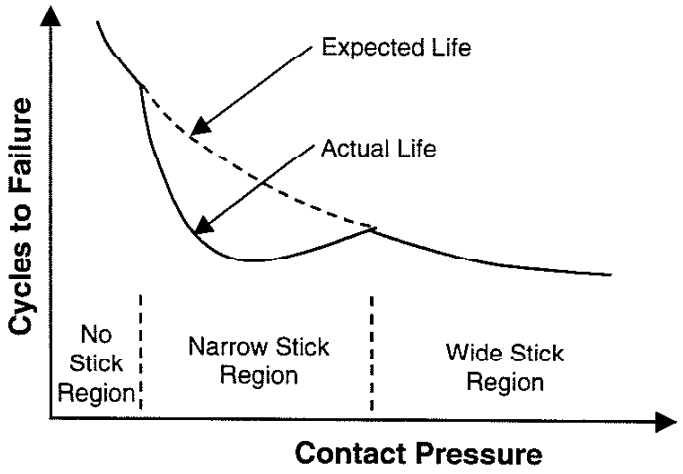

Figure 4.8: Fatigue life versus contact pressure.

Nakazawa and coworkers [83] found this reduction in life at medium pressure as shown in Figure 4.8. It is probably caused by a high concentration of frictional stress at the stick-slip boundry. Elsewhere in the figure, the contact pressure is proposed to be evenly distributed over the fretting area.

Nishioka and Hirakawa [53] suggest the use of the tangential force coefficient, which is a function of the contact pressure, tangential force, and coefficient of friction, to determine the size of the adhesive area. The relationship between the adhesion region, (b/a), and the tangential force coefficient, ϕ, is calculated in Equation (4.12).

$$\frac{b}{a} = \sqrt{1-(T/\mu P)} = \sqrt{1-\phi} \tag{4.12}$$

where

ϕ = Tangential force coefficient,

a = Contact region,

b = Adhesive region,

T = Tangential force,

μ = Coefficient of friction, and

P = Contact Force.

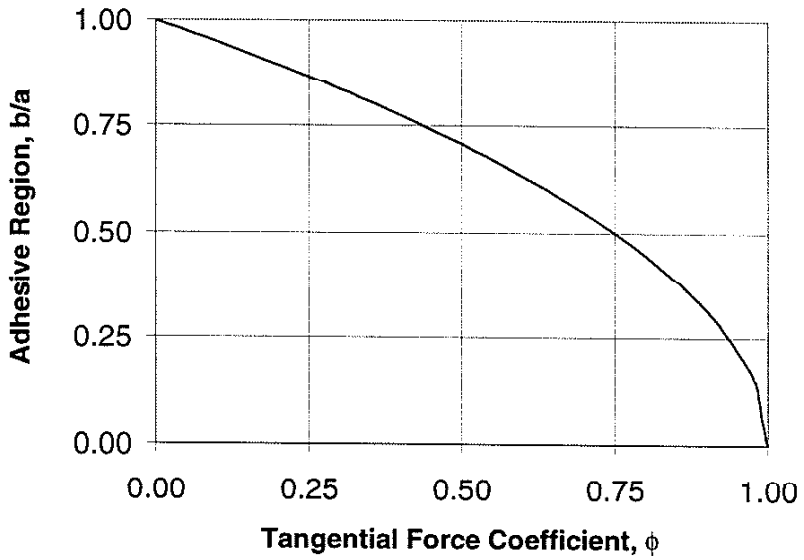

Figure 4.9: Adhesive region as a function of force coefficient.

This relationship is useful in relating the coefficient of friction to the size of the stick-slip region.

Note that on the left side of the graph in Figure 4.9, the coefficient of friction, the inverse of ϕ, increases along with the region of adhesion. In the case of splined couplings, a high tangential force usually ensures the tangential movement of the surfaces, and is the product of the contact pressure and coefficient of friction. Therefore, ϕ approaches unity. As indicated in the graph, the adhesion region disappears at that point. For low amplitude sliding, the slip area may be of interest, but for larger amplitudes, such as coaxial splines, the stick region disappears as well as its contribution to crack initiation and growth.

E. Damage Threshold Theory

Both Waterhouse and Hoeppner [67] proposed a fretting fatigue threshold that can be used to prevent and control fretting fatigue. It simply states that once damage occurs, if the fretting fatigue were eliminated, the fatigue damage would stop. The idea of a fretting fatigue threshold in fretting fatigue has existed since the early 1970's. As of 1992, however, insufficient studies regarding how it impacts fretting fatigue have been made [84].

Wharton [85] defines the fretting fatigue threshold limit as the number of cycles required to initiate a crack. Hoeppner [84], however, defines it as the point where premature failure will not occur if the fretting fatigue is eliminated.

It has been theorized that under certain conditions, fretting fatigue can produce mode I, II, or III cracks. After the cracks are produced, however, the fretting has no further effect on the fatigue life. The growth of the crack becomes the determining factor with respect to the part's life [67]. Endo and Goto [69] claim that fretting fatigue damage has an effect only in the first 20 to 25% of the component's life.

Hoeppner [84], found that for 7075-T6 aluminum, the normal pressure and damage threshold have an inverse relationship in that, as the pressure increases, the damage threshold decreases. It is suggested that this only occurs up to a certain pressure, after which the contact is mixed stick-slip [84]. It is also believed that there exists a critical

frictional stress which, when reached, causes the fretting damage to reach its threshold more quickly [86].

An increase in the maximum fatigue stress of the material may result in a decrease in the number of cycles to failure due to the fact that the fretting damage may reach the threshold limit much faster with this material. Because the stress concentrations in the stronger material may increase, the fretting damage can reach its threshold faster and initiate a crack [84].

F. Crack Initiation Criteria

Ruiz et al. [87] suggests that the likelihood of a crack initiating within a given number of cycles is a related to the product of three parameters: the maximum shear traction, τ, the slip amplitude at that same position, δ, and the bulk stress at the surface, σ. This theory seems to be consistent with experimental results, suggesting that it could be used to design components that resist fretting fatigue.

There are two possible ways to reduce the likelihood of fretting fatigue. One is to reduce the slip amplitude. If there is partial slip, reducing the coefficient of friction will increase the slip amplitude and decrease the traction force. This action should be carefully considered, however. As stated in this theory, it is the product of the slip amplitude and traction force which governs crack nucleation. The second method of fretting fatigue reduction is decreasing the bulk stress to prevent the cracks from growing. This theory suggests a proportional relationship between these stresses and the formation of a crack in a certain number of cycles [87].

G. Other Parameters

1. Surface Finish

Just as in fretting wear and corrosion, the surface finish can impact the resistance to fretting fatigue. It is responsible for the coefficient of friction, which in turn affects the tangential force and the ability to nucleate cracks. Scars from true fretting fatigue are generally rough but may be compacted and form a glaze on steel. The scars on steel are

reddish-brown and on aluminum they are black [70]. Small pits, which are 10 to 30 micrometers (.0004 to .0012 inches) in diameter, are found on fretted surfaces, as well as pits as large as 100 to 400 micrometers (.004 to .016 inches) [77].

Hoeppner suggests that, if lubricated, a surface with a finish greater than 63 microinches is better. However, if dry, a finish of 16 to 63 microinches should be avoided [67]. Cadmium, a soft metal, can be applied to the surface when the slip amplitude is small. The plating will shear with the movement, preventing the sliding motion which causes wear. Chromium, a hard plating, can also be applied to reduce fretting fatigue. It resists abrasion, thereby prohibiting the welding of the two surfaces together [57].

2. Coefficient Of Friction

The magnitude of, and transient changes in, the coefficient of friction are important in evaluating fretting. Lindley and Nix [88] believe that the coefficient of friction is more important than the sliding amplitude. While this can be debated, its magnitude is certainly important as it establishes the relationship between the contacting and tangential forces.

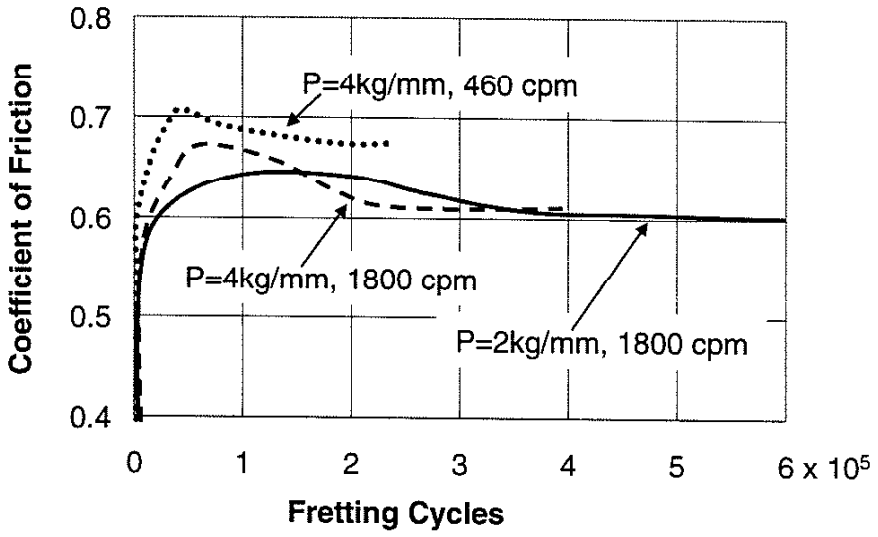

Figure 4.10: Initial coefficients of friction.

In the evaluation of fretting fatigue, several researchers have found the coefficient of friction between two surfaces to change with cycles or time, similar to Figure 4.10 [69].

As the load of cycle rate changes, so does the transient response. Additionally, it was found that if the test was stopped, and the faces inspected, the coefficient of friction changed as well as shown in Figure 4.11.

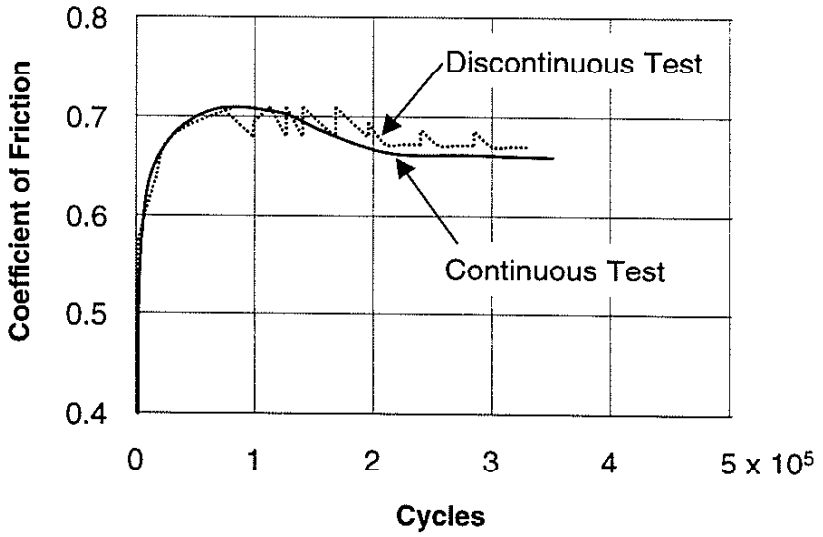

Figure 4.11: Effect of stopping tests on coefficient of friction.

The change in the coefficient of friction shown in Figure 4.11 is further demonstrated in observations of components with larger slip amplitudes that have an accumulation of oxide debris between the surfaces. With time, the oxide debris is removed from the surface and the tangential force increases quickly, just as demonstrated in Figure 4.11 [69].

During the initial stages of testing, when observations of crack size and growth are made, the changes in the coefficient of friction should be understood and accounted for in the evaluation.

The coefficient of friction can also affect where plastic deformation and damage occur. O'Connor [89] found that, for cylinders with a sufficiently large coefficient of friction, yielding would occur at the surface. Hamilton and Goodman found that for coefficients of friction of less than .3, yield occurs below the material surface. For larger coefficients of friction, yielding occurs on the surface.

3. Slip Amplitude

Just as the area of slip is important to the initiation and growth of cracks, so is the amplitude of the slip. Hills and Nowell [50] published relationships between slip amplitude and fretting fatigue life and wear similar to those shown in Figure 4.12. Their observations indicate that wear is not linear with slip amplitude. The fatigue life of the surface reaches its minimum value at about 10 micrometers of slip (.0004 inches). It is this point which differentiates between partial slipping and sliding, where sliding occurs over 10 micrometers.

This is conceptually consistent with the work of Nakazawa and coworkers [83] discussed earlier, where changing the pressure produced similar results.

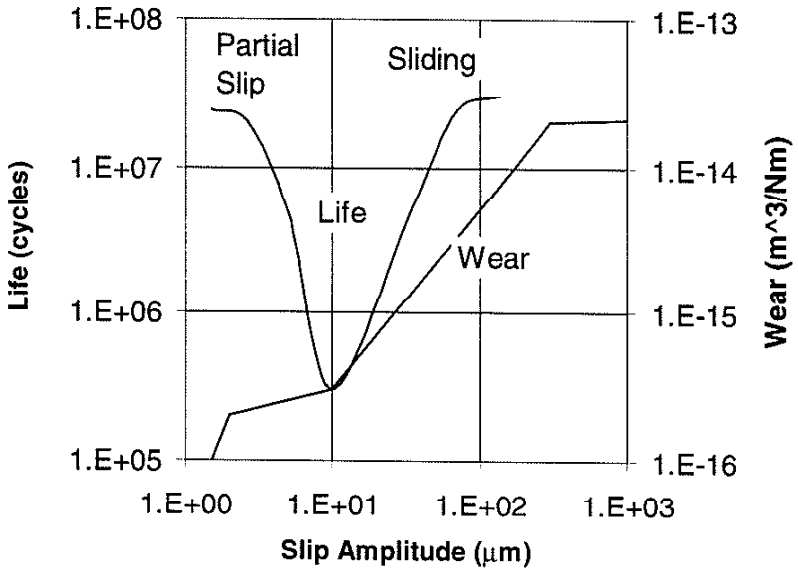

Figure 4.12: Typical fretting fatigue life and wear data.

Nishioka and Hirakawa [78] suggest that the fatigue strength can be reduced to about 20% of the original strength. The most significant reduction in strength occurs between 15 and 20 micrometers (.0006 to .0008 inches) of slip amplitude. If the amplitude is reduced to be less than 5 micrometers (.0002 inches), they expect significant fatigue strength improvement. Marsh [90], on the other hand, believes that the most significant decrease in fatigue strength has a wider slip amplitude range, 7 to 26 micrometers (.0003 to .0010 inches).

One key to reducing crack initiation is having knowledge of the slip amplitude. Johnson [91] calculates the slip amplitude in two contacting spheres as Equation (4.13).

$$\frac{\alpha}{a} = \frac{\pi(2-\nu)}{8}\frac{\mu p_0}{G}\left\{\left[1-\frac{\pi}{2}\sin^{-1}\left(\frac{a'}{a}\right)\right]\left[1-2\left(\frac{a'}{a}\right)^2\right]+\frac{\pi}{2}\left(\frac{a'}{a}\right)\left[1-\left(\frac{a'}{a}\right)^2\right]^{1/2}\right\} \qquad (4.13)$$

where the pressure and radius of no slip are Equations (4.14) and (4.15) respectively.

$$p_0 = \frac{3N}{2\pi a^2} \qquad a' = a\left[1-\left(\frac{T}{\mu N}\right)\right]^{1/3} \qquad (4.14, 4.15)$$

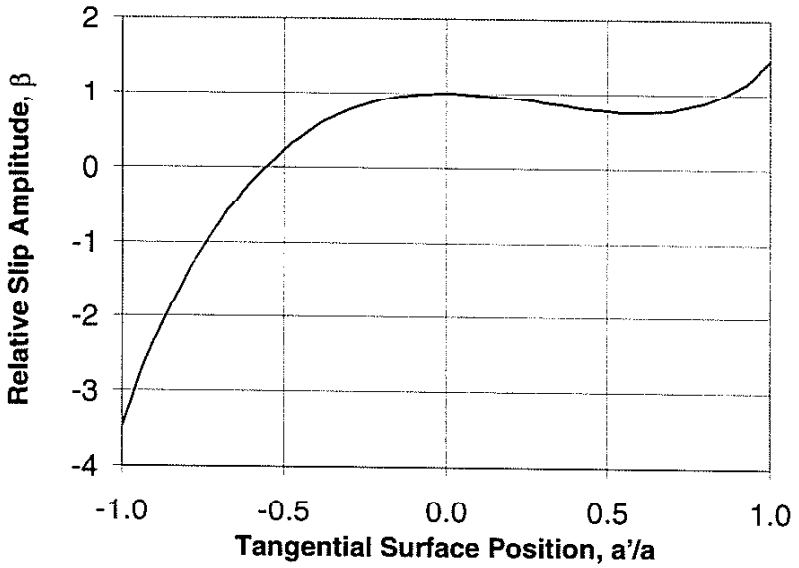

Figure 4.13: Slip amplitude of spheres.

Where the slip amplitude in Figure 4.13 is given in Equation (4.16).

$$\beta = \frac{\alpha}{a}\left(\frac{8G}{\pi(2-\nu)\mu p_0}\right) \tag{4.16}$$

and

α = Slip amplitude,

a = Sphere contact radius,

ν = Poisson's ratio,

μ = Coefficient of friction,

p_0 = Maximum Hertzian pressure,

G = Shear modulus,

a' = Radius of no slip, and

N = Normal force.

Note in Figure 4.13 that at the lagging position of contact, the left side, there is the greatest relative slip amplitude; nearly 4 times of that elsewhere in the contact region. When sliding occurs, the radius of the no-slip region becomes zero and the slip amplitude becomes Equation (4.17).

$$\frac{\alpha}{a} = \frac{\pi(2-\nu)}{8}\frac{\mu p_0}{G} \tag{4.17}$$

The slip amplitude is now linear with the radii of the sphere.

Another theory suggests that the slip amplitude of two surfaces in contact is better predicted as a relationship to the forces imposed on them. Nishioka and Hirakawa [53] derive a relationship between the slip amplitude, S, and the tangential force coefficient, ϕ, as shown in Equation (4.18).

$$S = -k\log_e(1-\phi) = -k\log_e\left[1-\left(\frac{T}{\mu P}\right)\right] \tag{4.18}$$

where

k = Material and surface constant,

ϕ = Tangential force coefficient,

T = Tangential force,

μ = Coefficient of friction, and

P = Contact Force.

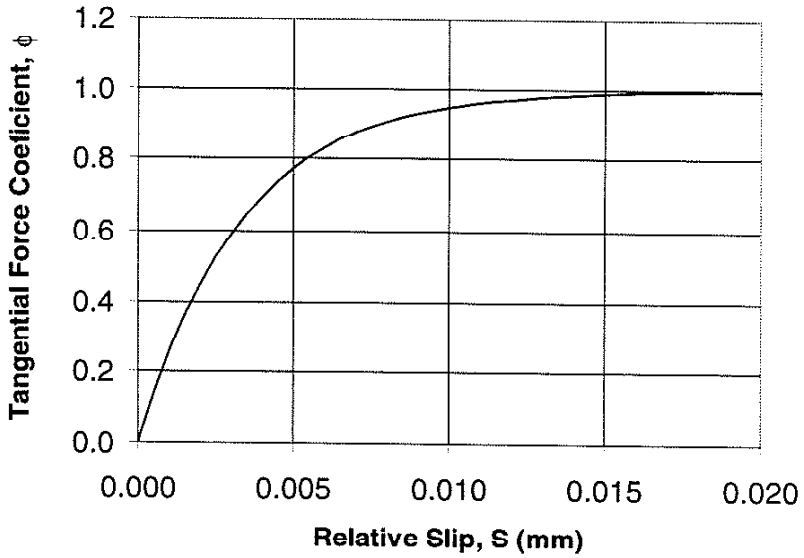

Figure 4.14: Tangential force coefficient and slip distance.

As shown in Figure 4.14, as the force coefficient, ϕ, approaches zero, so does the slip amplitude. In the case of splined couplings, the tangential force coefficient approaches 1, predicting the slip amplitude to be quite large, as expected. This suggests that with larger displacements, the most damaging zone of 7 to 26 micrometers may not be seen. Because of its predicted effect, however, it should not be ignored.

4. Material

In fretting fatigue, the material has a significant effect, as discussed in the damage threshold theory. Welding is more likely when the two materials in contact are identical

[66]. Similar materials, unprotected stainless, aluminum, and titanium should all be avoided [67].

In fretting fatigue, Hoeppner [67] claims the harder the material the better. Waterhouse and Taylor [74], however, observed that very hard surfaces, which do not produce fretting wear, can still produce fretting fatigue due to the stress concentration between the slip and non-slip regions. If this occurs, fretting fatigue can only be reduced by increasing the amplitude of slip or reducing the coefficient of friction.

H. Reducing Fretting Fatigue

The elimination of fretting fatigue from a design is empirical and dependent on the situation [57]. Methods include plating, material selection, shimming, reduction in the cyclic stresses, and the introduction of residual stresses into the materials.
Crack initiation can be reduced by lowering the coefficient of friction, increasing the fatigue strength of the material, or reducing the slip [53].

I. Summary

Fretting can reduce the fatigue strength of a material. Cracks from fretting fatigue can cause pits, debris, or fatigue failure. The cracks are most likely to be produced at the point of maximum adhesion. Once a crack grows into the material, it may become nonpropagating. Nishioka and Hirakawa have developed regions of stress and slipping distance which predict the evolution and result of cracks. Newell and Hills, along with Szolwinski, developed separate models to predict the effective stress due to the tangential forces. Nishioka and Hirakawa related the reduction in the fatigue strength to the slip amplitude. It is claimed that slip amplitudes of 7 to 26 micrometers produces fatigue strengths of 20% of the original strength. The concept of a damage threshold exists which is related to a cycle and pressure threshold.

V. Fretting Maps

As demonstrated in previous chapters, the various models that have been developed to explain fretting are at times conflicting. With time, it is likely that scholars will come to agreement regarding prediction models, and the phenomena will no longer be a mystery. As with most phenomena, there is a somewhat common chain of events by which it can proceed from an initial discovery to a widespread accepted practice or standard.

The development of plastics is a good example of this. Initially, the first plastic material was just a discovery. It was then considered for use in applications and markets. In attempts to find the limitations of the materials, more plastics were developed without specific needs. Classifications were created for the different types. Standards were made for their testing and to accommodate their special properties. Eventually, standard plastics were identified for specific applications. And today there are hybrid-engineered plastics with specific properties. Slowly plastics have moved from the realm of the unknown to the engineered.

As for fretting, the discovery of the existence has been made, many theories developed, and some classifications of the types of fretting have been identified. Now, the evolution of a model to predict fretting has reached the point where standards are being considered for the collection of information. There is a long way to go before the true impact of design changes will be known. Some of the standards existing today for wear testing are: ASTM G83-90, *Wear Testing With Cross Cylinder Apparatus*; ASTM G 99-90, *Wear Testing of Materials During Sliding With Pin-on-disk Apparatus*; and ASTM G 98-91, *Galling Resistance of Materials* [92].

With specific regard to fretting, a methodology which is in the infant stages on the way to becoming a standard is the evaluation of fretting by fretting maps. Vingsbo and Soderberg first published their idea of fretting maps in 1988 [49]. A fretting map is simply a graph involving the relationship of two variables and the indication of the three

regimes of fretting. It may also include the critical values where one regime changes to another.

The three regimes are sticking, mixed stick-slip, and gross slip. The stick regime is characterized by minimum surface damage by oxidation, limited wear, and no fatigue cracks at up to one million cycles of life. The stick-slip regime has low wear and oxidation effects, but there can be fretting fatigue. The last regime, gross slip, has severe wear whose damage is assisted by oxidation. Crack formation is limited in the gross slip region [49, 93].

The distinction of the three regimes is easily interpreted from the plot of tangential force versus displacement during the cycle. If, as shown in Figure 5.1 (a), the hysteresis loop is tight, the model is in the stick regime. If the hysteresis loop resembles that of Figure 5.1 (b), with a consistent tangential force limit, the regime is stick-slip. Figure 5.1 (c) depicts gross slip where the coefficient of friction changes from static to dynamic [49].

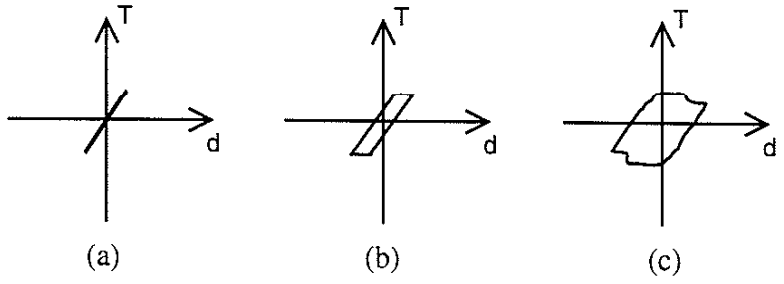

Figure 5.1: Tangential force versus displacement.

Figures 5.2 through 5.7 [49] reflect typical fretting map information. The last two also provide information about the fatigue life. Generally, the movement from the stick regime into the stick-slip regime is a gradual one. The movement into the gross slip regime, however, is typically more sharply defined.

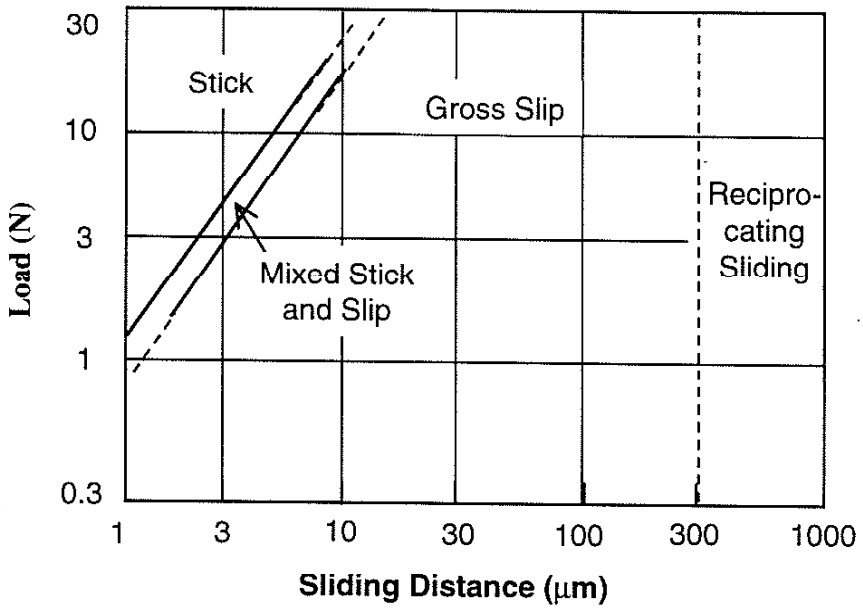

Figure 5.2: Load versus displacement.

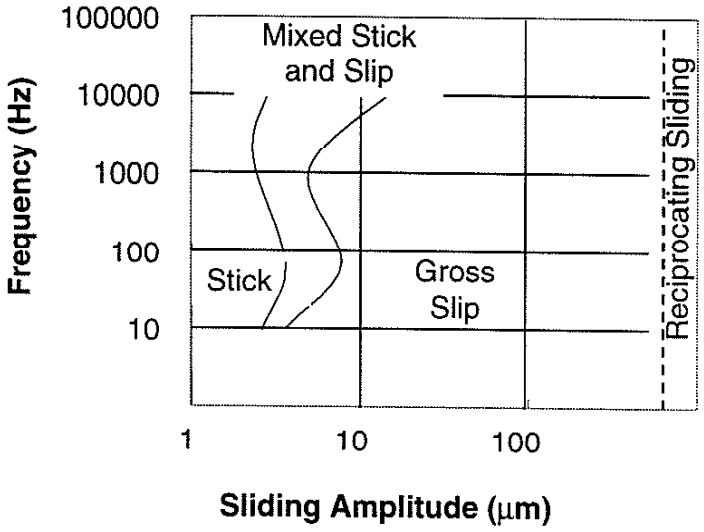

Figure 5.3: Frequency versus displacement.

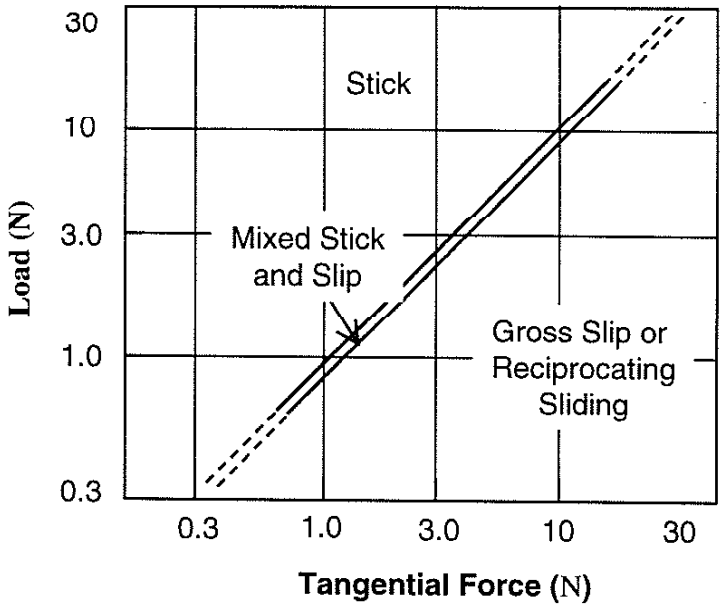

Figure 5.4: Load versus tangential force.

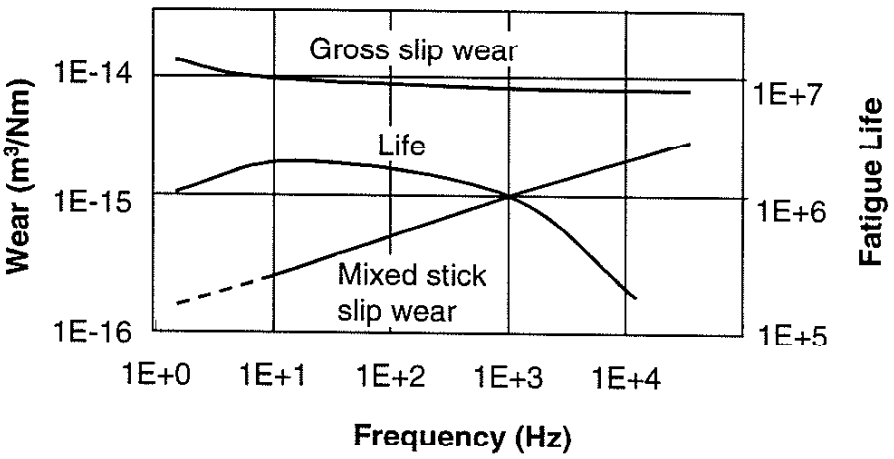

Figure 5.5: Wear and life versus frequency.

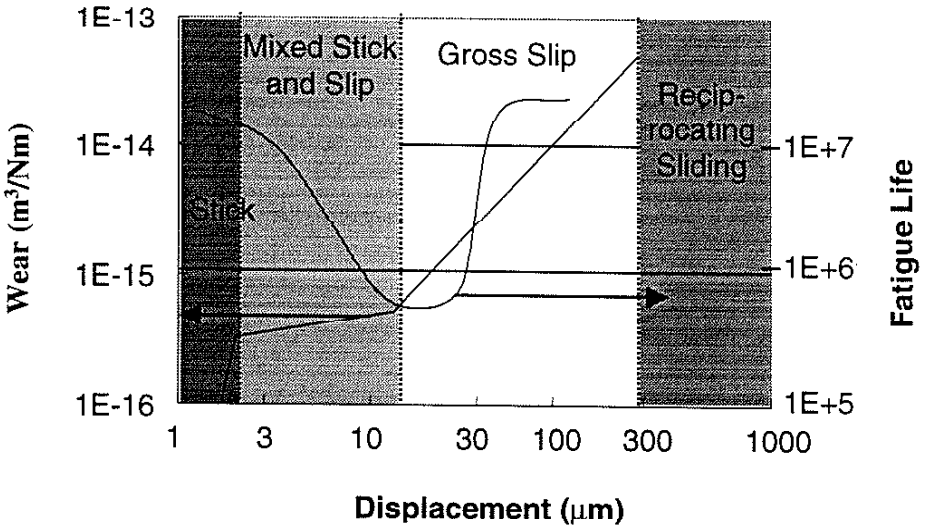

Figure 5.6: Wear and life versus slip amplitude.

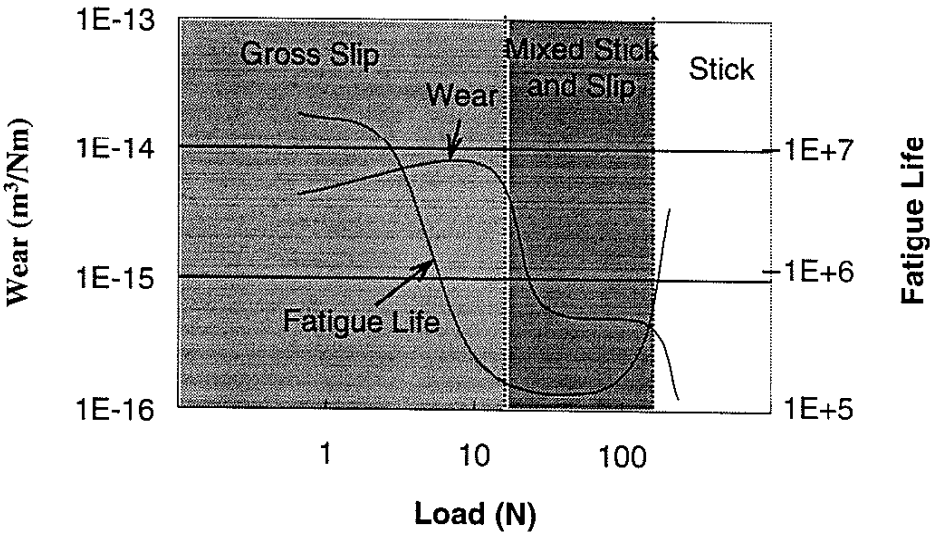

Figure 5.7: Wear and life versus load.

In the stick-slip regime, there are high cyclic stresses at the boundary between the stick and slip zones. This promotes contact fatigue and increases bulk fretting fatigue. The transition from the stick regime can be as low as 1 micrometer (.00004 inches), and the transition into the gross slip regime can be at slip amplitudes of 150 to 300 micrometers (.006 to .012 inches) [49].

Vingsbo and Soderberg have evaluated the work of several others for the transition amplitudes for different materials and applications. For example, a .33 weight percent carbon steel was tested by Nishioka and Hirakawa [45]. The material, as a cylinder on a flat, was subjected to 34 Newtons of force at 19 hertz. The transition points were 5 micrometers (.0002 inches) from the stick regime and 10 to 20 micrometers (.0004 to .0008 inches) into the gross slip regime [49].

While the fretting maps proposed by Vingsbo and Soderberg help to set a standard for evaluation, they might be improved to enhance usefulness. In the case of Figures 5.6 and 5.7, the ordinates remain identical while the abscissas change. While the displacement in

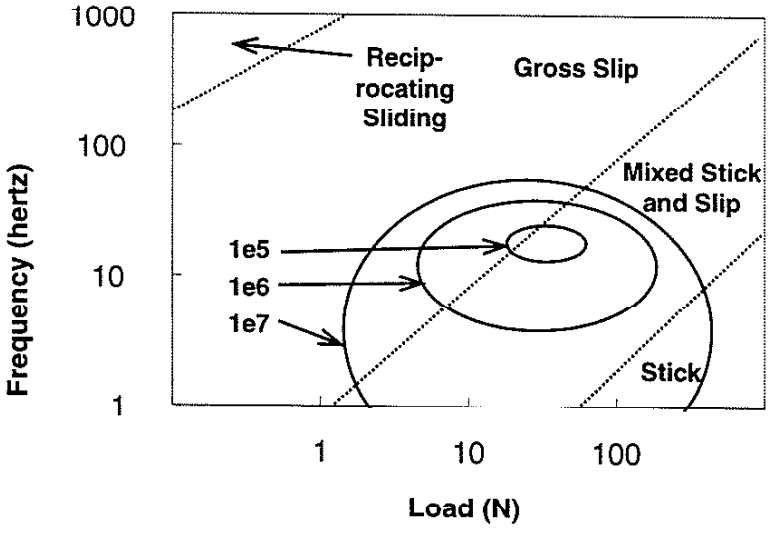

Figure 5.8: Three dimensional map of fretting life.

Figure 5.6 changed, the load must have been fixed, and visa versa for Figure 5.7. An suggestion would be to create each map at various displacements and loads. Then findings could be interpolated between them to form a three-dimensional map. This map could then be used to evaluate any displacement and force combination. Examples of such 3-D maps are shown in Figures 5.8 and 5.9.

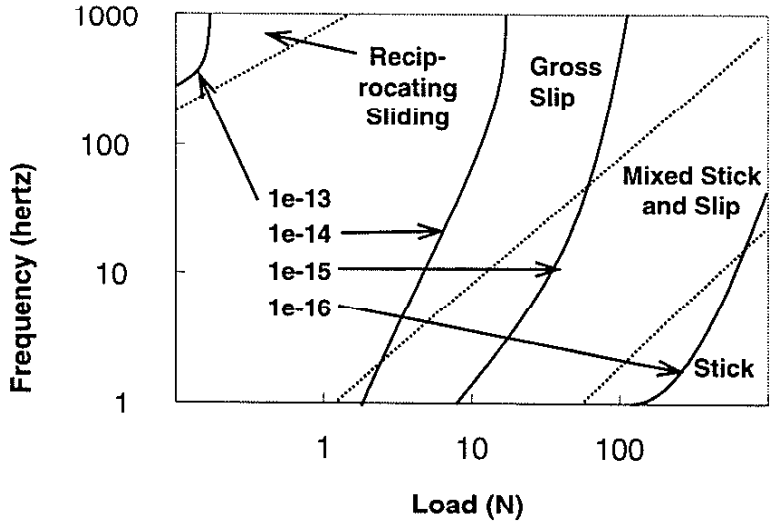

Figure 5.9: Three dimensional map of wear.

Clearly, fretting maps can be quite useful in the standardization and evaluation of fretting phenomena. Perhaps the identification of the critical transition points into the three regimes will become the standard for classification of fretting resistance.

VI. Wear

When the slip amplitude is over 300 micrometers (.012 inches), the removal of material from the mating surfaces is best analyzed using reciprocating wear models. Just as in the evaluation of fretting, reciprocating wear is a complex phenomenon involving many variables. Because of the number of parameters involved, there is not a single wear model for all applications [94]. Scoring, a common surface conditions in gears, is the result of higher speeds and loads, and is a severe form of adhesive wear. In 1953, Archard developed an adhesion theory model, which is the most widely used and which serves as a point of comparison for other theories [71].

A. Archard's Adhesion Theory

Archard's [95] adhesion theory relates the wear volume to sliding distance, normal loads, and hardness. His premise is that wear is proportional to the load divided by the contact area. This is true if the flow pressure of the material and the probability of a contact producing a wear particle are constant. Therefore, the wear rate is not a function of sliding speed.

Archard [95] begins his theory with a study of the contact area's relationship to the load as shown in Equation (6.1).

$$A = kP^n \tag{6.1}$$

where

P = Load,
k = Constant, and
n = Constant based on deformation type.

The value of k is a constant based on conditions, whereas n is a function of the type of deformation and the nature of the contact resistance. The value of n must be less than 1,

and is 4/5 for elastic contact with multiple areas of contact. For just a single area of contact, n drops to 2/3.

Bowden and Tabor [60] also predict the number and size of contacts made between two steel plates as presented in the Figure 6.1. The resulting n from this analysis is about .75.

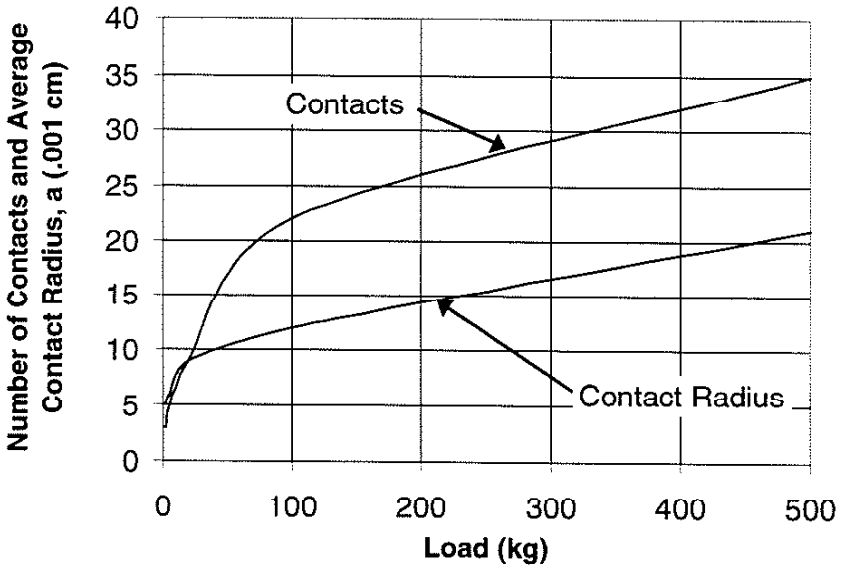

Figure 6.1: Flat plate contacts versus load.

Notice that the contact area is not proportional to the load. Therefore the wear rate needs to be related to both the load and area.

Archard's wear theory is based on four assumptions: (1) Asperities are only on one surface and are spherical with equal radii. They also have an even depth distribution. (2) Once the sliding distance moves from zero, the contact area reduces and moves towards zero as the sliding distance approaches the contact width. Therefore only the initial area of contact is included in the evaluation. (3) The depth to which material is worn away is constant. (4) Even with different materials under different conditions, the probability of wear remains constant.

Archard's prediction of wear rate, W, is presented in Equation (6.2) [95]:

$$W = KE\left[P/C\right]^{\left[(1+q)/(1+p)\right]} \tag{6.2}$$

where

K = Probability factor for the combination of materials over a range of conditions,

E = [M/(1+q)]e,

M = Number of asperities per unit of depth,

q = .5, layer removal,

= 1.0, lump removal,

$e = .5R^{1/2}\beta$, layer removal,

$= R\gamma$, lump removal,

β, γ = Constants,

R = Asperity radii of curvature,

P = Load,

p = 1, plastic deformation, and

= 3/2, elastic deformation,

If hemispherical wear particles having the same contact area and radius were assumed, the wear rate reduces to Equation (6.3).

$$W = \frac{KP}{3a} \tag{6.3}$$

where

K = Constant and

a = Radius of contact area.

Here the wear rate becomes a simple function of the pressure and contact area.

In 1956, Archard [96] revised his wear model so that it could incorporate the material hardness. He proposed a nondimensional wear coefficient, k, as given in Equation (6.4).

$$k = \frac{3PV}{LX} \tag{6.4}$$

where

P = Indentation hardness of the softer material,

V = Volume of material lost,

L = Load. and

X = Total sliding distance.

The resulting wear coefficients for various materials and conditions have been found as listed in Table 6.1.

Author	Material	Frequency (Hz)	Amplitude (μm)	Wear Coefficient, k ($x10^{-3}$)
Feng-Rightmire [42]	Mild steel SAE 1018	1.3	45	.110
Feng-Uhlig [97]	Mild Steel SAE 1018	1-50	10-227	.115-.125
Charney [98]	Silver	1.0	12-200	.007-.18
Halliday-Hirst [33]	Mild Steel	50-200	20-300	.1-.00004
McDowell [99]	Hardened Steel SAE 4340	20	90-130	.500
Uhlig [50]	Mild steel SAE 1018	1-50	10-227	.098-.17

Table 6.1: Wear coefficients.

Stowers and Rabinowicz [27] then proposed the model in Equation (6.5) relating the coefficient of friction, f, to Archard's wear coefficient, k.

$$k = Kf^n \tag{6.5}$$

Stowers and Rabinowicz found the constant K to be based on material combinations and to be typically about .0005 [27]. Additionally, the value for n has been found to be about 4. The wear coefficient, k, versus friction coefficient, f, would then look like Figure 6.2 [100, 101]:

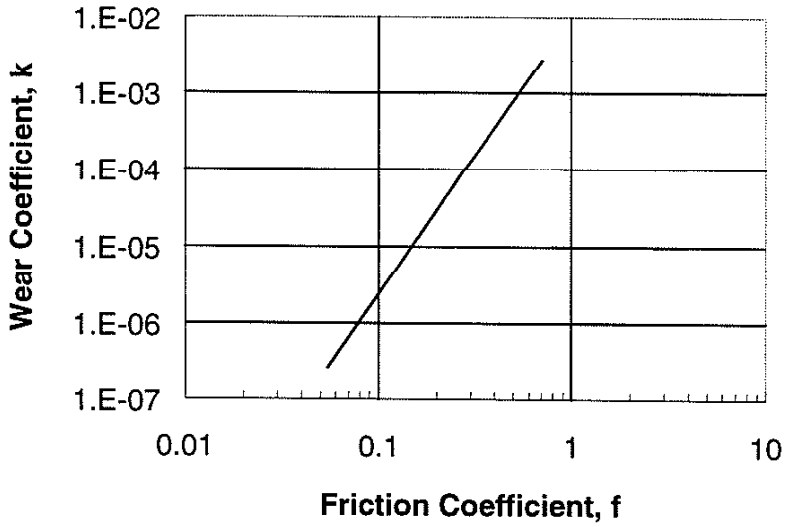

Figure 6.2: Wear coefficient versus coefficient of friction.

This constant K is considered to be a modified Archard's wear coefficient, which can be calculated by Equation (6.6) [27].

$$K = \frac{3PV}{LXf^n} \tag{6.6}$$

The wear rate in volume per unit of sliding distance can now be written as shown in Equation (6.7).

$$\frac{V}{X} = K\frac{Lf^n}{3P} \tag{6.7}$$

Various publications suggest that the wear coefficient, k, changes with slip amplitude. In support of Archard's adhesion theory, Stowers and Rabinowicz [27] have found this is not true for amplitudes as small as 10 micrometers.

B. Simplified Wear Models

There are many forms of engineering equations describing wear, such as Equations (6.8) [94].

$$W = KLS \tag{6.8}$$

$$W = KL(S-S_i)+ S_i \quad \text{(break-in)}$$

$$W = KL^{m\geq 1} S^{n\leq 1}$$

$$W' = KL^{m\geq 1}$$

$$h = KPV$$

$$W = KL^{m>1} N \quad \text{(rolling)}$$

where

W = Wear,

W' = Wear rate,

h = Wear depth,

S = Sliding distance,

L = Load, and

K = Wear Coefficient.

Archard, using his adhesion concepts, created the early sliding wear relationship, W=KL. While this works well in some systems, some claim that the volume of wear is nonlinear with the load, giving rise to a model with load to the power m. The value of m typically ranges from 2 to 3 but has been reported to be over 5 at times. The larger the value of m, the greater the association with a fatigue or stress-dependent mechanism. The addition of sliding distance to the power n accounts for contact area changes such as those that exist when going from a sphere to a flat [94].

The method using the height of wear, h=KPV, is related to plastics and the PV limit. The PV limit is the transition from mild to severe wear. It assumes that the area of contact remains constant. For non-lubricated systems, particularly plastics, a sliding temperature criteria usually dictates the PV limit [94].

For abrasive wear, the wear is evaluated as the product of load, distance, and a constant. The constant, K, is proportional to the hardness, H, to the m power. If the abrasive and the abraded material are the same hardness, m is –10. If the abrasive is harder, m is –1. If it is softer, m is –5 [94].

There exists a zero wear model, which allows the magnitude of the wear depth to reach half the roughness of the courser of the two surfaces. This model has two approaches, one using constant energy and the other, variable energy. The identification of the correct model to use is typically empirical. The constant energy model in Equation (6.9), however, is characteristic of nonlubricated systems which have significant abrasive wear.

$$dQ = CdN \tag{6.9}$$

where

Q = Cross sectional area of the wear scar,

C = Empirically determined wear coefficient, and

N = Number of passes.

C. Severe Wear

In mild wear, there is the relatively slow removal of material from the tops of the highest asperities. The lower material on the surface does not distort significantly. An oxide layer builds on the sliding surfaces. The debris contains oxidized particles as well [102].

Archard [59] identifies mild wear as when the surfaces remain smooth and are usually protected by a surface oxide layer. This usually occurs at low speed, load and temperature. All of these conditions allow for the oxide layer to be developed. When severe wear occurs, the wear rate increases by as much as two orders of magnitude over mild wear. Severe wear occurs between two transition loads as shown in Figure 6.3. The

maximum particle sizes suddenly increase and become metallic at the transition load [102].

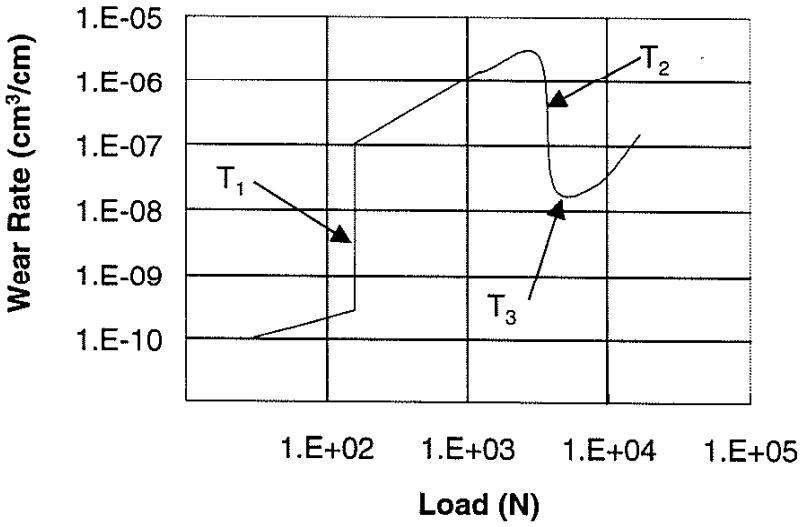

Figure 6.3: Severe wear.

Severe wear can be affected by the hardness of the material. In the case of steel, increasing hardness raises T1 and lowers T2 and T3. There is a hardness level where T1 and T2 merge and severe wear is eliminated [102].

The wear rate in severe wear is linear with time, sliding distance and load. Mild wear, however, has two distinct linear functions of time or distance, as shown in Figure 6.4 [102].

The appearance of the wear surfaces and their debris can be an indicator of the type of wear that is taking place. In the early stages of mild wear, the wear tracks, as well as the metallic debris, are bright. After some time, the tracks and the debris become dark due to oxidation. It is the production of oxides that cause mild wear to occur. Mild wear is also dependent on the production of hard transformation products that reduce surface damage. These help the oxide layer to stay intact [102].

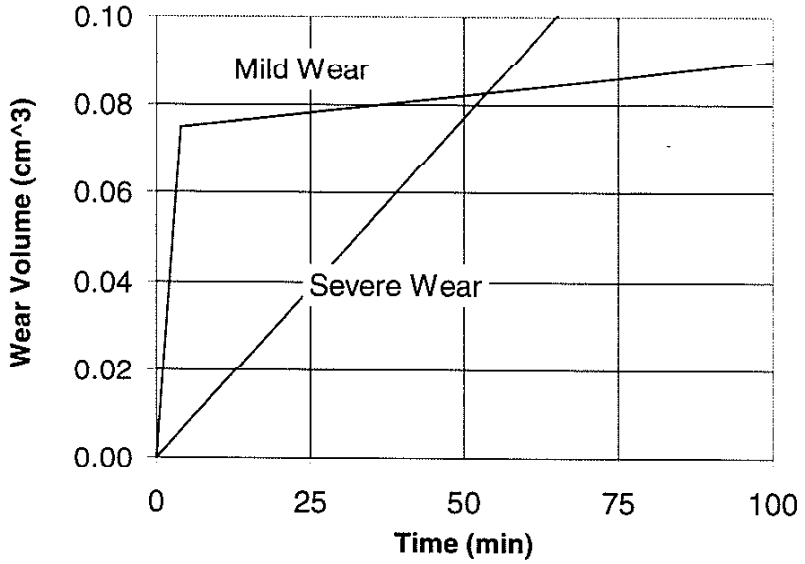

Figure 6.4: Mild and severe wear volume.

Sometimes gears are run-in before large loads are imposed in order to build the oxide film up to a sufficient thickness. The layer beneath the oxide film must, however, be of sufficient strength. Otherwise it will deform and allow gross material removal. Severe wear can only occur if the oxide film is removed and the core material is sufficiently soft [102].

Although not characterized as severe wear, another form of gross material removal is plowing. Plowing, abrasion scoring or scratching, occurs when a very hard, rough surface contacts a softer one. The asperities on the hard surface wear the softer one [18]. Another type of plowing is when sharp hard particles are caught in the surface. They temporarily embed into the softer surface, producing wear on the harder one. The particles that provide plowing wear must be greater than 20 micrometers [18].

D. The Delamination Theory

Suh [103] is critical of Archard, claiming that he completely ignores the physical metallurgy and physics of the metal deformation. Suh contends that in Archard's

mathematical derivation, the assumptions are arbitrary and unreasonable and that the theory does not provide any insight into the wear of metals in different conditions.

Suh [103] proposes the delamination theory for predicting wear as opposed to Archard's adhesion theory. It is based on how the dislocations at the surface behave, as well as sub-surface cracks, voids, joining of cracks, and the shear deformation of the surface. It predicts that the surface undergoes large plastic deformation, producing flat thin sheets.

1. Voids and Particles

In the delamination theory, void formation is one of the most important mechanisms. Voids are created by the formation of cracks around hard particles. In most common grade metals, hard particles such as oxides, borides, carbides and nitrides are common. When the hard particles are at low fractions, the formations of major voids are as if there were no hard particles at all. If the shear deformation is small, many cracks must form before a particle becomes loose. And, unless there is sufficient shear deformation in a given direction, wear particles may not form unless additional cracks are created. Suh [103] says this might explain why fretting wear decreases with decreasing displacement amplitude once the displacement is below a critical value. This critical amplitude can be found by observing the spacing of the holes and cracks.

The particles that are formed start out as sheets. With ductile material, they can either remain unchanged or roll into a larger particle. Metals like zinc, lead, and cadmium form larger particles than those produced by less ductile steels, because they also produce thicker sheets to begin with.

2. Material

The wear of a soft metal against a harder one, such as copper against steel, is also explained by the delamination theory. The overall contact stress may be less than the bulk stress for the harder material, but the stress at the asperities may be large enough to produce local dislocations. As these dislocations accumulate at the hard particles, a crack forms in the harder material. The nucleation rate of the crack is slow, because the

cohesive strength and friction stresses are both high and the plastic shear deformations are quite small at the surface. Therefore, before the particle can become loose, many cracks must form. This explains why a hard material has a much lower wear rate than a soft material [103].

In copper, the cracks grow more perpendicular to the surface than in steel, as the majority of the voids, or cracks, created are around the hard particles. The voids eventually elongate by large shear deformations, and then join to form a wear sheet. The thickness of this sheet for steel is between 2 and 5 micrometers. The steel particles produced are between 1 and 2 micrometers, whereas bronze particles are about 5 micrometers. Close examination of the particles show that the majority of them are actually thin sheets [103].

For a 3 percent silicon iron material with low dislocation density, the surface layer is about 1/10 of a micrometer thick. That same layer is about 10 to 20 micrometers thick for annealed pure copper. In general, the layer is thicker for face-center cubic materials then body-center cubic materials. This is because in face-center cubic materials, the friction stresses are higher. Some hexagonal close-packed materials like cadmium, zinc, and magnesium are expected to form thin sheets because their c/a ratio (the unit cell height divided by the hexagon's side dimension) is large compared to other hexagonal close-packed materials such as titanium and beryllium [103].

3. Shear Deformation Requirement

Rabinowicz [48] could not find wear particles when sliding gold against gold with a normal load of less than 5 grams. He explained this in terms of the surface energy. Hauser [104] found that because there was no gross plastic deformation on the surface, nickel, cobolt, chromium, 52100 steel, and tungsten produced no wear when slid against graphite-fiber-reinforced epoxy. Metals such as zinc, copper, and 316 stainless steel all have substantial plastic deformation and show wear. This indicates that plastic shear deformation is required to produce appreciable wear.

4. Wear Prediction

Suh [103] used the previous observations and some assumptions for his wear prediction. The first assumption is that metals wear layer by layer. The number of sheets per layer is assumed to be proportional to the average number of asperities in contact. Lastly, the void and crack nucleation rate as well as the shear deformation is expressed in the critical sliding distance. Equations (6.10) and (6.11) best describe the delamination theory of wear.

$$W = \kappa LS \tag{6.10}$$

$$\kappa = \frac{b}{4\pi}\left[\frac{K_1 G_1}{\sigma_{f1} S_{01}(1-\nu_1)} + \frac{K_2 G_2}{\sigma_{f2} S_{02}(1-\nu_2)}\right] \tag{6.11}$$

where

W = Wear rate,

L = Load,

S = Sliding distance,

b = Burgers vector,

K_I = Surface topology constants,

G_I = Shear modulus,

σ_{fi} = Friction stress,

S_{0I} = Critical sliding distance, and

ν_I = Poisson's ratio.

This equation is quite similar to Archard's equation for wear, except it does not directly depend on hardness. It does, however, elaborate on the constant κ, which includes material properties and surface finish.

One conclusion of the delamination theory is that when the slip amplitude is less than a critical value, the wear coefficient is a function of the amplitude [103].

The delamination theory explains many wear phenomena that are experimentally observed. It suggests that adhesive, fretting and fatigue wear are produced by the same mechanisms. If the shear deformation of the surface layer is prevented, the wear rate is significantly reduced. Finally, the inclusion of excessively hard particles in metals can accelerate the wear [103].

E. Coefficient of Friction Model

In many of the theories presented, the coefficient of friction is an integral part of the wear model. Contrary to the adhesion theory of friction, this newer theory, the genesis of friction, by Suh and Sin [105], suggests that the coefficient of friction and its force change with sliding distance and environment. There are three components that cause the coefficient of friction to change; deformation of asperities, plowing of wear particles and hard asperities, and adhesion of the flat portions of the contact surfaces. This theory was developed due to the fact that the more popular adhesion theory often disagrees with experimental data. Wear results obtained experimentally are usually higher than those predicted by the adhesion theory [105].

Adhesion theory says that the asperities of sliding surfaces contact to form weld junctions which end up shearing. The frictional force is a function of the actual area of contact, which is a result of the normal and tangential loads. Adhesion theory has relied on the idea that the actual contact area is larger when some of the junctions are under tensile load, requiring a larger shear force at the interface. This may explain the difference between experimental coefficients of friction and those obtained theoretically using the adhesion theory [105].

1. Observations of the Material

It has been found that when the two contacting materials are identical, the coefficient of friction and wear rates are higher than if a hard stationary material is sliding against a moving soft material. If, however, the moving material is hard and the stationary one soft, the coefficient of friction is nearly the same, and the wear rate is much higher than with the two identical materials [105].

For stationary hard materials and soft moving materials, once the delamination process as discussed in the previous section is complete, the new high spots will be polished to a mirror finish. If the materials are identical or the stationary material is softer, this does not occur, and the surfaces remain rough as a result of plowing [105].

If a hard slider with a high Young's modulus contacts a softer metal with a lower Young's modulus, the dislocations in the softer metal cause its particles to break from the surface. Unless the particles find an obstacle to stop their motion, they are driven into the softer material, causing strain-hardening [103].

2. Observations of the Coefficient of Friction

Experiments have demonstrated that the coefficient of friction is dependent on certain conditions and can change for a given set of materials. For example, the change in coefficient of friction over time will be similar to Figure 6.5.

Figure 6.5 also shows the relative effect of pairing like and different materials. The reason the coefficient of friction decreases for dissimilar pairs of materials is that the two surfaces polish each other. This is more likely to occur when the stationary surface is the harder of the two.

Experiments have also shown that the coefficient of friction decreases when the wear particles are removed form the interface. It then increases until it reaches a steady state value, just as was found in Chapter 4.

In the absence of a significant interfacial temperature rise, the coefficient of friction effects the mechanical properties of the material more than the chemical properties. When the interface is lubricated, the time scale of the friction coefficient response extends itself so much that the total time in service for the well-lubricated surface may be equivalent to the early stages of dry sliding [105].

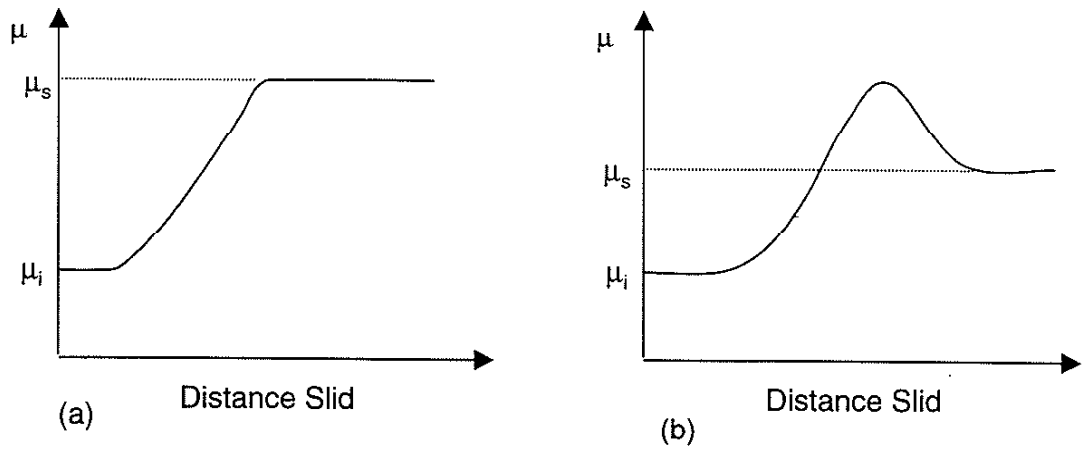

Figure 6.5: Coefficient of friction versus distance: (a) similar materials; (b) hard slider, soft specimen.

Even for materials that are chemically identical, the coefficient of friction can vary by as much as .2, depending on which member is moving. With or without a lubricant, the initial kinetic coefficient of friction is typically between .12 and .17, but it can be .1 to .2 for steel on steel and brass on steel [106, 107]. Suh and Sin [105], also claim that, regardless of material or the presence of a lubricant, the initial coefficient of friction between two surfaces is always about .1 to .2. Their final observation of the coefficient of friction is that if the mating surfaces are well polished, plowing grooves are formed from the very beginning of friction testing.

Suh and Sin theorize that the static coefficient of friction is determined by asperity deformation. Since asperities form continuously, they affect the dynamic coefficient of friction as well. Because their deformation occurs rapidly, their contribution, however, is small compared to that of plowing and adhesion.

3. The Theory of Friction

The postulate of the genesis of friction between sliding surfaces is that the coefficient of friction between sliding surfaces is a result of: (1) Asperity deformation; (2) Plowing by wear particles and hard surface asperities; and (3) Adhesion of flat surfaces. The relative impact of each of these phenomenon to the coefficient of friction depends on the

condition of the mating interface, materials, history of sliding, surface topography, and the environment.

Referring to Figure 6.6, the time-dependent behavior of friction according to the theory can be explained.

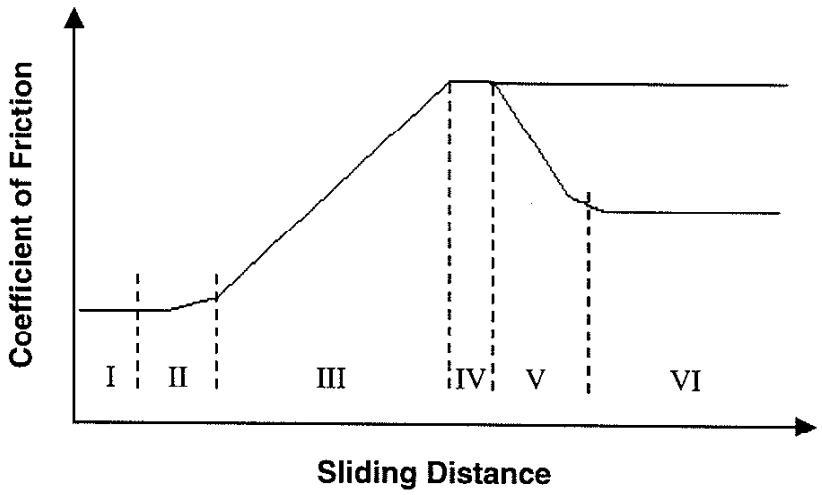

Figure 6.6: Six stages of the frictional force.

In the first stage, the coefficient of friction appears to be governed by plowing from asperities. Because the surface is contaminated, adhesion does not play a major role. Once sliding begins, the asperities deform, affecting the static coefficient of friction. This, however, is not the major contributor to the coefficient of friction, as the surfaces are easily polished. At this stage, the coefficient of friction is fairly independent of material combinations, surface, and environmental conditions.

There is an increase in the coefficient of friction in the second stage due to the onset of adhesion. The slope of stage two becomes steeper if the wear particles are trapped between the surfaces, promoting plowing. If the system is lubricated, stage two may never be reached.

The third stage has an even steeper increase in its slope. This is caused by the increase in the number of wear particles caught between the surfaces from the first two stages. Again, these particles can cause plowing. If the materials are of nearly equal hardness, the plowing will be greater because the wear particles will penetrate both surfaces. Since the newly formed surface is also clean, there can be an increase in adhesion. And as long as asperities are present, they continue to contribute to the coefficient of friction as well.

The fourth stage is established when the number of entrapped wear particles as well as the amount of adhesion reaches a steady state. Because in most cases the frequency of new asperity generation is low, asperity deformation becomes less significant than plowing. If the two metals are identical, the coefficient of friction in stage four is the same through steady state. When the hard surface is moving, the harder surface remains rough. There are no changes in stages five and six.

When the stationary member is harder, its asperities are slowly removed in stage five, producing a mirror finish. The coefficient of friction then decreases as plowing and adhesion decrease. When stage six is reached, the softer material aquires the same mirror finish as the harder material. At this point, however, there are always "pot-holes" from the delamination of wear particles [105].

4. Asperity Deformation Coefficient

The contribution of asperity deformation to the static coefficient of friction is significant, but not in stage one. This is due to the fact that, once the asperities deform, interaction between them cannot take place. If new asperities, however, are generated during steady state wear, they can also contribute to the coefficient of friction. The asperity deformation is determined through slip line field analysis. It is a function of the leading and lagging surface angles of the asperity with relation to the sliding direction. Once the surface angles of the asperity are known, the coefficient of friction, μ_d, can be determined, from Figure 6.7.

The coefficient of friction due to asperity deformation is usually between .43 and .75 for asperities with slopes between 4° and 20°.

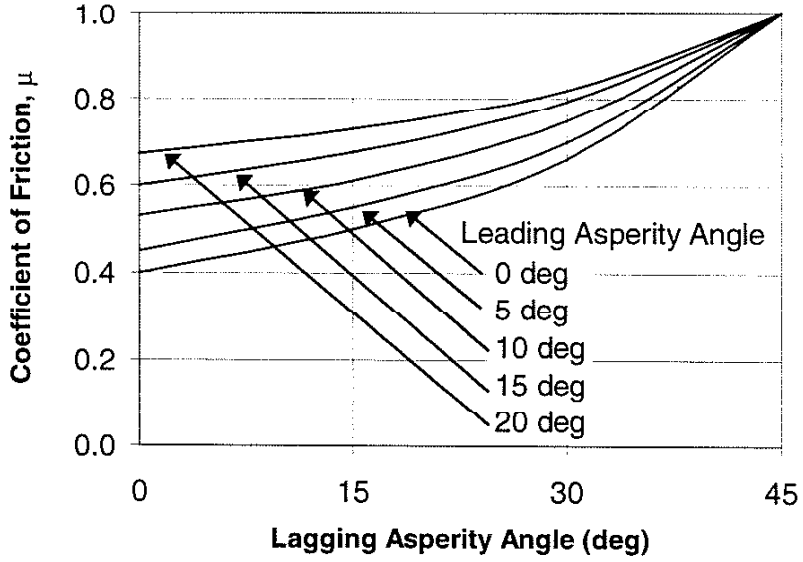

Figure 6.7: Asperity deformation coefficient of friction.

5. Adhesion Coefficient

Experimentally, the contribution from adhesion has been shown to be negligible at the beginning of sliding. This is thought to be due to contaminants on the surface. Challen and Oxley [108] have developed Equation (6.12) and (6.13) for the coefficient of friction due to adhesion, μ_a.

$$\mu_a = \frac{A\sin\alpha + \cos(\cos^{-1} f - \alpha)}{A\cos\alpha + \sin(\cos^{-1} f - \alpha)} \tag{6.12}$$

$$A = 1 + \frac{\pi}{2} + \cos^{-1} f - 2\alpha - 2\sin^{-1}\left[\frac{\sin\alpha}{(1-f)^{1/2}}\right] \tag{6.13}$$

where

α = Asperity angle and

f = Strength of adhesion.

The strength of adhesion, or interfacial film strength, is the ratio of the film strength to the flow stress acting parallel to the slip line of the softer material.

As the strength of adhesion varies from 0 to 1, the adhesion coefficient of friction changes from 0 to .39. Experiments were conducted with hard AISI 1095 steel as the slider against soft Armco iron. This produced a steady-state coefficient of friction of .51. Both surfaces were polished smooth, indicating that the primary contributor was adhesion [105].

The adhesion coefficient, which theoretically reaches a maximum of .4, depends on the interaction of the two surfaces. This value is lower for well-lubricated surfaces and higher for identical metals that do not have surface contaminants or oxide layers.

6. Plowing Coefficient

Plowing occurs whenever particles are trapped between the two surfaces or when asperities themselves cause plowing. The plowing coefficient of friction can be a result of hard asperities or wear particles. When two surfaces of equal hardness are involved, the particle can penetrate both. As the surfaces move, grooves can then be produced in one or both surfaces. If one surface is quite hard and smooth, little damage will occur as the particle will slide along the surface. If, however, the hard surface is rough, the wear particles will tend to stay in the grooves of the rough surface and plow the softer material.

Sin et al. [109] determined the contribution of plowing to the coefficient of friction, μ_p, as Equation (6.14).

$$\mu_p = \frac{2}{\pi}\left[\left(\frac{2r}{w}\right)^2 \sin^{-1}\left(\frac{w}{2r}\right) - \left\{\left(\frac{2r}{w}\right)^2 - 1\right\}^{1/2}\right] \qquad (6.14)$$

where

r = Particle radius and

w = Width of penetration.

By measuring a worn specimen, the w/r ratio was found to be about .8. This ratio produces a coefficient of friction due to plowing of .2. In tests with Armco iron against Armco iron and Armco iron against AISI 1095, the plowing coefficients of friction were .31 and .16 respectively [105].

Theory holds that the plowing contribution can be from 0 to 1, but it is typically less than .4. This value is higher for identical metals with deeply penetrating wear particles and lower when wear particles are absent or a soft material is slid against a hard surface with a mirror finish [105].

7. Contributions to the Total Coefficient of Friction

The relative contributions of the three coefficients of friction are difficult to determine. The coefficients for both asperity deformation and adhesion assumed the total normal load was applied to either the asperities or flat areas. In reality, the loads are apportioned between asperities, adhesion joints and trapped particles [105].

The major points of this theory are that adhesion is not always present and that the asperities sliding over each other also impacts the coefficient of friction. In many cases, wear particles can effect the coefficient of friction more than adhesion. It also demonstrates that the coefficient of friction changes with the time of sliding. And finally, the theory shows that the static coefficient of friction is determined by the asperity deformation and can range from .43 to .75 as the slope of the asperity changes [105].

F. Asperity Deformation Model

The asperity deformation model by Challen and Oxley [110] provides coefficients of friction and wear rates that are consistent with the two basic laws of friction; that the friction force is proportional to the normal load and independent of area. This model is in contradiction to Archard's adhesion theory, but it is in agreement with experimental data [110]. Part of the basis for this model is that under all conditions, with a constant force, the coefficient of friction increases with increasing roughness. The asperity deformation

model includes three separate models: (1) the rubbing model, (2) the wear model, and (3) the cutting model. These models are all functions of the asperity shape and the interfacial film strength.

The first contribution to the asperity deformation model is the rubbing model. It is the same as the Challen and Oxley [108] model, which was used for the genesis of friction model. This model is applied when the lagging asperity angle to the horizontal is larger than the leading asperity angle but less than 45°. It is also limited to cases where the coefficient of friction is less than 1.

When the coefficient of friction is greater than 1, and the asperity angle is still less than 45°, the wear model should be used. The wear model coefficient of friction, μ, is calculated by Equations (6.15) and (6.16).

$$\mu = \frac{\left\{1 - 2\sin\beta + (1-f^2)^{1/2}\right\}\sin\alpha + f\cos\alpha}{\left\{1 - 2\sin\beta + (1-f^2)^{1/2}\right\}\cos\alpha - f\sin\alpha} \tag{6.15}$$

$$\beta = \alpha - \frac{1}{4}\pi - \frac{1}{2}\cos^{-1} f + \sin^{-1}\frac{\sin\alpha}{(1-f)^{1/2}} \tag{6.16}$$

where

α = Asperity angle and

f = Interfacial film strength or strength of adhesion.

The predicted wear rate for the wear model, W, is found through Equation (6.17).

$$W = \frac{1}{2k}\frac{\sin^2\alpha + \frac{1}{2}\sin 2\alpha}{1 + \sin 2\alpha} \tag{6.17}$$

where

k = Shear flow stress.

The cutting model describes the formation of chips. It applies when the asperity angle is greater than 45 degrees, and the coefficient of friction is greater than 1. It is also a function of the asperity angle and film strength as shown in Equation (6.18).

$$\mu = \tan(\alpha - \frac{1}{4}\pi + \frac{1}{2}\cos^{-1} f) \tag{6.18}$$

And the wear rate is predicted by Equation (6.19).

$$W = \frac{1}{\sqrt{2k}} \frac{\cos(\alpha + \frac{1}{2}\cos^{-1} f)}{\cos\left\{\pi + (\alpha - \frac{1}{4}\pi + \frac{1}{2}\cos^{-1} f)\right\}} \tag{6.19}$$

The results from the three models can then be plotted on one graph. The combined coefficients of friction and wear rates are as shown in Figures 6.8 and 6.9 respectively. In Figures 6.8, 6.9, and 6.10, the are numerous lines. Each are results of the asperity deformation model as the strength of adhesion, f, changes from .1 to .9 in .1 increments.

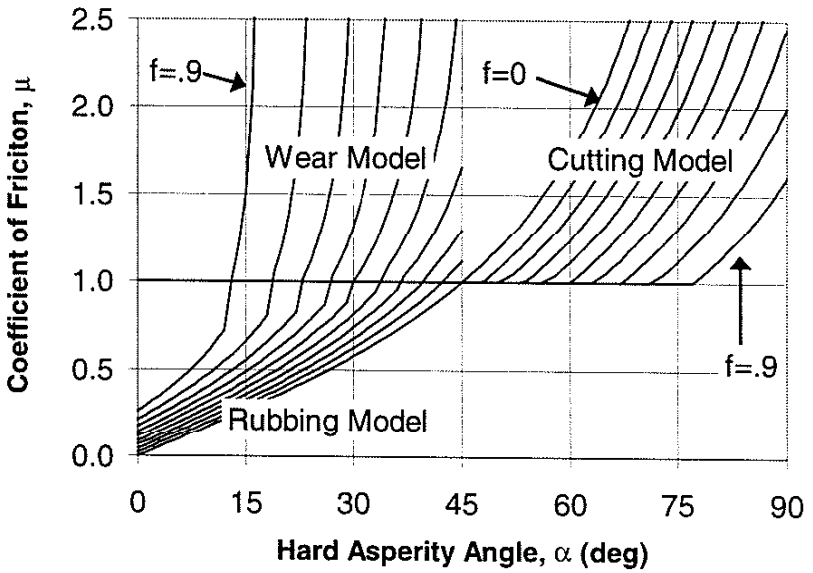

Figure 6.8: Asperity deformation friction model.

If the asperity angle, α, remains constant, and the force decreases, the coefficient of friction increases in the cutting model and decreases in the rubbing and wear models.

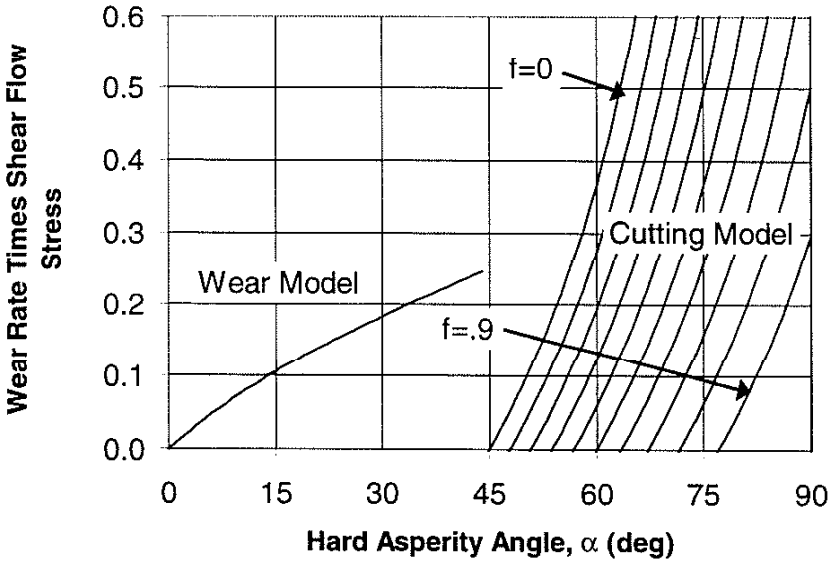

Figure 6.9: Asperity deformation wear model.

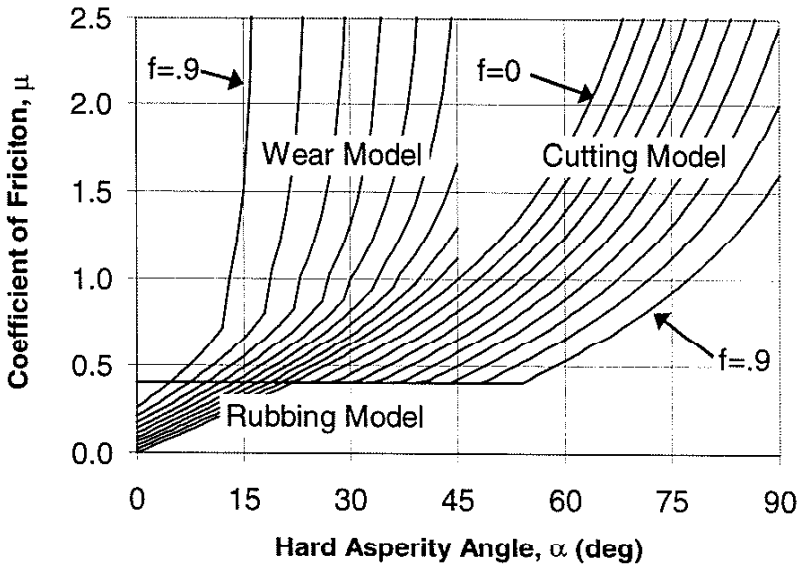

Figure 6.10: Modified asperity deformation friction model.

According to the prediction, before chips can be produced, the asperity angle must be greater than $\pi/4$. Chips have experimentally been produced with a smaller α, and so the graph of the coefficient of friction is modified by reducing the lower limit in the cutting model as shown in Figure 6.10.

This model demonstrates the importance of asperity shape for producing both wear and friction. It also relates the wear and friction to the strength of adhesion.

G. Other Parameters

1. Material

In the fretting process, hardness is important, as hard materials tend to fret less. Buckley [111] suggests that in adhesive wear this may not be true, as indicated by the crystal structure concept. It says that the hexagonal metals have lower adhesive wear characteristics than body or face-centered cubic metals. In an oxidizing environment, the greater the adhesive wear, the greater the fretting. The crystal structure has been shown to affect the adhesive wear one hundred fold. This, as so many other theories, is contrary to the long-standing Archard theory.

Fowle [18] identifies many ways to reduce the wear of gear teeth. He found that materials with more carbon have better wear properties. Tungsten, molybdenum, and white cast irons can increase wear resistance, as well as higher levels of austinite. The presence of chromium and nickel also serve to reduce scuffing. Small concentrations of carbon in iron are quite efficient at reducing adhesion.

Fowle also has a theory that explains stainless steel. He suggests that in low alloy steels, the oxide layer that occurs on high spots can break the exposed bare metal. These oxide fragments cut the oxide film on the mating part, promoting adhesion and wear. In 18/8 austenitic stainless steel, there is a thin brittle oxide layer. This, rather than its austenitic structure, may be why it is difficult to avoid scuffing it [18].

Sulfur can be more effective than oxygen in the reduction of adhesion. When sulfur is used, varying the load does not affect adhesion. The practical application of this, however, is not reasonable. Once a sulfide film is exposed to oxygen, the sulfur is completely displaced, leaving only oxygen on the surface [111].

2. Polymers

The study of polymers and how they wear has been of interest for some time now. Their use as bearings, gears, and other components has increased significantly over the past several years, as they have become engineered materials. Some of the nonlubricated plastics used for bearings include nylon, acetal, tetrafluoroethylene (TFE), polyimide, and phenolics. When nonlubricated rubbing occurs with plastic parts, wear will also occur [112].

The traditional wear rate for plastics is simply the product of pressure, velocity and a constant. This is true, but the surface finish of the metal counterpart must also be taken into account. Hollander and Lancaster [113] found the relationship between the metal's

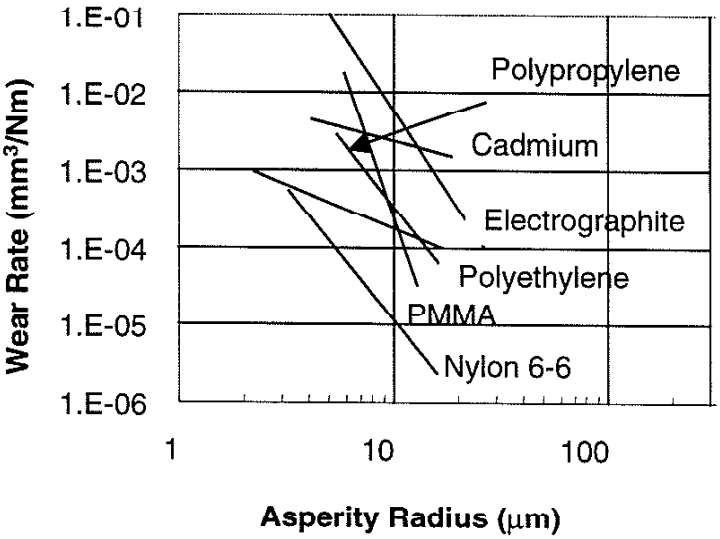

Figure 6.11: Effect of asperity size on wear rate.

asperity size and wear rate for several plastics is shown in Figure 6.11. Note that, depending on the capability to produce a smooth surface, some plastics will give varied results. An example of this is polyethylene. If the manufacturing capability could produce asperities with radii of 5 to 20 micrometers, the wear rate would be .00008 to

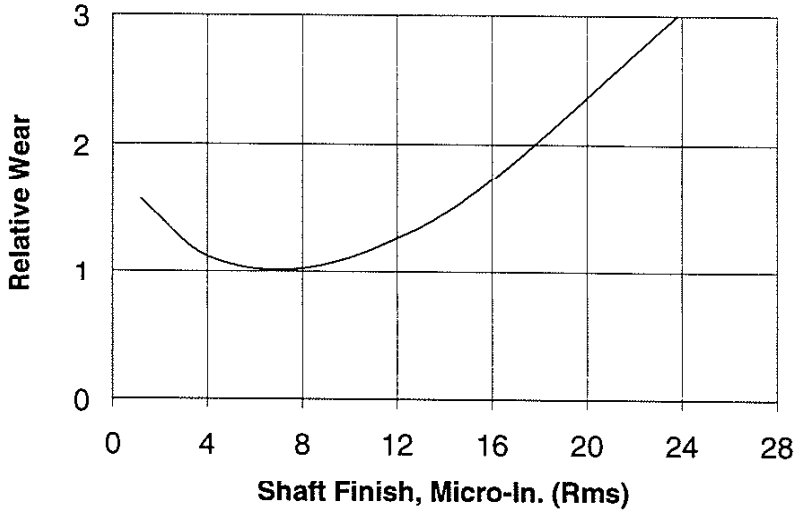

Figure 6.12: Wear versus surface finish.

.0008 mm^3/Nm. PMMA, over the same range of asperity size, will have a wear rate of .00002 to .01 mm^3/Nm. With larger asperities, each material performs almost as well as the other. For smaller asperities, however, the polyethylene is ten times superior to the PMMA. If the asperity size were always larger than 20 micrometers, the PMMA material would always wear less than the polyethylene.

In Figure 6.12, Bower [112] presents the relation of bearing wear with shaft finish for TFE. In this case, notice that the wear increases if the shaft is too smooth. While demonstrated experimentally, the cause for this has not yet been identified.

3. Speed and Load

Although no model exists relating the coefficient of friction to the load, there is a phenomenon where the coefficient of friction has been found to decrease with increasing

load. Earles and Powell [114] have studied this and found the coefficient of friction, μ, to be as calculated by Equation (6.20).

$$\mu \alpha N^{1/2} U \tag{6.20}$$

where

N = Load and

U = Speed.

4. Lubricant

In 1939, Blok [115] predicted that unless the contact temperature exceeds a critical level, scuffing would not occur. This temperature is the most widely used criteria for scuffing in gear applications, but it has been shown that the temperature measured just before scuffing occurs is inconsistent and varies with testing conditions. One interesting observation from this study is that at rolling speeds at least four times greater than the sliding speed, no scuffing occurs [116]. Instead of a critical contact temperature, Bell and Hadley [116] suggested that fractional power intensity be used to evaluate scuffing. The fractional power intensity is the product of the coefficient of friction, the mean Hertzian contact pressure and the sliding speed.

H. Summary

Reciprocating wear is studied at amplitudes over 300 micrometers (.012 inches). There are many theories to predict wear and the coefficient of friction. Archard's wear theory is the most popular relating wear to the load divided by the area. The delamination theory of wear is based on the formation of sheets of wear debris during the wear process. Its prediction is a function of the load, sliding distance, and properties of both materials. The asperity deformation model predicts the wear rate and coefficient of friction by rubbing, wear, and cutting of material. All of these values are a function of the angle of the asperities and the surface strength of adhesion.

Suh and Sin produced a model of the coefficient of friction that involves components for asperity deformation, adhesion, and plowing. They also explain the change in coefficient of friction with time through six stages.

Severe wear is identified as an increase in wear within a load range by as much as two orders of magnitude. Changing the material hardness can effect the occurrence of severe wear.

Wear is also dependent on material for a variety of reasons. Increases in the amount of carbon were found to reduce wear, and materials with hexagonal crystal structures were found to be more effective at resisting adhesion. Finally, the asperity size was found to impact the wear rate of polymers.

Regardless of the mechanism by which wear occurs, an important part of the evaluation of coaxial gear tooth wear is the determination of the stresses on the tooth's surface. Additionally, the sliding amplitude and the product of the contact pressure and velocity of the two surfaces need to be determined to establish the type and quantity of wear.

The Hertzian stresses on the tooth are not easily obtained. Since the two coaxial shafts are not perfectly concentric, all of the spline teeth are not necessarily in contact and do not have the same stress levels. Consider, for example, a set of perfectly rigid coaxial gears with a loose fit, mounted on two shafts with centerlines that are slightly offset, as shown in Figure 7.1. Only one or two pair of teeth would ever make contact with each other at one time.

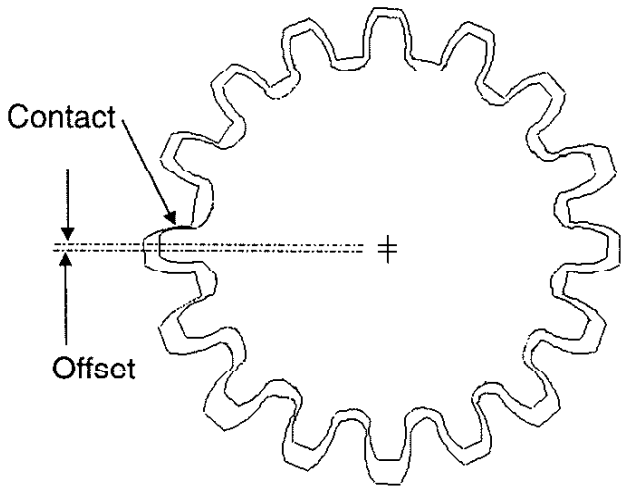

Figure 7.1: Tooth contact.

In actuality, due to tooth bending, more teeth do make contact. For instance, plastic splines have been shown to exhibit better wear properties than rigid steel gears, despite their inferior material properties. It is their ability to deflect that makes them superior.

One rule of thumb which has been used by gear engineers is to design the spline with the assumption that half of the teeth make contact. Whereas this may produce a functional design, it is not based on an understanding of the limits of the gear set and therefore, it is not a good method of predicting their performance. Clearly, depending on the loading and geometry, more teeth may be in contact in one design than another. Additionally, out of those teeth actually making contact, the loads on some will be higher on some than on others.

To obtain a clearer picture that will allow a more accurate prediction of the behavior of the gear set, it is important to understand the nature of the contact stresses. This chapter presents the "coaxial spline model", which was developed during the course of this study in order to better understand and explain coaxial spline interaction. The evaluation of the contact stresses begins with the evaluation of the bending capacity of the tooth itself. It serves to relate the tooth's stiffness to its geometry, as well as to identify the location where a pair of teeth make contact. The remainder of this chapter involves the evaluation of a system of spline teeth. For an internal and external set of splined teeth, the deflections, forces, Hertzian stresses, sliding amplitude, speed, and product of stress and speed product can be calculated for any set of conditions.

A. Tooth Geometry

In order to determine the deflection of the tooth under load, the thickness of the tooth along its entire length must be known. The geometry of a spline tooth is found in the study of involutometry. Equations (7.1) through (7.4) calculate tooth thickness for an external spline at any radius as depicted in Figure 7.2.

$$t(r) = 2r\left(\frac{t_p}{2r_p} + \text{inv}\phi - \text{inv}\varphi\right) \tag{7.1}$$

$$\text{inv}\phi = \tan\phi - \phi \tag{7.2}$$

$$\text{inv}\varphi = \tan\varphi - \varphi \tag{7.3}$$

$$r = \frac{r_b}{\cos\varphi} \tag{7.4}$$

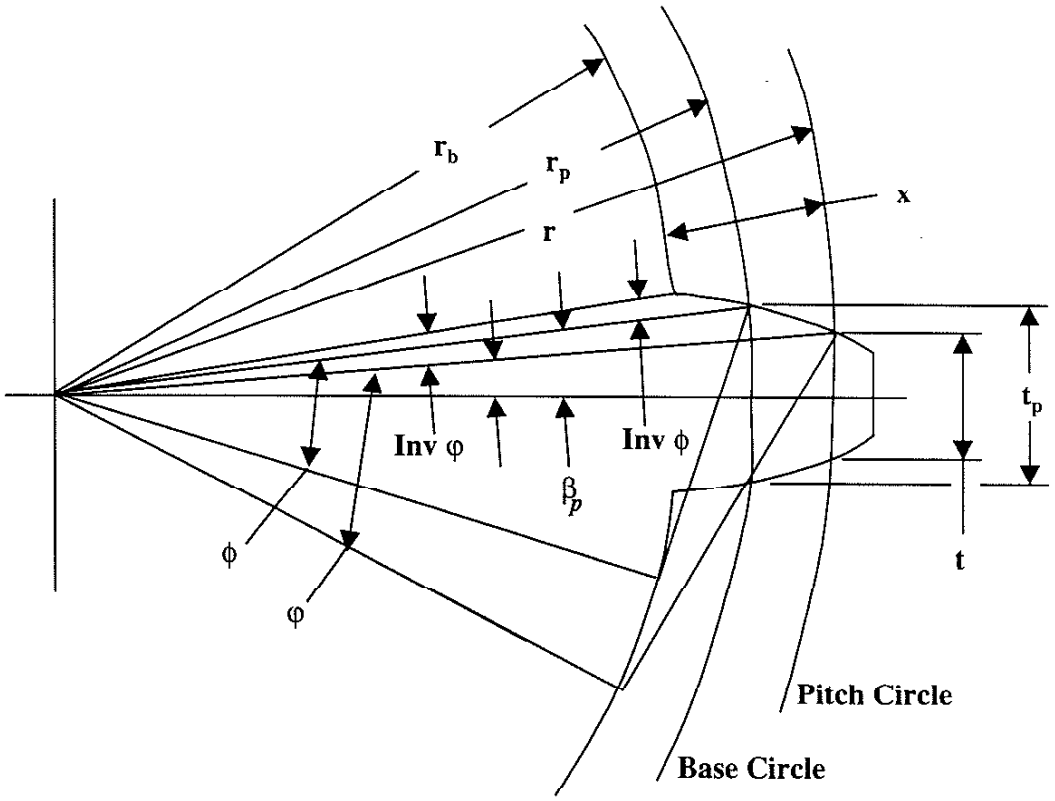

Figure 7.2: Tooth geometry.

Variables in Figure 7.2 are

t = Arc thickness of the tooth,

r = Radius where the thickness is calculated,

t_p = Arc tooth thickness at the pitch circle,

r_p = Radius of the pitch circle,

ϕ = Pressure angle at point r_p,

φ = Pressure angle at point t, and

r_b = Radius of base circle.

If x were defined as the distance from the radius of the base circle, r_b, to the radius of interest, r, the tooth thickness as a function of x reduces to Equation (7.5).

$$t(x) = 2(x + r_b)\left[\frac{t_p}{P_d} + \tan\phi - \phi + \cos^{-1}\left(\frac{r_b}{x + r_b}\right)\right] - \frac{2}{r_b}\sqrt{x^4 + 4x^3 r_b + 5x^2 r_b^2 + 2x r_b^3} \qquad (7.5)$$

where

P_d = Pitch diameter.

Unfortunately, this equation yields the arc thickness of the tooth. In order to determine the area moment of inertia, which is required to calculate the tooth deflection, the cross sectional thickness, t', of the tooth is required, not the arc thickness. The tooth thickness, t', can be determined by taking the sine of the arc angle at r times the radius at r as shown in Equation (7.6) and Figure 7.3.

$$t'(x) = 2r\sin\left(\frac{t(x)}{2r}\right) \qquad (7.6)$$

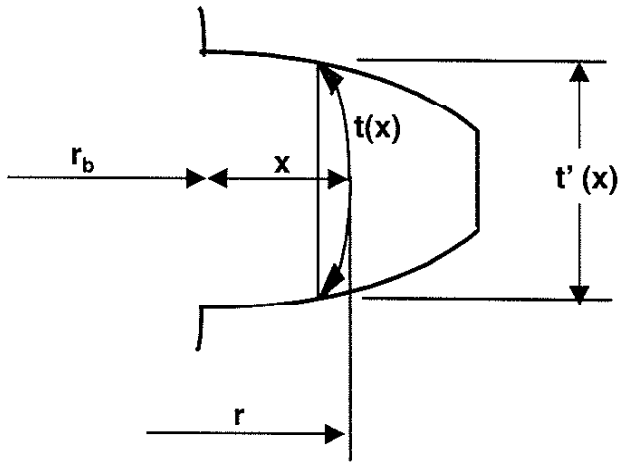

Figure 7.3: Tooth thickness.

This, however, will result in a thickness that is actually at a radius less than r, and it is the tooth thickness at the radius that is desired.

A direct solution is not readily available because the tooth thickness is a complex function of r. The exact value at r may be found by iterative solutions. For the purpose of this evaluation, however, an approximate adjustment to r will be made. The adjustment is equal to the residual of the cosine component to produce r' as calculated in Equation (7.7) and shown in Figure 7.4. The remaining error will then be less than the difference in tooth thickness at r and r'.

$$r' = r\left\{2 - \cos\left(\frac{t}{2r}\right)\right\} \qquad (7.7)$$

For a 25-tooth spline with a pitch of 10 teeth per inch, the adjustment to the tooth's thickness by changing r to r' is a maximum of .004 inches, or 2 percent of the tooth's thickness. To adjust the radius more closely would have a minimal effect on the solution. The arc thickness and normal thickness can be calculated at the new position r' to provide a sufficiently accurate tooth thickness value.

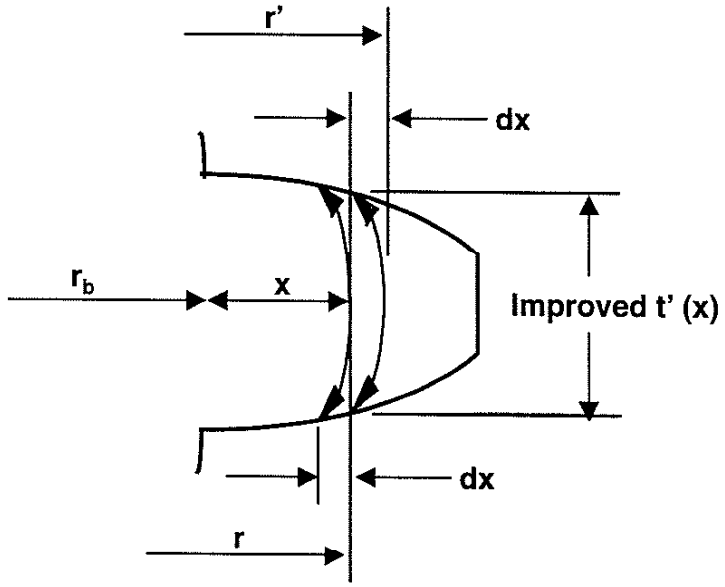

Figure 7.4: Improved tooth thickness.

The previous evaluation is for an external splined tooth. The calculations for an internal tooth are the same, except that its circular tooth thickness, t_p, would be the circular space width at the pitch line. The circular space width, $t_E(x)$, could then be calculated for the external spline, and the internal tooth thickness along the length of the tooth, $t_I(x)$, would become Equation (7.8).

$$t_I(x) = \frac{2\pi}{N}(x + r_b) - t_E(x) \tag{7.8}$$

where

N = Number of teeth.

B. Tooth Bending

The evaluation of the tooth's ability to bend can be made assuming it is a cantilever beam. Using the convention shown in Figure 7.5, the problem is solved by integration of Equation (7.9).

$$\frac{\partial^2 y(x)}{\partial x^2} = \frac{M(x)}{EI(x)} \tag{7.9}$$

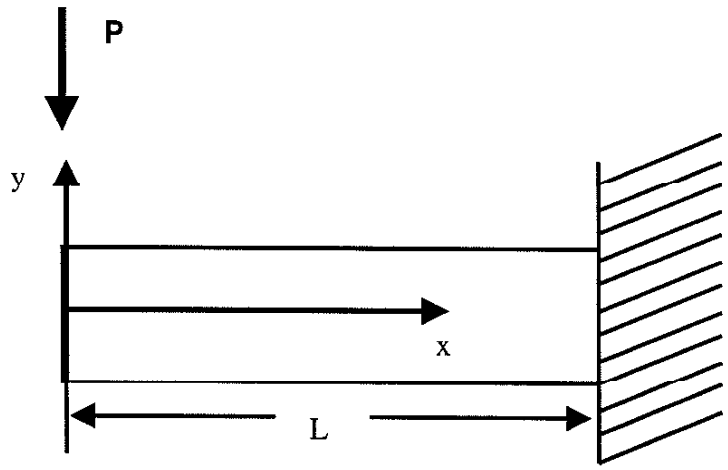

Figure 7.5: Tooth coordinate system for integration.

Equation (7.10) is the area moment of inertia.

$$I(x) = \frac{bt(x)^3}{12} \tag{7.10}$$

where

x = Radial position on tooth,

y(x) = Tooth deflection,

M(x) = Moment created by tooth load,

E = Young's modulus,

I(x) = Area moment of inertia,

b = Tooth width, and

t(x) = Tooth thickness.

By assuming small angles and defining the boundary conditions as zero slope and deflection at the base of the tooth, the problem becomes Equation (7.11).

$$y(x) = \frac{1}{E}\int_0^x\int_0^x \frac{M(x)}{I(x)}dx - \int_0^L \frac{M(x)}{I(x)}dxdx \tag{7.11}$$

Which reduces to Equation (7.12).

$$y(x) = \frac{12}{Eb}\int_0^x\int_0^x \frac{M(x)}{(t(x))^3}dx - \int_0^L \frac{M(x)}{(t(x))^3}dxdx \tag{7.12}$$

Due to the complexity of the tooth thickness equation, the deflection is best solved using numerical integration. In this evaluation, the rectangular rule was used with 100 divisions of the tooth. Now a load can be applied and the moments determined for each location on the tooth. Because the actual loading is unknown at this time, a point load on the tooth will be assumed. The resulting moment diagram and deflection curves are shown in Figures 7.6 and 7.7, respectively, for a 10 pitch, 25 tooth spline.

The same evaluation is then performed for the internal tooth. The only change required is the tooth width and direction of the force.

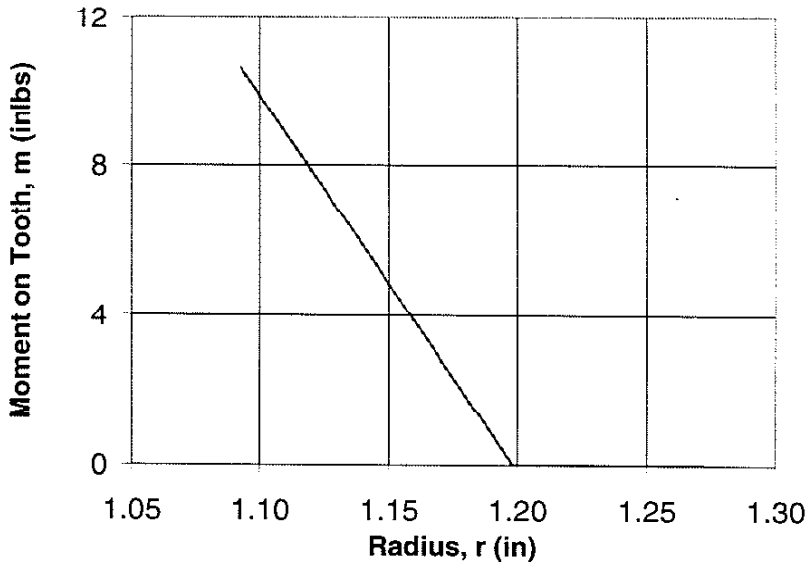

Figure 7.6: Moment along the tooth length.

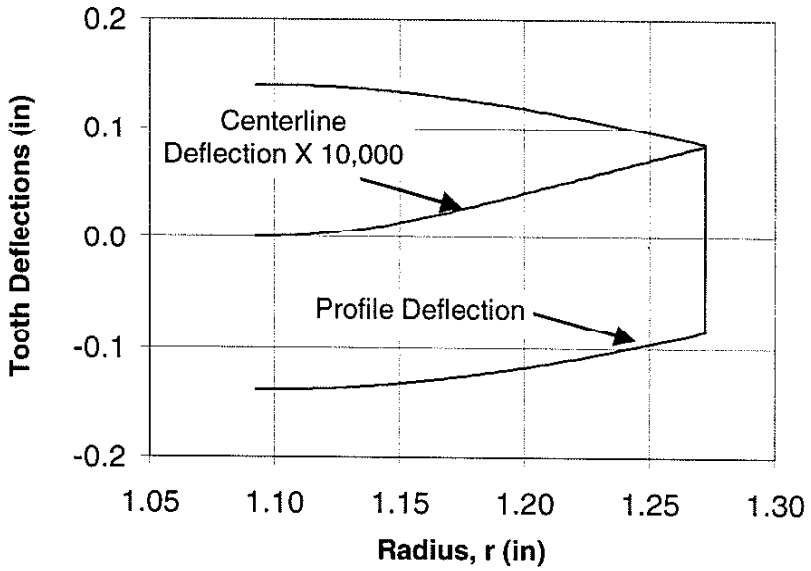

Figure 7.7: Deflected tooth surface and centerline.

C. Contact Of Two Opposing Teeth

Since the deflections of the internal and external teeth are known, their interaction can be considered. It is reasonable to assume that when the two teeth come into contact, the contact will not be made along the entire length of the tooth. The load would be concentrated at one position. This assumption is valid provided the gap between the teeth exceeds the surface deformation of the teeth. Figure 7.8 is the predicted gap for a set of steel coaxial spline teeth which have a pitch of 10, 25 teeth, and are under a 100 pound load.

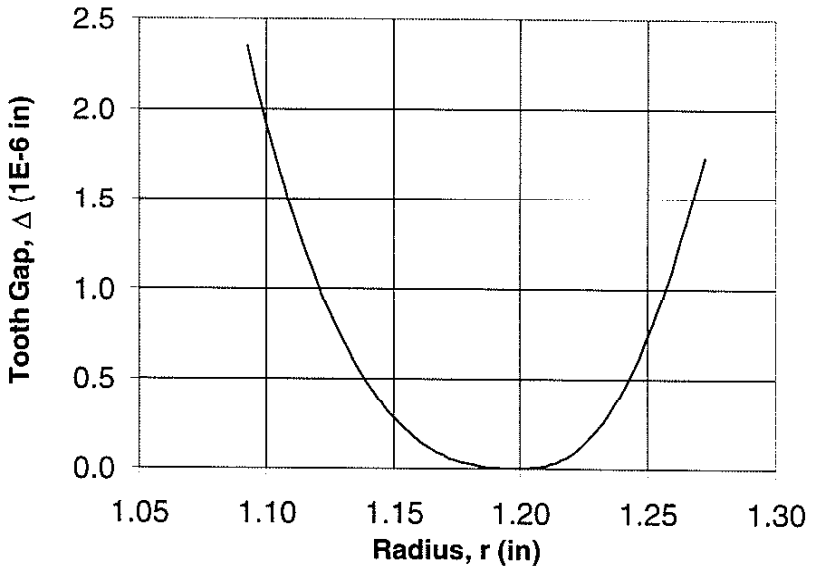

Figure 7.8: Gap between teeth with a 100 pound load.

Notice that there is a gap between the teeth surrounding the point of loading and that the load is concentrated near the center of the tooth. Although there are gaps at the ends of the teeth, they are extremely small, millionths of an inch. This suggests that it is possible for the teeth to make contact over their entire length, depending on their surface finish and deformation due to contact stresses. For the purpose of this evaluation, however, the contact can be assumed to occur at one point.

Although the gap surrounding the point of contact is small, the deflection of both teeth under a 100 pound load at the point of contact is about 8 (10^{-6}) inches, creating a gap that is equal to as much as 25% of the deflection. The nature of the involute produces zero gap at zero deflection. While being deflected, the curvature of the two faces are nearly the same and have been calculated as .506810 inches for the external tooth and .506880 inches for the internal tooth. The interaction of the two surfaces is, therefore, best evaluated as a cylinder inside a cylindrical socket.

Since the deflection has been found to be linear with the load, a constant spring rate of the pair of teeth can be calculated as the force divided by the displacement. Additionally, under these conditions, the point of contact is constant as the load changes.

The process of determining the point of contact and gap size is not necessarily straightforward. First, the deflection curves are determined through the double numerical integration mentioned earlier. The shape of the teeth contacting surfaces are then determined, as well as the radius where contact occurs. Next, the position of the load is adjusted until it sufficiently agrees with the radius of contact. Finally, the gap between the two teeth surrounding the point of contact can be determined, as well as the deformed radius of the deflected surface at the point of contact.

Evaluations of the tooth thickness, deflection curve, and contact with an opposing tooth have all been made with a program written in TK Solver™. TK Solver™ is a simultaneous equation solver with the ability to easily change independent and dependent variables. This, coupled with its ability to easily graph data, makes it very suitable for this type of analysis. A listing of the TK Solver™ code written to solve the tooth deflection problem is in Appendix A.

D. Gear Teeth Deflections

Now that the deflection shape of a pair of teeth is known, the possibility of multiple teeth in coaxial spline drives can be considered. If the two members, internal and external, were perfectly concentric, all of the mating teeth would contact each other and deflect

uniformly. If there were no torque load, they would not deflect at all. When the gear centerlines are not concentric, without any torque applied, the teeth may or may not make contact or deflect.

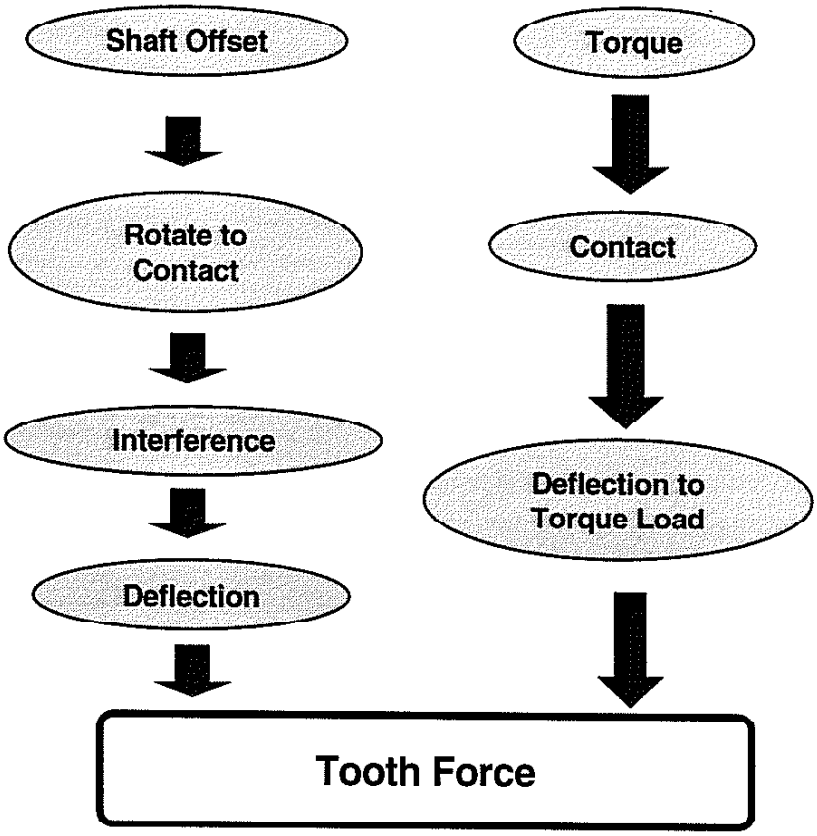

Figure 7.9: The analysis process.

The case for consideration, then, is when the shafts are offset. Referring to Figure 7.9, the analysis process, before the teeth can deflect, the shafts must first rotate to accommodate all the misalignment possible. If the remainder of the system is perfectly rigid, the teeth must accommodate all the required deflection. Any deflection in the system other than the teeth will degrade the concentricity between the splines. When there is compliance in the system, the concentricity of the splines will improve. An example of a compliant component is ball bearings. Their internal clearance can allow both axial and radial movement of their races, decreasing the required deflection of the spline teeth. Once system deflection is considered, the remaining interference needs to

be accounted for through tooth deflection. It is this deflection which determines the load on the tooth due to misalignment.

This loading of the teeth is then added to any torque load that may be applied. The torque load is determined by first establishing which teeth are in contact. Then through iterations, their required deflection which will drive the torque load is found. Throughout the evaluation, the gap between the teeth is continuously checked to properly identify those in contact.

In the analysis of a set of teeth, the conventions in Figures 7.10 and 7.11 will be used.

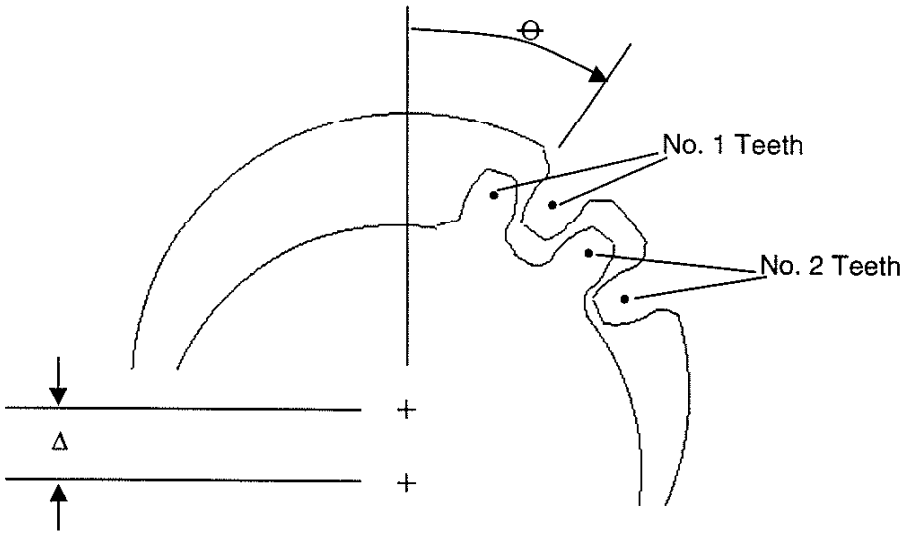

Figure 7.10:Teeth position and numbering.

The variables in Figures 7.10 and 7.11 are

θ = Angular offset from top dead center,

Δ = Gear centerline offset,

$\Delta_{i,j}$ = Tooth deflection,

$t_{i,j}$ = Tooth arc thickness,

$L_{i,j}$ = Arc length between teeth,

δ_j = Gap between teeth,

i = Tooth, 1 = external, 2 = internal, and

j = Tooth pair number.

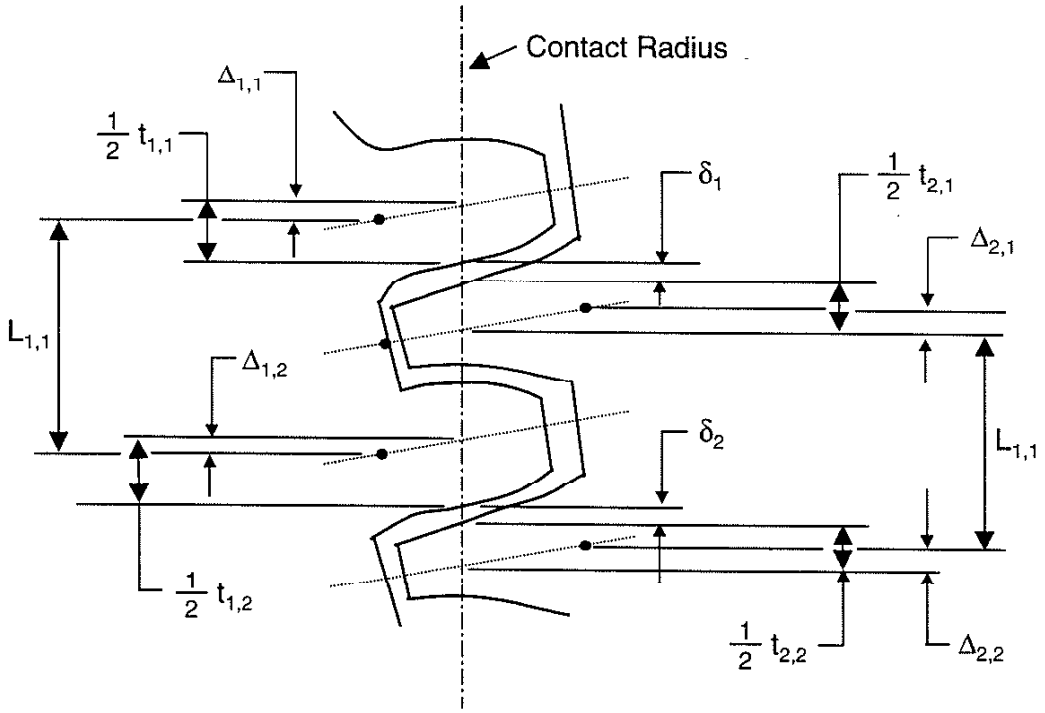

Figure 7.11: Definition of teeth arc lengths.

The angular offset, θ, is used to evaluate different discrete tooth locations. Using these definitions, the relationship between tooth spacing and deflection due to load can be established as the matrix Equation (7.13).

$$[I]\{L_1 - L_2\} = [B]\{t_1 - t_2 + \Delta_1 + \Delta_2 - \delta\} \tag{7.13}$$

Where for each pair of teeth

L_1 = Arc length between two external teeth,

L_2 = Arc length between two internal teeth,

t_1 = Arc tooth thickness of the external tooth,

t_2 = Arc tooth thickness on the internal tooth,

Δ_1 = Deflection of the external tooth from the load,

Δ_2 = Deflection of the internal tooth from the load,

δ = Gap between the teeth,

$$[B] = \begin{bmatrix} 1 & -1 & 0 & 0 \\ 0 & 1 & -1 & 0 \\ 0 & 0 & 1 & -1 \\ 0 & 0 & 0 & 1 \end{bmatrix}^{ect}, \text{ and}$$

[I] = Identity matrix.

The arc distance between the teeth, L, and the tooth thickness, t, are known from the geometry of the problem. The arc length between teeth, L, is determined through the geometric relationship of the arc length between the teeth to one center. This is where the offset, Δ, has a significant effect. The deflections due to the offset and gap between the teeth are unknown. Therefore, Equation (7.13) becomes Equation (7.14).

$$[B]^{-1}\{L_1 - L_2\} - \{t_1 - t_2\} = \{\Delta_1 + \Delta_2 - \delta\} \tag{7.14}$$

The value for the right hand side of the above equation can then be calculated. Now the freedom of rotation needs to be accommodated. First the minimum result from the right hand side of the equation is subtracted from each tooth gap. Then the manufacturing clearance and wear are added to each tooth gap from the right hand side of the equation. Some teeth now have gaps between them, whereas others have interference.

If there is interference, the gap between the teeth, δ, is set to zero and the force from the deflection can be calculated as in Equation (7.15).

$$F_i = K\Delta_i \tag{7.15}$$

where

F_i = Tangential force on the tooth pair and

K = Tooth pair spring rate.

If, however, the gap is greater than zero, the force on that tooth is set to zero. Additionally, the deflection of those teeth in contact, which are required to drive the torque, is considered. A deflection is estimated and adjusted to produce the required torque. These deflections are added to the deflections required from the offset. This allows the complete solution to the set of coaxial splines.

The remainder of the analysis involves the evaluation of a set of gears using the coaxial spline model. It is assumed that the teeth are of perfect form and that the gear set has the properties listed in Table 7.1.

Number of Teeth	25
Pitch	10 /in
Pressure Angle	30 degrees
Offset	.010 in
Torque	50 ftlbs
Material	Mild Steel
Class of fit	6
Wear	0 in

Table 7.1: Baseline gear teeth properties.

The resulting load distribution on the teeth is that shown in Figure 7.12:

There are actually two curves in the graph, one for zero torque applied and the other with 50 ft lbs. These are the results if the clearances between the teeth are at their maximum, .0088 inches for a class 6 fit. Clearly there must be a distribution of these clearances. They are not expected to decrease to zero, however, otherwise, axial movement could not occur. The analysis was repeated with an estimate, based on experience in industry, of the tightest clearance likely to be produced, .001 inches.

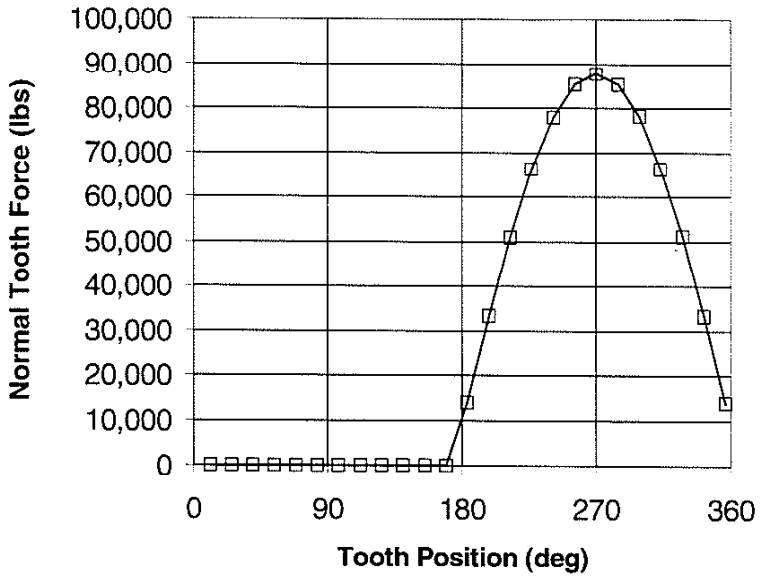

Figure 7.12: Tooth loads.

With the tighter clearance, as shown in Figure 7.13, the tooth stresses are nearly double, and almost all of the teeth make contact at the same time. Now consider the case where the teeth are worn by .018 inches, with the .001 inch manufactured clearance as shown in Figure 7.14. Not only are there fewer teeth in contact, the maximum load on the teeth is significantly reduced.

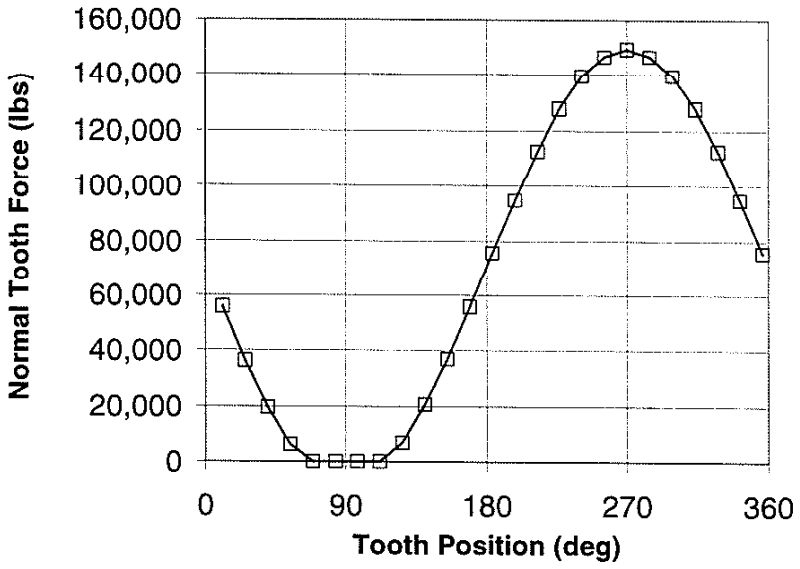

Figure 7.13: Tooth loads at .001 inch tooth clearance.

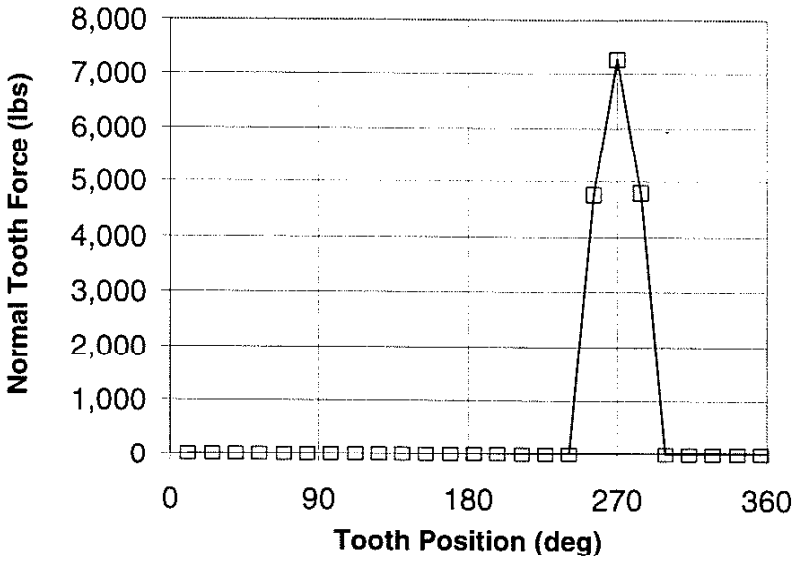

Figure 7.14: Tooth loads with tight clearance and wear.

Several observations can be made from the results shown in Figures 7.12, 7.13, and 7.14. The first is that the tighter the fit, the more each tooth will have to deflect, increasing its load. Second, as the teeth wear, fewer teeth carry the load. Also, the load imposed on the teeth by torque is insignificant compared to the load from the teeth deflections.

The last and most important observation is that the tooth forces due to the offset shafts are extremely high. If the surrounding system is truly rigid, the teeth would be expected to fracture. In applications such as clutches, which are the focus of this paper, the system surrounding the gear teeth is not rigid. The friction faces of the clutch may slip, placing a ceiling on the load and the gear tooth requirement to bend. The amount of slippage is not always a known quantity. Early in the life of the clutch, the force can be easily determined with Equation (7.16) as a relationship between the torque, coefficient of friction and mean radius.

$$F = \frac{T_q}{\mu r} \tag{7.16}$$

where

F = Force,

T_q = Torque,

μ = Coefficient of friction, and

r = Mean friction face radius.

The typical clutch which would be used with this spline would have 750 lbs. of maximum radial retention force. Considering this to be the case, the model can be adjusted so that the force acting in any radial direction is calculated. Then the offset is adjusted so that the force is not exceeded. This produces the tooth loading in Figure 7.15.

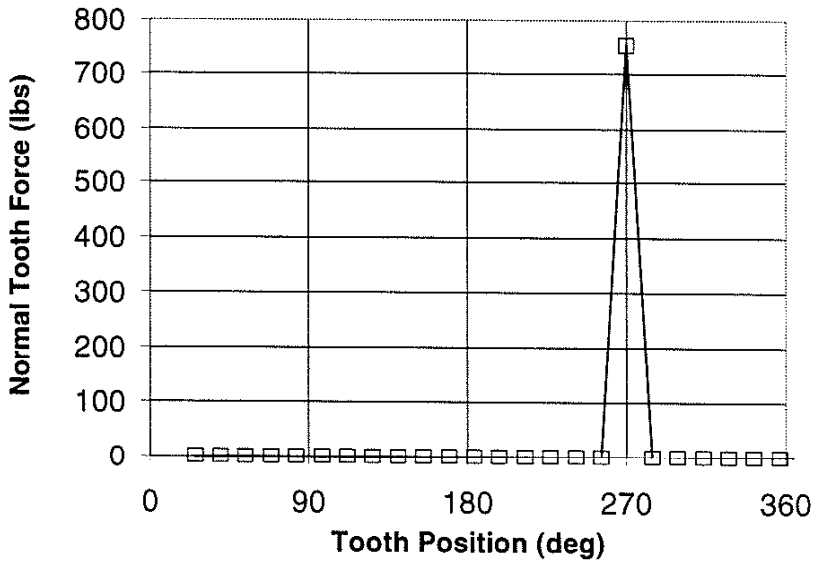

Figure 7.15: New clutch tooth loads.

As the friction faces wear, as shown in Figure 7.16, the determination of this force is not as straightforward. Grooves are cut into the face, causing the radial load ceiling to increase. The force would be dependent on the size of the groove, its material, and many other factors. Assuming the contact in the groove can be modeled as a rigid, static, inclined plane, an estimate of the radial force, F_r, can be made with Equation (7.17).

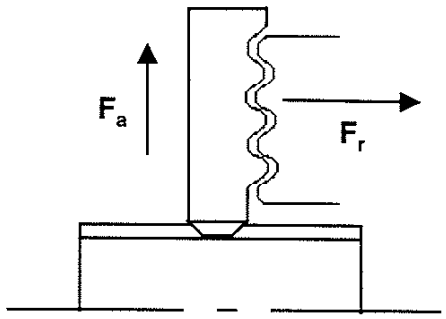

Figure 7.16: Worn clutch face.

$$F_r = F_a\left(\frac{\mu Cos\lambda - Sin\lambda}{Cos\lambda - \mu Sin\lambda}\right) \tag{7.17}$$

where

F_a = Axial clutch force,

μ = Coefficient of friction, and

λ = Contact plane angle to friction face.

The contact plane angle is a key factor in determining the axial force. If an angle of 25° and a coefficient of friction of .5 were assumed, the radial force would be about 2000 lbs. Under these conditions, the tooth loads should be as predicted in Figure 7.17.

Figure 7.17 is a much better representation of the load sharing between teeth that is produced. Figure 7.15, at a 750 lb. axial ceiling, would be representative when the clutch is new. After wearing in, the loads would increase to those in the Figure 7.17. Therefore, these are the loads used to determine the steady-state stresses in the teeth.

There are two more items regarding this evaluation. Because of the complex nature of modeling the gap and deflection between the teeth, solutions for the torque load and radial force limit are found through iteration. The equivalent deflections required to produce those loads are estimated and adjusted accordingly until the desired loads are

achieved. Secondly, it should be noted that these tooth forces are tangential to the gear radius at the point of contact. They have normal and tangential components with respect to the tooth's surface, which are trigonometric functions of the pressure angle.

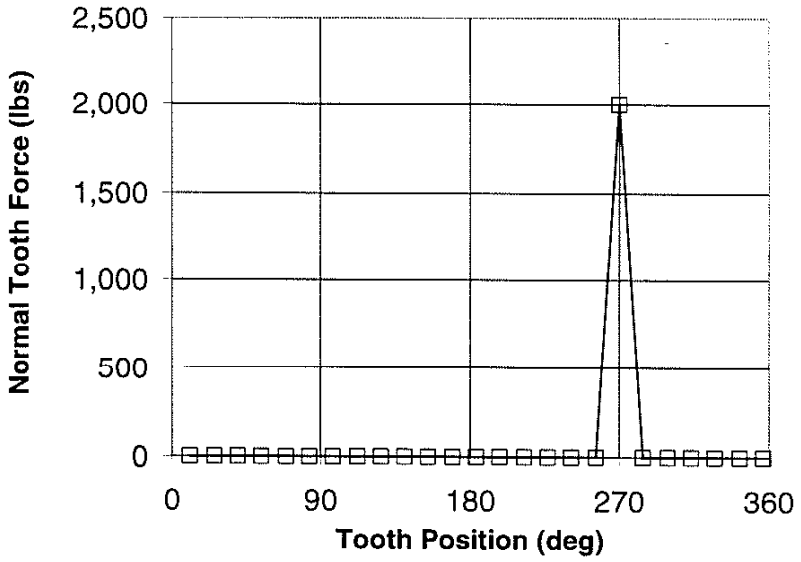

Figure 7.17: Worn clutch tooth loads.

E. Hertzian Stresses on Tooth Surfaces

Now that the loads on each tooth can be found, the stresses need to be determined. The Hertzian stresses and contact areas of the tooth to tooth interface can be evaluated several ways, including a sphere on a plate, a sphere on a spherical socket, a cylinder on a flat plate, or a cylinder in a cylindrical socket [117]. In some of these cases, elastic surface deformations can be calculated as well.

Due to the curvature of the teeth, the use of the cylinder in a cylindrical socket best describes the interface. This assumes the teeth are quite long, have contact across their entire width, and that the surfaces are large arcs. Splined teeth are not necessarily always long, however. Additionally, contact across the entire tooth width may not occur if there is angular misalignment. The best estimation of surface conditions for that case may be the sphere in a spherical socket.

The Hertzian contact stress for a cylinder in a cylindrical socket is given by Equations (7.18) through (7.20).

$$\sigma_c = 0.798\sqrt{\frac{p}{K_D C_E}} \tag{7.18}$$

$$K_D = \frac{D_1 D_2}{D_1 - D_2} \tag{7.19}$$

$$C_E = \frac{1-\nu_1^2}{E_1} + \frac{1-\nu_2^2}{E_2} \tag{7.20}$$

where

σ_c = Contact stress,

p = Load per unit length,

D_i = Contact surface diameter,

ν_I = Poisson's ratio, and

E_I = Young's modulus.

The contact width, b, is found through Equation (7.21).

$$b = 1.6\sqrt{pK_D C_E} \tag{7.21}$$

In the case of the baseline model, the radius of the teeth surfaces are .506880 and .506810 inches for the internal and external teeth, respectively. Evaluating them as a cylinder within a cylinder produces a Hertz stress of 3770 psi with a contact width of over 3 inches. Clearly, the contact width is larger than that available on the tooth. By allowing only the radial tooth length to make contact, the predicted stress is more realistic. The constant K_D for the proper tooth length becomes Equation (7.22).

$$K_D = \left(\frac{b}{1.6}\right)^2 \frac{1}{pC_E} \tag{7.22}$$

Where b is the radial length of the tooth. Now a stress of 63.5 ksi is predicted. As expected, this is just slightly higher than the contact stress calculated if the load were divided by the entire tooth area. That stress is 57.4 ksi.

F. Sliding Distance and Speed

Sliding distance and speed are both measures used to predict the fretting or wear of materials. In the case of coaxial splines, the contact of the teeth is periodic. The time of contact is a function of the maximum number of teeth which can make contact. This is seen in Figures 7.12, 7.13, and 7.14. While the sliding distance is fairly constant, cycle to cycle, the sliding speed changes with angular position during the cycle.

If, using the earlier convention, the shafts were offset by an amount, Δ, the relative position of two opposing teeth to each other, S(t), at a speed, ω, would be found with Equation (7.23).

$$S(t) = \frac{\Delta \mathrm{Sin}(\omega t)}{\mathrm{Cos}(\phi)} \tag{7.23}$$

And the sliding amplitude, dS, would be determined with Equation (7.24).

$$dS = \frac{\Delta\left(1 - \mathrm{Sin}(\beta)\right)}{\mathrm{Cos}(\phi)} \tag{7.24}$$

Here, β, is the angle where contact is first made. In Figure 7.12, β is 170 degrees. The sliding distance during one cycle is twice the sliding amplitude.

The velocity, V(t), can now be found with Equations (7.25) and (7.26) by taking the absolute value of the first derivative of S(t).

$$V(t) = \left| \frac{\Delta \omega \mathrm{Cos}(\omega t)}{\mathrm{Cos}(\phi)} \right|, \quad 2\pi - \beta > \frac{\omega t}{2\pi n} > \beta, \quad n = 1,2,3.... \tag{7.25}$$

$$V(t) = 0, \quad \beta > \frac{\omega t}{2\pi n} > -\beta, \quad n = 1,2,3.... \tag{7.26}$$

For the preceding spline evaluation, the sliding distance would be .0116 inches and the amplitude .0058 inches. The sliding velocity of the teeth while they are in contact is predicted as shown in Figure 7.18.

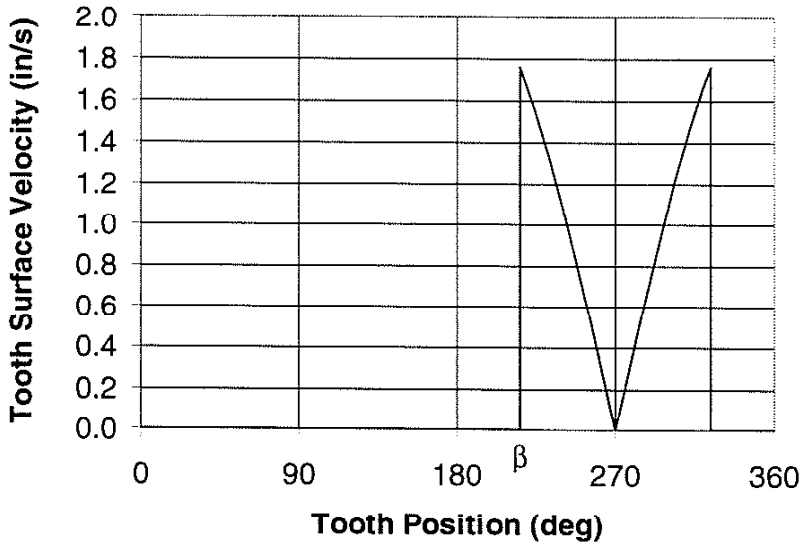

Figure 7.18: Tooth surface speed.

Note that when the teeth first make contact, at β, the velocity is not zero. This is because the relative velocity between the teeth exists, even when they are not in contact.

Now that the sliding distance and the velocity profile can be determined, they can be applied to fretting and wear theories.

G. PV Limit

The evaluation of plastic gear teeth wear requires the calculation of the PV value for comparison to the PV limit. The previous sections evaluated the maximum stress. That stress occurs when a tooth reaches a position normal to the offset. At that point, however, the sliding velocity becomes zero, producing a zero PV value. This is seen in Figure 7.18. By adjusting the offset angle of the teeth, and repeating the analysis, the

condition where the maximum product of the load and velocity can be found. This, then, is the position where the maximum PV value is calculated.

It is recognized that the PV value calculated only exists for a moment during the cycle. The same is true for the maximum stress. The proper solution would be an integration of the changing stress of PV value, with time, while the teeth rotate, similar to Miner's rule for fatigue stresses. For the purposes of this paper, however, the focus is on determining the maximum values, based on the assumption that they cause the majority of the damage. Any reduction in the maximum value is assumed to reduce the damage.

H. Summary

Using the coaxial spline model, several key characteristics relating to fretting and wear can be predicted. They include the maximum load, stress, and PV value.

The evaluation begins with the gear tooth's stiffness. The tooth is treated as a cantilever beam whose profile is given in Equation (7.5). Tooth deflection is then found through the double numerical integration of Equation (7.12). Next, the interaction between mating teeth is evaluated to determine the point of contact. Once the point of contact agrees with the load point, the stiffness of the teeth is known.

Reactions of the teeth pair are then used in the evaluation of the gear set. Teeth contact is a function of the space between the teeth and the deflection of the surrounding teeth. The gears set is evaluated by Equation (7.13), which relates the system of teeth deflections to their gaps. The space between the teeth is governed by the offset of the two gears whereas the deflection of the teeth is determined by their interference with mating teeth and the torque load applied.

Evaluations made with the coaxial spline model were made with clutches and couplings. The clutch evaluation limits the radial load on the teeth to the maximum slip load of the friction faces. The coupling evaluation, however, does not have this restriction. In both

evaluations, the loads on the tooth from torque are less than the loads from offsetting the two gears.

Once the teeth in contact as well as their loads are known from Equation (7.13), analysis of contact stresses, sliding distances and velocities, and PV values can be made. These properties are then used in the evaluation of wear and fretting. Therefore, use of the coaxial spline model allows the engineer to evaluate changes to the design and better understand the effects prior to actual testing.

VIII. The Clutch Evaluation

A. Approach

There are many theories that predict the life and wear rates of components subjected to fretting and wear. These were presented in Chapters 2, 3, 4, and 6. In order to reduce coaxial gear failures due to these mechanisms, the results of the coaxial spline model described in Chapter 7 need to be interpreted in light of those theories.

The theories presented in Chapters 2 through 6 predict not only wear and wear rates, but also maximum stresses, the position of those stresses, the angle at which cracks are most likely to occur, and coefficients of friction. The discussions also include how sliding amplitude, frequency, temperature, humidity, and other application parameters effect wear and fretting. Some of these characteristics, including humidity, temperature, surface finish, material elements, and debris, are not described by the coaxial spline model, and therefore will not be addressed during the course of this analysis. The analysis does, however, provide results with respect to pressure, force, sliding amplitude, frequency, and the product of velocity and pressure.

Once these results are obtained, they need to be interpreted, using the theories described earlier to predict the life and wear rate of the components. Selection of the most appropriate theory is based on a variety of questions. Does the application involve fretting wear, corrosion, or just wear? Is fretting fatigue fracture likely? Is the material best described with a PV value? How does the coefficient of friction change? Once questions such as these are answered, the best model can be identified and a wear rate, fretting rate, or life prediction identified.

A review of the various theories shows that some trends are evident. First, with only a few exceptions, the stresses and rates of wear are all linear with the load. Therefore, a reduction in load can be expected to provide at least a linear increase in life. The theories

also generally agree that the amount of wear is linear with distance traveled. Additionally, if plastics are being used, the maximum product of the load and velocity is a significant factor.

The remainder of this chapter will show how design changes with respect to the tooth geometry, material, tolerances, radial slip force, torque, and speed will impact the key elements of contact stress, sliding amplitude, and maximum PV values.

B. Baseline Design

The baseline design is the same as that of the example used in Chapter 7 to describe the coaxial spline model. The spline will be used to transmit 50 ftlbs of torque. Since the application is a clutch, the splines will have a 2000 lb radial load limitation, with the assumption that, beyond that point, the clutch will slip. It is also assumed that this is steady-state with respect to the radial force and the change in clearance due to wear. The spline will be assumed to have the maximum clearance allowed for a Class 6 fit. The contact will be assumed to be a point load, and the Hertzian stresses will be evaluated using the modified K_D for a limited contact area.

C. Tooth Geometry

In the evaluation of the ability of a set of coaxial splines to resist fretting and wear, the stiffness of the tooth affects the number of teeth that will simultaneously make contact. Changes in the geometry of the tooth, therefore, need to be evaluated for their effect on stiffness, as well as for their impact on fretting and wear characteristics.

1. Pitch

The design was evaluated at three different pitches to determine the effect of pitch on pressure, force, and the product of pressure and velocity. The first condition was the baseline design with 10 teeth per inch. The second and third conditions were 12 and 16 teeth per inch, respectively. Each of these conditions maintained the same pitch diameter of 2.5 inches, changing only the number of teeth in the spline. Increasing the pitch from

10 to 16 teeth per inch results in the number of teeth increasing from 25 to 40. This change produces only slight changes in the radius where contact is made and the average surface radius. It has a significant impact, however, on the stiffness of the teeth, as indicated in Figure 8.1. The resulting spring rate goes from 7.9 to 6.6 million lbs/inch, a decrease of 16%.

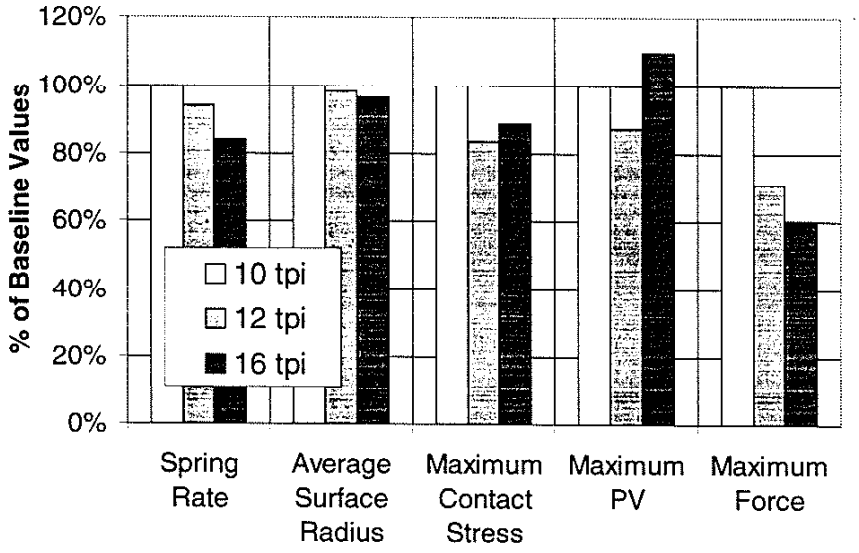

Figure 8.1: Changing pitch.

Changing the pitch also produces changes in the contact stress. Changing from a 10 to 12 tooth pitch produces a 16% reduction in contact stress. However, increasing the pitch still further to 16, rather than providing an even greater improvement, reduces the stress reduction by only 11% from the baseline. This can be explained by observing the maximum force produced and number of teeth in contact. As the pitch increases, the force decreases, in fact by nearly 40% when moving from a 10 to 16 pitch. As the force decreases, however, the contact area of the tooth face also decreases. The major contributor to this inconsistent behavior is the number of teeth in contact. The effect of changing the number of contacting teeth on the tooth force is shown in Figure 8.2. In the baseline, the number of opposing teeth in contact can be as little as one. In the other two

cases, there are always at least two teeth in contact. When this happens, two teeth now share the maximum load produced by torque and the faces slipping, which, in the case of the baseline, was completely absorbed by one tooth. The increase in stress in going from the second to the third case is then clearly related to the tooth area decreasing faster than the force. Therefore, any benefit due to increasing the number of teeth is only obtained if the minimum number of teeth in contact is increased. Otherwise increasing the pitch is detrimental.

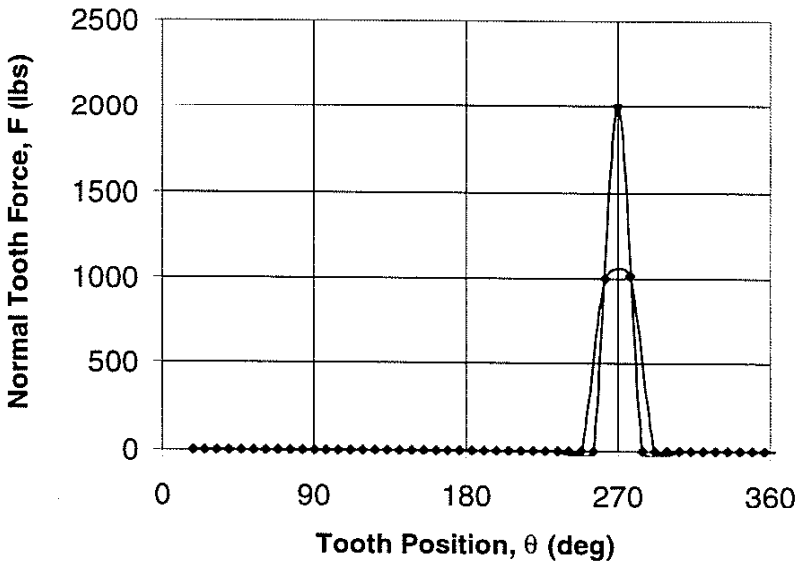

Figure 8.2: Changes in tooth force.

The effect of the number of teeth in contact is also seen in the maximum product of pressure and velocity, PV. There is a 12% reduction in the maximum PV when the pitch is increased from 10 to 12, and a 10% increase when the pitch is changed from 10 to 16. This, as in the case of contact stress, is a result of the number of teeth in contact and the change in contact area.

2. Pitch Diameter

This evaluation involves maintaining the same tooth pitch and changing the number of teeth by increasing the pitch diameter. The pitch diameter was changed from the 2.5 inch

baseline to 2.7 and 2.9 inches for the second and third evaluations. This changed the baseline of 25 teeth to 27 for the second case and then to 29 teeth for the third case.

Referring to Figure 8.3, while there is the expected large increase in contact radius, the spring rate is only slightly reduced by these changes. It is interesting to note that the average surface radius increases somewhat significantly as well. The coaxial spline model presented in Chapter 7 suggests that a change in the average surface radius would have minimal effect on the fretting and wear characteristics. This is because they assume the curvature of the teeth surfaces to have perfect relative positioning with respect to each other. As discussed earlier, due to deformation, the tooth surface is best evaluated as being in complete contact. Intuitively, however, as the surfaces of the teeth approach that of flat plates, their contact pressure can be expected to be more uniformly distributed, potentially reducing any stress, fretting, or wear.

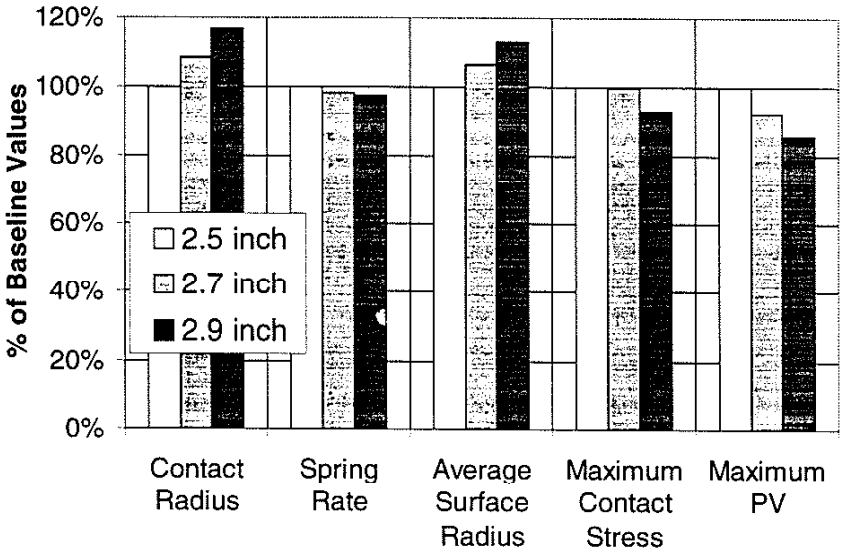

Figure 8.3: Changing pitch diameter.

Once again, the minimum number of teeth in contact plays an important role in the reduction of stress. Increasing the pitch diameter by 8% has no effect on the peak tooth

stress, because the minimum number of teeth in contact is still one. Once the pitch diameter is increased by 16% to 2.9 inches two teeth are in contact, and the maximum contact pressure is decreased by 7%. This result is as expected for this application, since the clutch limits the radial slip force that can act on the spline. When the slip force significantly exceeds the torque driven through the spline, it becomes the major contributor to tooth loading. The load on the teeth will be constant, therefore, as long as the number of teeth in contact is constant, regardless of the pitch diameter.

Increasing the pitch diameter has a more consistent effect on the PV value. Increasing the pitch diameter by 8% and 16% decreases the maximum PV value by 8% and 14%, respectively. This is because, as discussed earlier, the maximum PV value occurs not when one tooth is in contact, but when two are sharing the load.

3. Pressure Angle

All of the evaluations to this point have been made with a 30-degree pressure angle. The other two standard involute spline angles are 37.5 and 45 degrees. At the two larger pressure angles, the teeth become quite rigid, forcing contact at the base of the external tooth. Their ability to maintain a good contact surface is minimal, and therefore, their use should be avoided if possible.

4. Tooth Width

Changing the width of the tooth in the axial direction has a linear effect on the spring rate of the teeth. As shown in Figure 8.4, there is no change in the maximum force unless the number of teeth in contact changes. In the case of the .2 and .4 inch wide teeth, there is only one tooth in contact. When the width is reduced to half of the baseline model, .1 inches, number of teeth in contact increases to two and the maximum force is reduced. The maximum contact stress and maximum PV value also change linearly with the tooth width, provided the contacts do not change. In the case of the baseline model, doubling the tooth width cut the loads in half as well. If, however, more than one tooth were in contact, the load reductions would not be as significant.

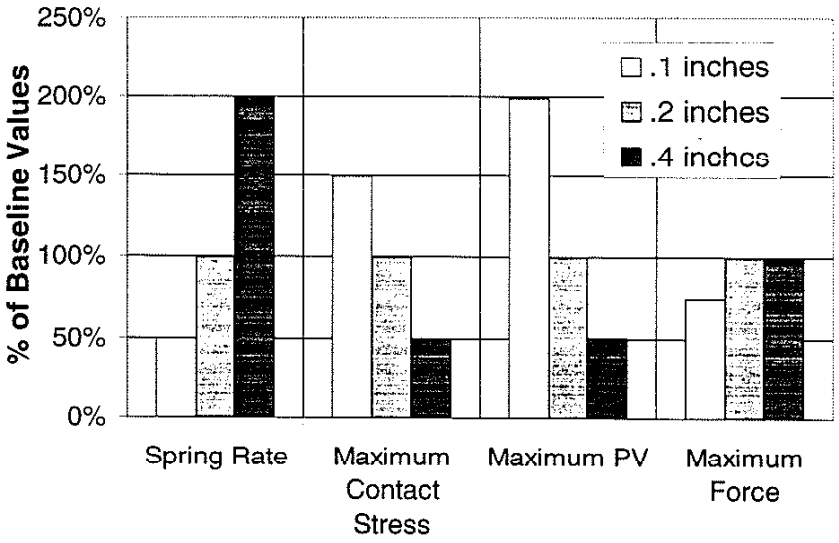

Figure 8.4: Changing tooth width.

D. Material

1. Young's Modulus

a. Identical Change For Both Internal and External Teeth

Young's modulus can be substantial changed by using different materials. As shown in Figure 8.5, changing the Young's modulus on both gears at the same time has a significant effect. The spring rate of the tooth is found to be proportional to the changes in the Young's modulus. The baseline model evaluation uses the Young's modulus of steel, $30(10^6)$ psi. The subsequent two evaluations were done with Young's modulus of $30(10^5)$ psi and $30(10^4)$ psi. These resulted in significant reductions of 58% and 80%, respectively, in the maximum contact pressure. This reduction is similar to the reduction in the maximum force, and can be completely attributed to the increase in the minimum number of teeth in contact. The baseline model had one tooth in contact. Decreasing the Young's modulus by a factor of 10 brought three teeth into contact. Decreasing it further by another factor of 10 meant that eight teeth were in contact.

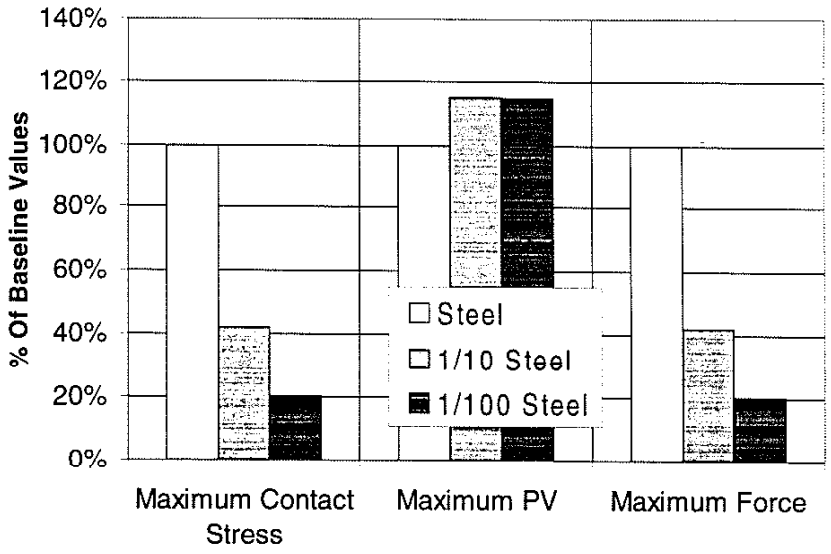

Figure 8.5: Changing Young's modulus of both members.

The impact that changing the Young's modulus had on the maximum PV value, however, was mixed. The first decrease in the Young's modulus, which resulted in the number of teeth in contact increasing from one to three, produced a 15% increase in the maximum PV value. With further reduction of the Young's modulus, however, the PV value remained unchanged. The reason for this is, again, the number of teeth in contact. In the baseline case, the maximum PV value occurs when two teeth are in contact. In the second case, where the Young's modulus is one-tenth that of steel, the maximum PV value occurs when there are four teeth in contact. The PV value increases because, as the fourth contacting tooth is added, the increase in velocity on one of the teeth is greater than its decrease in surface pressure. When the Young's modulus is further decreased to $30(10^4)$ psi, again, the contact pressure does not decrease faster than the velocity increases with the additional teeth in contact. This results in the PV value remaining nearly the same as that for the previous case.

b. Independent Change for Internal and External Teeth

Having a different Young's modulus for the internal and external teeth may be a result of an attempt to take advantage of the benefits of using dissimilar materials or a result of manufacturing advantages. Figures 8.6 and 8.7 show the results obtained by changing the Young's modulus of, first, the external teeth and second, the internal teeth. The changes were by a factor of 10, made in the same manner as in the previous section. In both cases, these changes produced significant changes in the average surface radius.

This is a result of the deflection that takes place in the weaker tooth. If the external tooth is weaker, it bends the most, resulting in a contact radius closer to its minor diameter. The radius of the contacting surfaces also decreases. Young's modulus reductions in the internal tooth result in similar but opposite changes. In both cases, the spring rate of the pair of teeth decreases substantially, but not as much as the decrease caused by changing the Young's modulus equally in both teeth.

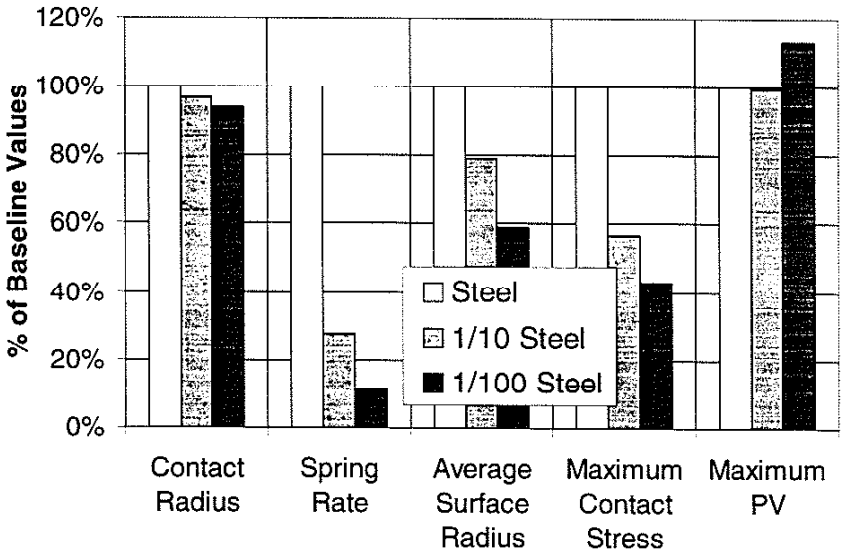

Figure 8.6: Changing Young's modulus of external teeth.

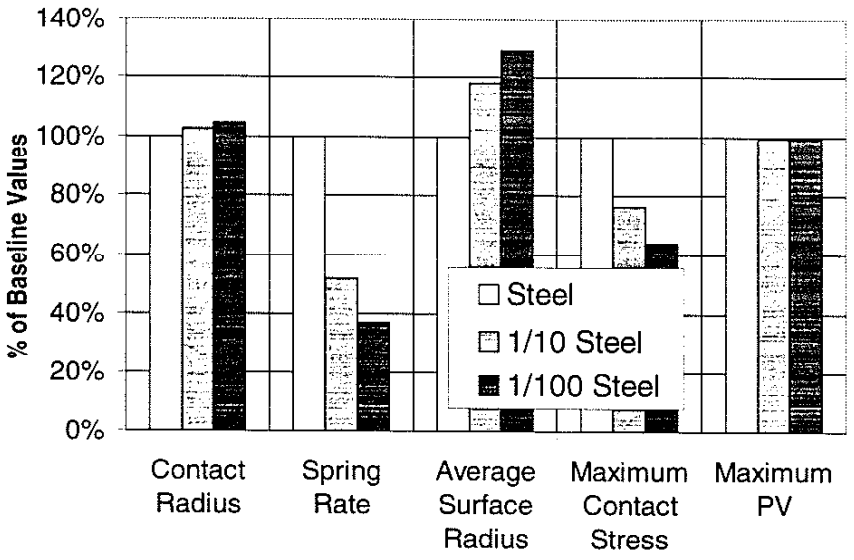

Figure 8.7: Changing Young's modulus of internal teeth.

As both of the preceding figures show, the resulting effect on the system of multiple teeth is similar to that of changing the Young's modulus of both teeth. The minimum number of teeth in contact increases, decreasing the contact force and pressure. Changing the material of the external teeth has a more significant effect than changes to the internal teeth. Changing the Young's modulus of the external teeth cause the number of teeth in contact to increase from one to two to three with each order of reduction in the modulus. These reductions produce a 43% and 57% reduction in contact pressure. The same changes in the Young's modulus of the internal teeth produce, at most, a minimum of two teeth in contact and contact stress reductions of 24% and 36% for each order of magnitude reduction in the Young's modulus.

In each case, the average surface radius changes significantly as the weaker of the two teeth accommodates all of the bending. The weaker tooth deforms, whereas its mating surface is nearly unchanged.

As for the maximum PV value, in the case of the internal tooth, this value is unchanged. This is because it always occurs when two teeth are in contact. In the case of the external tooth, once there is a minimum of three teeth in contact, at a Young's modulus one one-hundredth that of steel, the maximum PV value increases 13.5%. This maximum PV value occurs when four teeth come into contact. Just as before, as more teeth are caused to come into contact, the relative speed is increasing faster than the load in decreasing.

2. Poisson's Ratio

Poisson's ratio is a key variable used in the calculation of the Hertz stress. But when K_D is back-calculated to account for a smaller contact area, as explained in Chapter 7, the contact stress is no longer a function of the material's Poisson ratio. Therefore, changes to Poison's ratio have no effect on the model.

E. Wear of Teeth

With the exception of tooth-to-tooth variations in the circular tooth pitch, each tooth has an equal opportunity to slide and wear on the opposing teeth. Because the teeth are assumed to all be contacting on the same side, if the contacting surface were to wear, the tooth-to-tooth pitch would remain unchanged. In a clutch, it is the radial force limit that eliminates the effects of wear. The wearing of the teeth does, however, reduce their stiffness, allowing more deflection. This was determined to have a negligible effect, however, and was not included in the model.

F. Tolerances

1. Angular Misalignment

Angular misalignment of the two splines results in contact at the axial edges of the teeth, producing a stress concentration. If there are only a few teeth in contact, the result is simple. Since the pair of contacting faces does not change, it is hypothesized that the edge will wear consistently until the contact area becomes sufficiently large to support the load without wear. It will eventually either (1) stop wearing or (2) distribute the load across the entire tooth and wear as if it had zero angular misalignment. If there are more

teeth in contact the problem becomes quite complex. In that case, continuous fretting or wear action occurs.

2. Class of Fit

Initially, if the pitch were to change from tooth to tooth and multiple teeth were making contact, the tooth with the higher surface would deflect more, taking more of the load and reducing the load on the adjacent teeth. In doing so, the high tooth will wear until the load is properly shared in the steady-state condition, as indicated in the coaxial spline model. Changing the class of fit would present a similar solution to that produced by the wear of the teeth.

G. Radial Slip Force and Torque

As explained earlier, in evaluating a spline applied to a clutch, there exists the ability for the radial load on the teeth to be limited. The value of the limit becomes a function of the torque and friction surface conditions of the clutch. The load on the teeth in a clutch, therefore, is a direct result of the radial slip force and torque. The baseline model was modified to evaluate the effect of the radial slip force. The results are shown in Figure 8.8.

Once the effect of the number of teeth in contact is taken into account, the contact stress is found to be proportional to the slip force. In this model, reducing the force by half did not change the number of teeth in contact, but it did cut the stress in half. Doubling the slip force, however, required two teeth to make contact, producing only a 50% increase in contact pressure. The PV value, on the other hand, is almost directly proportional to the slip force.

If the torque in the spline were increased, the radial slip force for a clutch would have to increase proportionally as well. In the model, the radial slip force has the most influence over the load on the tooth. Therefore, the effect of changing the applied torque is the same as that of changing the radial slip force.

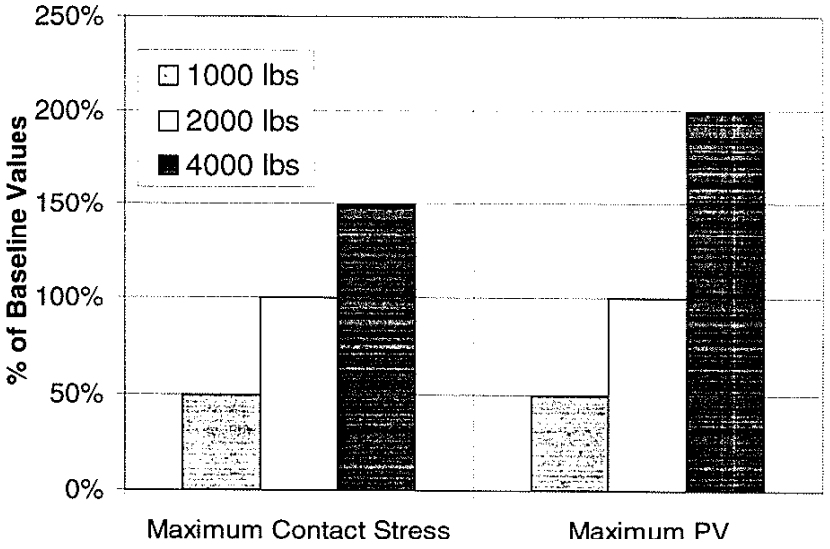

Figure 8.8: Changing radial slip force.

H. Offset

The offset, or concentricity, of the two splines is actually a result of tolerances in the application and is thought to be the most significant cause of wear or fretting of the teeth. The baseline model has an offset of .010 inches. The key characteristics of the teeth were evaluated at .005 and .020 inches of offset with the results shown in Figure 8.9.

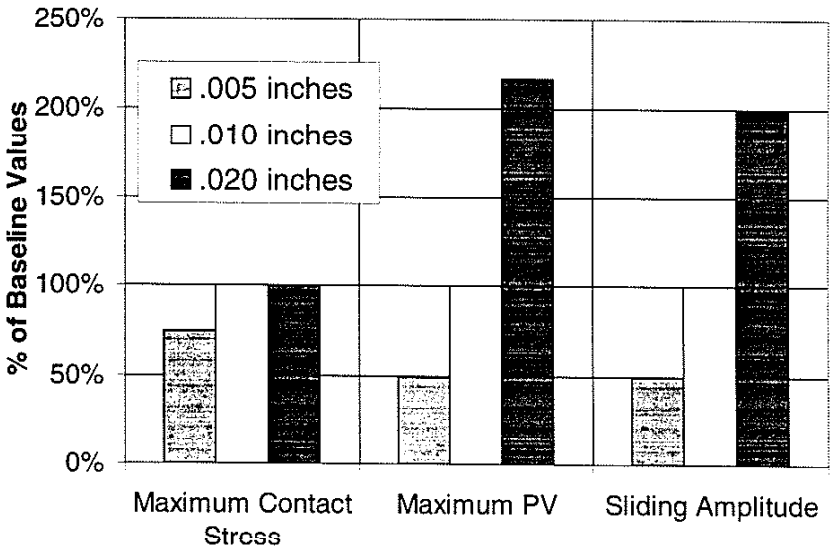

Figure 8.9: Changing offset.

By reducing the concentricity by 50%, the contact stress decreased by 25%. This is a result of the number of teeth in contact increasing from one to two. Doubling the offset, however, to .020 inches, did not change the number of teeth in contact, and therefore had no effect on the contact stress. The contact stress became a limit of the ability of the clutch faces to slip.

The change in the PV value, however, was different than that of the contact stress. Cutting the offset in half also reduced the PV value by half. When the offset was doubled, however, the PV value increased by over 200%, demonstrating the significant impact of the offset on this characteristic. The reason for the extra increase is most likely due to the relative velocity of the tooth surfaces.

The offset is also the only variable evaluated that significantly affects the total sliding amplitude. As can be seen in the above figure, the amplitude change is proportional to that of the offset.

I. Rotation Speed

The speed of the rotation affects the frequency of the sliding action and is not a factor in determining stresses and PV values. At 1800 rpm, the most common speed for applications of this nature, the frequency of sliding is 30 hertz. Perhaps just as important as the frequency is the distance between the contacting teeth during the cycle. When the teeth are not in contact, the gap between them allows oxidation to occur more easily. This may effectively increase the frequency that is required for oxidation to take place. Another characteristic of a clutch application, not accounted for in this model, is that when the teeth are in contact, the sliding in bi-directional.

J. Optimum Design

Once the effects of various design changes are understood, this knowledge can be used to optimize the design of a set of coaxial gears. Three key characteristics will be considered in optimizing the design: contact stress, PV value, and sliding amplitude.

1. Contact Stress Reduction

Significant factors in reducing the contact stress include the tooth width and amount of slip force. Change in the slip force has a nearly linear effect on the stress. The tooth width does as well, provided the number of teeth in contact remains unchanged. Increasing the pitch diameter has a small effect, and only when the number of teeth in contact can be increased. Increasing the number of teeth by increasing the pitch increased the stress more than the pitch diameter. However, if changing the pitch does increase the number of teeth in contact, a fair reduction in stress can be achieved. Reductions in the offset produce stress reductions slightly larger than those achieved by changes in the pitch.

The most effective factor in the contact stress reduction was the Young's modulus. Reducing the Young's modulus in both members is the most effective means of reducing stress. Changing the external tooth's Young's modulus is more effective than changing the internal tooth's material. Provided the materials do not significantly loose wear resistance, reductions to the Young's modulus may produce the most resistance to fretting and wear.

The variables are discussed in generalities here because they are highly interdependent. One of the key factors in reducing the contact stress, however, is increasing the number of teeth in contact.

2. Maximum PV Reduction

The maximum PV value response changes linearly with the slip force. It is also linear to the tooth width if the number of contacts is consistent. The maximum PV value is nearly linear to the amount of offset. Unlike the effect on maximum stress, changing the Young's modulus on either material seems to have only a small effect on the maximum PV value. A change in the pitch has mixed results regarding the PV value ,depending on

the number of teeth in contact. Any increases in the pitch diameter produce a fair reduction in the maximum PV value.

3. Slip Amplitude Reduction

The only variable that has an effect on the slip amplitude is the offset, and the relationship between the two is linear.

IX. The Coupling Evaluation

A. Approach

The approach to the evaluation of splined couplings will be the similar to that used for clutches in the previous chapter. In fact, some variables, including the pressure angle, Poisson's ratio, tooth width, angular misalignment, and rotational speed evaluations produce the same results as in the clutch evaluation and need not be described again here. The design parameters that do produce different effect for couplings than for clutches are the pitch and pitch diameter, Young's modulus, tolerances, torque applied, offset and amount of wear.

B. Baseline Design

The baseline design for the coupling is the same as for the clutch with only two exceptions: (1) Since the coupling is rigid, there will not be a ceiling on the radial force produced by the spline loading. (2) The baseline evaluation of clutches was made with a .010 inch shaft offset. If that offset were introduced to theoretically rigid splines, such as those in couplings, the stresses would be unreasonably large, suggesting immediate failure. The baseline for couplings, therefore, will have an offset of .004 inches.

C. Tooth Geometry

1. Pitch

The coupling was evaluated at the same pitches as the clutch, 10, 12 and 16 teeth per inch, while maintaining the same pitch diameter of 2.5 inches. Results from this evaluation are shown in Figure 9.1. The spring rate of the teeth and teeth surface radius for each of the coupling evaluations are identical to those obtained in the clutch evaluations. This is due to the fact that the offset has no effect on the response on the individual teeth. The remaining results are nearly identical for the coupling as those for the clutch. The increase in the number of teeth allows more teeth to make contact, causing a decrease in contact stress. But when the same number of teeth are in contact

and the total number of teeth increased, the stresses increase as well. The maximum PV value follows this same trend.

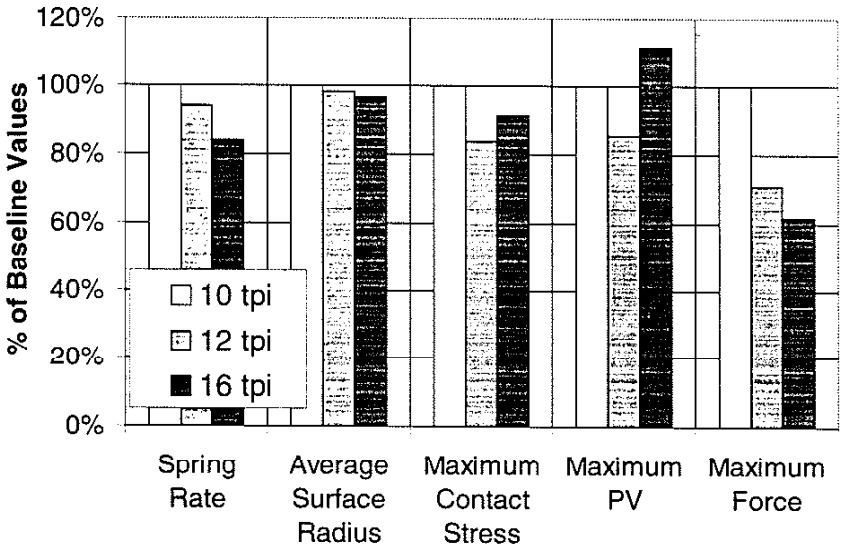

Figure 9.1: Changing pitch.

2. Pitch Diameter

Again, the pitch diameter is increased from 2.5 inches to 2.7 and 2.9 inches while maintaining the same pitch of 10 teeth per inch. This results in an increase in the number of teeth from 25 to 27 and 29, respectively.

Referring to Figure 9.2, the changes in contact radius, spring rate, and average surface radius are again identical to those of the clutch evaluation. The maximum contact stress, however, increases by 8% as the spline diameter goes from 2.5 to 2.7 inches. This deviates from the performance of the clutch due to the fact that there is no clutch face slipping in the coupling. The minimum number of teeth in contact, one, remains the same as in the baseline, just as in the clutch. Once the diameter increases to 2.9 inches, there are two teeth in contact, and the maximum contact stress decreases by 7% from that resulting from the 2.7 inch pitch diameter. This change in diameter allowed the

additional tooth to make contact, reducing the stress, although it is still higher than the baseline 2.5 inch diameter.

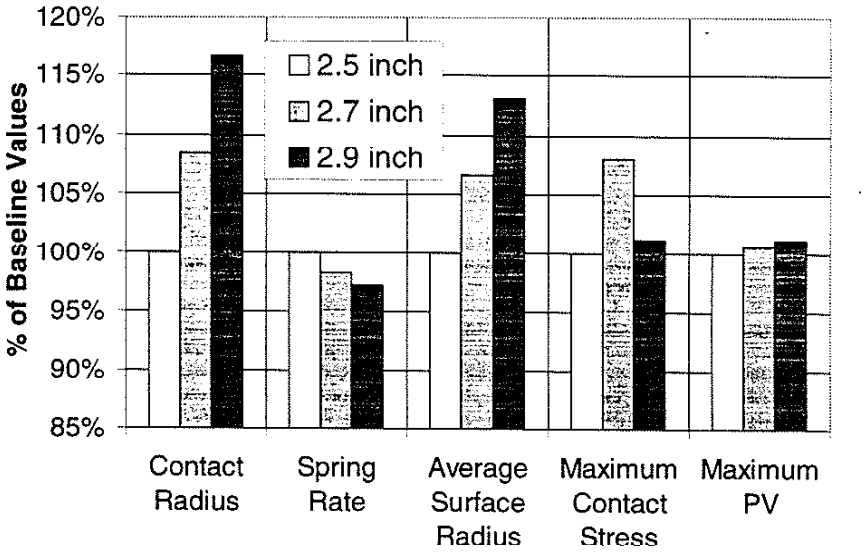

Figure 9.2: Changing pitch diameter.

Another difference between the clutch and the coupling is the maximum PV value obtained. In the clutch, the PV value decreased by 14% when the pitch diameter is increased from 2.5 to 2.9 inches. In the coupling, it increased by 1%. This demonstrates again that, as the pitch diameter increases, the load on the teeth due to their required deflection increases at a significantly faster rate than the torque decreases.

D. Material, Young's Modulus

1. Identical Change for Both Internal and External Teeth

Decreasing the Young's modulus in the coupling has a slightly greater effect on reducing the maximum contact stress than it does for the clutch. Figure 9.3 shows the stresses are reduced by over 80% when there is a one hundred-to-one reduction in the Young's modulus.

The maximum PV value in the coupling, however, has a different response to changes in the Young's modulus than it had in the clutch. In the clutch, as the Young's modulus decreases, and the number of teeth in contact increase from one to three then eight. The maximum PV value, however, increased when three teeth were in contact and remained stable thereafter. In the coupling, the number of three teeth in contact remains the same as for the clutch, but the maximum PV value occurs when three teeth are in contact, and then drops when eight teeth are in contact. Close examination of the clutch data reveals a slight reduction in the PV value by the increase in contact teeth from three to eight. This, along with the coupling results, is believed to be a subtle result of changes in the number of teeth in contact and the faster increase in velocity than decrease in pressure.

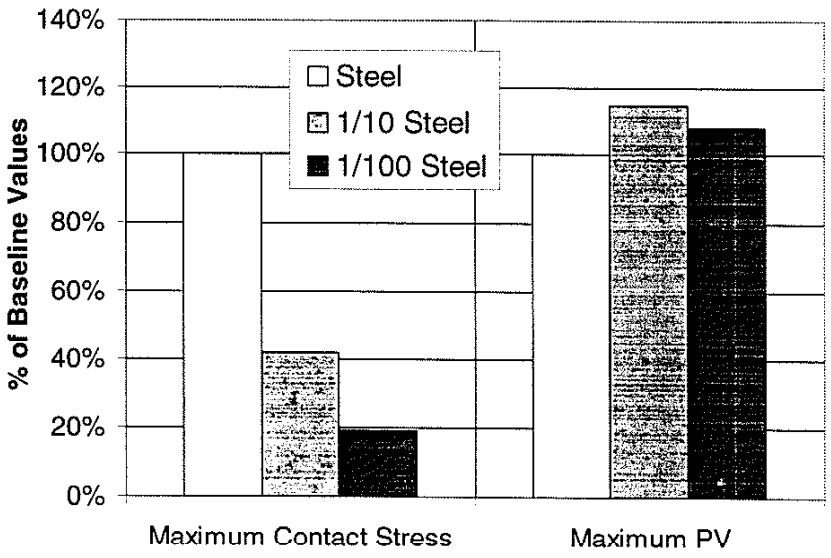

Figure 9.3: Changing Young's modulus of both members.

2. Independent Change for Internal and External Teeth

The reductions in stress due to a decreasing Young's modulus are slightly larger in the coupling than in the clutch, but only for the external teeth. Figure 9.4 and 9.5 show the results of changing the external and internal teeth respectively. In the case of the internal teeth, the clutch produces slightly more stress reduction.

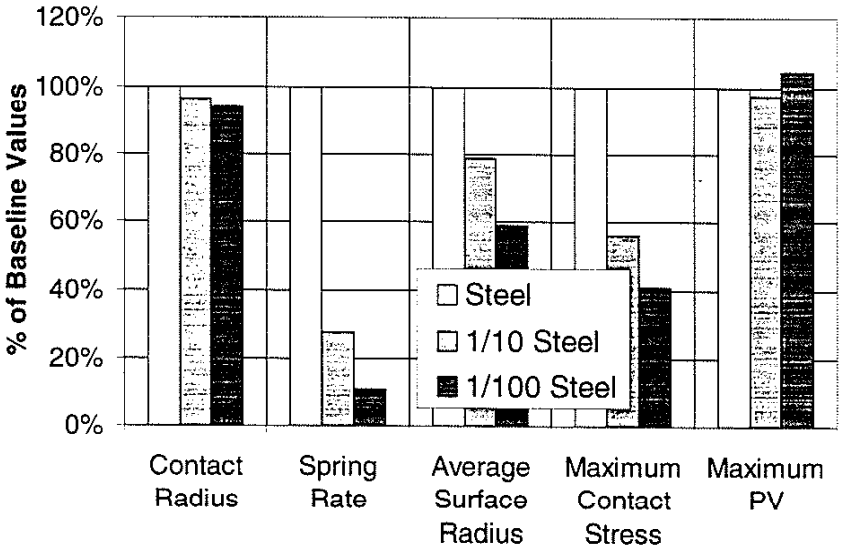

Figure 9.4: Changing Young's modulus of external teeth.

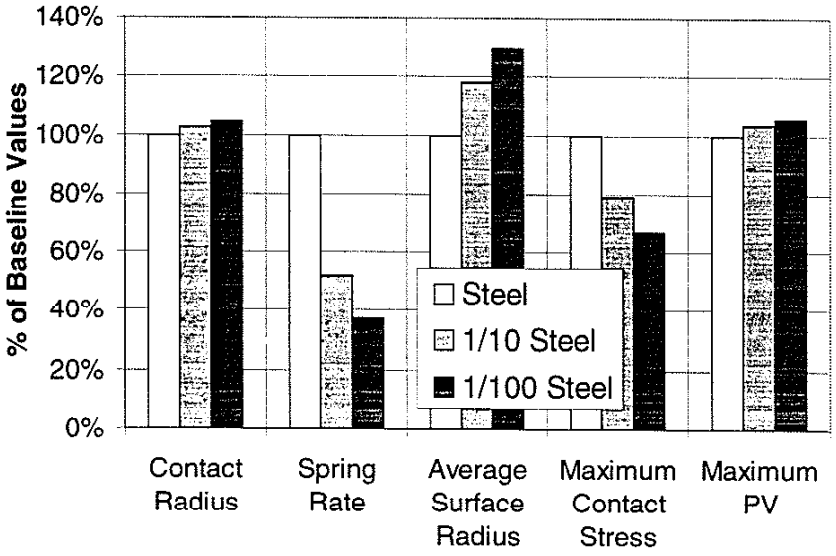

Figure 9.5: Changing Young's modulus of internal teeth.

Both the internal and external splines in the coupling have the same number of teeth in contact as they did in the clutch evaluation of Young's modulus changes. The internal teeth in the coupling experience very slight increases in the maximum PV value, whereas

the PV value in the clutch remained constant. The maximum PV value in the external tooth, however, fluctuates a small amount as the Young's modulus decreases. This is most likely due to the changing number of teeth in contact.

E. Wear of Teeth

The effect of the teeth wearing in the coupling is different than for the clutch. In the clutch, the slip force limits the loading on the teeth, and it is the slip force that controls that loading when the gap between the teeth changes. In the coupling, however, the gap between the teeth is integral to their sharing of the load. Figures 7.13 and 7.14 of Chapter 7 demonstrate the effect of wear in a coupling. Initially, there are several teeth in contact. As they wear, the teeth in contact reduce in number until only one remains. The maximum load on the teeth also decreases significantly, because the spline is allowed to rotate, reducing the amount of interference. The figures in Chapter 7 show the number of teeth in contact starting at 13, with a maximum stress of 150 ksi. After .026 inches of wear, there are only 3 teeth are in contact and the maximum stress is reduced to 7.1 ksi.

F. Class of Fit

The effect of changing the class of fit is identical to the effect wear has on the teeth. Results obtained by decreasing the class of fit is shown in Figures 7.13 and 7.14 of Chapter 7. In the example, as the fit changes from .0088 inches to .001 inches, the stresses increased from 88 ksi to 150 ksi. The number of teeth in contact increases as well, from 7 to 21. The coaxial spline model demonstrates the advantages of a loose fit for splines used in a coupling.

G. Torque

In the coupling, as in the clutch, the change in maximum contact pressure between the teeth is related to the torque driven through the spline. As shown in Figure 9.6, doubling the torque increases the load, in this case by 50%. Doubling it again increases the stress still more, but not proportionately. This is, again, related to the number of teeth in

contact. Just as in the clutch, the maximum PV value is nearly linear with the increase in torque.

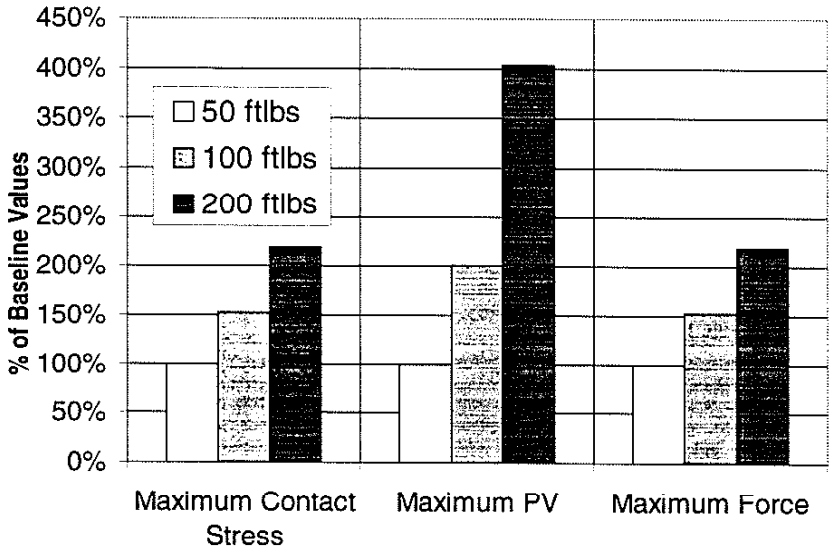

Figure 9.6: Changing torque.

H. Offset

The offset of the two splines can have the most significant impact on the life of the teeth, just as in the clutch. Results of the evaluation are given in Figure 9.7. The evaluation of the offset for a coupling reveals some interesting results. When the offset is reduced from .004 to .002 inches, the stress decreases 24% and the maximum PV value is cut in half. More importantly, the .002 inch offset is small enough so that the load is shared by at least two teeth.

If, however, the offset were increased by .001 inches to .005, the stresses increase by a factor of ten, and the maximum PV value is over 60 times greater. These increases are caused by the forced displacement of the teeth. At the lower offsets, the gears compensated for the misalignment by rotating. At larger offsets, gear rotation became limited and the teeth were forced to deflect.

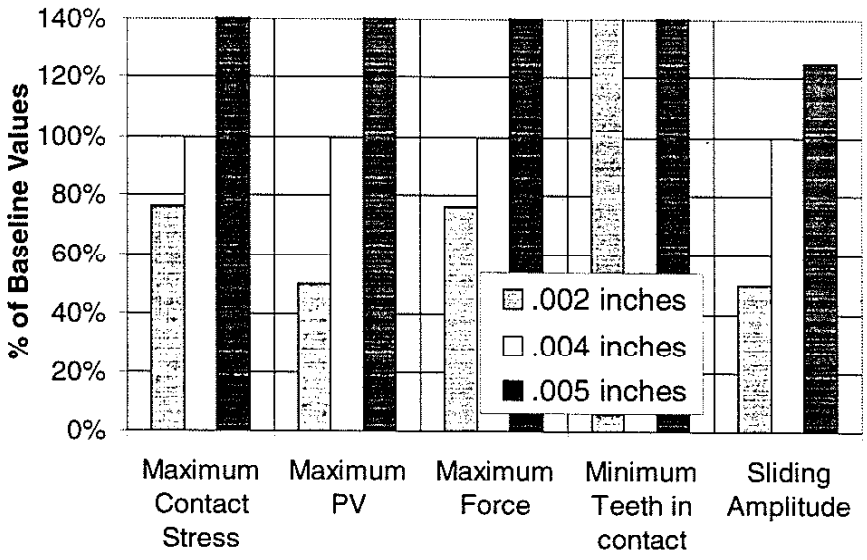

Figure 9.7: Changing offset.

The offset is the only variable that contributes to the sliding amplitude, which increases proportionally to increases in the offset. The coaxial spline model clearly demonstrates the susceptibility of a rigid coupling to radial offsets.

I. Optimum Design

As stated in the beginning of this chapter, several variables have either no effect on the results or have the same effect for couplings as for clutches. They include the pressure angle and Poisson's ratio. Additionally, just as in the clutch, changes to the width of the tooth have a proportional effect on the contact stresses and maximum PV values, unless the spring rates of the teeth change enough to allow a different number of teeth in contact.

Whereas the tightness of fit either from manufacturing tolerances or wear have no effect on the clutch, they have a significant effect on the coupling design. If the fit is tight, more teeth make contact and the stresses increase. In the interest of contact stresses, the looser the spline fit the better. If, however the fit is tight when new, and the teeth do not fail by fracture, their surfaces will wear until the loads are sufficiently distributed such that wear stops.

The effects of the other variables are quite similar to those in the clutch. The one with the greatest exception is the pitch diameter. In the clutch, as the pitch diameter increased, the contact stress remained relatively constant or decreased, and the maximum PV value decreased. The same changes in pitch diameter to the coupling produced slight increases in both the contact stress and maximum PV value. The result of increasing the pitch, a decrease in the PV value and increase in pressure if the number of teeth in contact remain the same, is the same in both the coupling and the clutch. The material changes, which are the most effective, produce nearly identical results in each application as well. Any change in the coupling's torque produces a proportional change in the PV limit and a related change in the maximum contact stress, just as the radial force does in the clutch. Also, just as in the clutch, the more teeth that make contact the lower the surface loads.

The most significant variable in the coupling is the radial offset. Decreasing it by 50% produced a 22% decrease in the stress and a 50% decrease in the maximum PV value. The sliding amplitude was also reduced proportionally. But if the offset were increased beyond .004 to .005 inches, the stresses and PV values grew exponentially. The offset, therefore, can be the most detrimental element to the life and performance of a rigid splined coupling.

X. Summary

There have been many factors presented that influence the wear of spline teeth, and they are associated with a wide variety of gear design, fatigue, and wear theories. While each theory is unique, they do have common elements. The theories used in conjunction with the results of the coaxial spline model, should provide a better understanding of and the ability to improve, coaxial spline designs.

A. Type of Wear

The literature does not identify a direct relationship between the slip amplitude of gears and wear. The results when slipping occurs, however, are well known and include scoring and pitting. Outside of gear design, a major characteristic that determines the type of wear which will occur is the slip amplitude. With slip amplitudes less than about 300 micrometers, the wear mechanism will be fretting, while with higher amplitudes it is reciprocating wear. Below about 70 micrometers, fretting corrosion through oxidation produces the only wear. Above 70 micrometers, both fretting wear and fretting corrosion can occur. Fretting fatigue can either result in the fracture of the gear tooth or the production of debris. The slip amplitude required for the fretting fatigue wear mechanism to occur would be the same as that for fretting wear.

The use of fretting maps, as discussed in Chapter 5, can be quite useful in establishing the effect of the slip amplitude. One outcome of the maps is the identification of the contact region as stick, mixed stick-slip, gross slip, or reciprocating sliding. This can aid in identifying the type of wear mechanism taking place. Results from the coaxial spline model can be used in conjunction with fretting maps to establish the effectiveness of changes to the design.

B. Wear Prediction

The life prediction models used for gears are of little use in evaluating coaxial splines for two reasons. First, they rely on the existence of lubrication. Secondly, although they are

the result of decades of experience, they are also focused on gear reducers with external teeth. Two parameters used to determine scoring criteria for gear wear are load and velocity. Should their product fall below a limit, scoring will not occur.

While true models have not yet been developed that predict fretting wear, there are several observations that are useful. For example, it is usually found that the fretting wear rate is nearly proportional to the load. Fretting fatigue theories do not address the issue of wear either. The majority of the models predict crack behavior and effects on the fatigue life diagram.

Reciprocating wear, on the other hand, has many published theories, including: Archard's wear theory, Equation (6.2); the PV limit model; the zero wear model; the delamination theory, Equations (6.10) and (6.11); and the asperity deformation model, Equations (6.17) and (6.19). The PV limit model is quite similar to the scoring criteria for gears. Both of them are temperature related, one of lubricant, the other of plastic.

C. Stresses

The calculation used in standard gear design for gear tooth surface stresses , as shown in Chapter 2, uses the Hertzian equations for contacting cylinders, Equations (2.1) through (2.5). For mating internal and external spline teeth, however, this is not the correct model. Instead, the model for cylinders within cylindrical sockets should be used, Equations (7.18), (7.20), and (7.22). The coaxial spline model in Chapter 7 can be used to determine the effect of centerline offset and sharing of the load by multiple teeth due to deflection. The model's result, which is the load on each tooth, can be further used to calculate the stress.

In fretting wear, corrosion, and fatigue, the amount of stress on the surface and the sliding amplitude determine whether the surface sticks, sticks and slips, or completely slips. The type of slip then determines the fretting mechanism. In fretting fatigue, it is the cyclic stresses that determine crack nucleation and propagation. There are models predicting these stresses and their effect on the fatigue stress diagram. Researchers, however, are

finding the greatest decrease in fatigue life occurring when there is mixed stick and slip. In the wear models, the wear is usually proportional to the load or a function of the shear flow stress. Some of the simpler wear models use the load to a power greater than one.

D. Coefficient of Friction

The coefficient of friction between two surfaces in contact can significantly impact their wear. In gear design, the use of lubricants is primarily to reduce oxidation of the surfaces, but it also significantly reduces the coefficient of friction. Whereas the coefficient of friction does not seem to have an impact on fretting wear or corrosion, it can affect whether there is stick, slip, or both. Additionally, in fretting fatigue, crack nucleation is most likely to occur when there is high adhesion, a result of friction. This may occur either early in the life of the part, or when they are disassembled for inspection and then reassembled. Chapter 6 describes numerous models for the coefficient of friction in reciprocating wear under conditions of asperity deformation, adhesion, plowing, wear, and cutting. The wear and cutting models predict the wear rate along with the coefficient of friction.

E. Adhesion

Adhesion is not a term typically used in gear design. It does, however, relate to fretting and wear. Adhesion involves material transfer or the production of debris. Sikorskii [47] predicts it to be a function of the surface energies. As mentioned earlier, crack nucleation is thought to occur at the time of maximum adhesion. The adhesion of asperities was found to be a key element in the study of wear.

F. Abrasion

Abrasion, just as adhesion, plays an important role in the theories regarding wear. Abrasion is the plastic deformation of asperities and the production of particles. These particles can then abrade the surface. There were no models for abrasion found, however, Midlin [50] developed a model of elastic asperity deformation, Figure 3.1. In gear applications, abrasion occurs at low speeds and high loads.

G. Crack Initiation and Growth

Cracks can either lead to fatigue failure or debris production. At higher stresses and low slip amplitudes, surface cracks are found. At the same high stresses and high slip amplitudes, part fracture occurs. The delamination theory of Chapter 6 describes how debris is produced after the cracks grow around hard particles. The cracks can grow, through shear, to form sheets of debris. Even if the component does not fracture, it is the initiation and growth of cracks that contribute to the surface wear.

H. Severe Wear

Severe wear can only occur if the oxide layer is removed and the core material is sufficiently soft. It is a function of load, and produces an increase in the wear rate of up to two orders of magnitude. Observations of severe wear shows that it occurs when the load is between two limits. Increasing the material hardness reduces the range of the load. The initial wear rate of two surfaces is severe wear, after which the wear either becomes mild or remains severe.

I. Parameters

1. Sliding Amplitude

Reductions in the sliding amplitude not only reduce the amount of work performed, they can change the type of wear mechanism, as stated earlier. The lowest sliding amplitude range, that involving stick, produces no wear and is most favorable. The next range is stick-slip which produces the greatest reduction in fatigue life. Higher sliding amplitudes produce slip, gross slip and reciprocating sliding.

The sliding amplitude for the coaxial spline model is linear with the offset of the shafts, making the identification of type of wear quite simple.

2. Material

One of the easiest ways to reduce fretting and wear is to change materials. In gear design this is often accomplished through harder or less abrasive surface treatments. Harder materials have been found to better withstand both fretting and abrasive wear. Their

stress concentrations in the stick-slip regions, however, can be detrimental with respect to fretting fatigue. In fretting corrosion, it is the hardness of the oxidized particle itself that is of interest, as it may eventually interact with the two surfaces.

Wear theories suggest that the crystal structure is important, as hexagonal materials have lower adhesive wear than body or face-centered cubic materials. Chapter 6 identifies several chemical elements that can be added to the material to impact the wear of the material. The use of identical or similar materials has mixed results. Their adhesion is usually higher, but if their hardness and surface finish are different, wear reductions can be achieved.

The coaxial spline model identified the Young's modulus of the material as an effective contributor to the deflection and sharing of the loads by the teeth. A reduction allows the contact stresses and maximum PV values to decrease, possibly reducing the wear rate.

3. Surface Finish

Surface finish plays an important role in gears as it usually effects the function of the lubricants. If one surface is rougher than the other, they will eventually wear to the same level of roughness. In fretting wear, however, a hard rough surface is beneficial, as it allows a place for debris to collect without causing future damage. If the debris is allowed to oxidize, however, the benefit is lost. To reduce fretting fatigue of dry surfaces, Hoeppner [67] recommends a finish of less than 16 or greater than 63 microinches.

4. Environment

Temperature and humidity have been identified as less important parameters in gear tooth wear. That is, with the exception of the effect of temperatures on lubricant. In reciprocating wear and fretting fatigue, they are not critical factors either. In fretting corrosion, however, temperature and humidity play an important role. A ten percent humidity level is the most detrimental to fretting wear and corrosion. As for temperature,

the effect becomes increasingly severe as the temperature falls below 50 C. Damage also increases as temperatures goes from 70 C to 150 C.

5. Cycles

In gear design, scoring occurs first, and then pitting is said to occur after 20,000 to 500,000 cycles. There are mixed opinions regarding the type of wear that occurs in the early stages. It is debated as to whether severe wear occurs or not. In fretting fatigue, cycles do not have a significant effect on the life. It is observed, however, that the growth rate of the crack decreases as it moves further from the surface, due to the decreasing effect of the surface stresses. In reciprocating wear theories, the number of cycles has not been identified as an influencing parameter.

6. Slip Speed

A key wear parameter for gears is speed. Higher speed increases the possibility of scoring the surfaces. In review of the theories, the relative speed of the surfaces does not seem to have an effect on fretting wear, corrosion, or fatigue.

7. Contact Area

While a larger contact area reduces the contact stresses, it also creates more of an opportunity for wear particles to become trapped, producing plowing wear. In the case of gear teeth, this is less of an issue because the teeth are not always in contact, allowing particles to freely escape.

8. Cycle Frequency

The cycle rate of sliding only has an effect on fretting wear and corrosion. With mild steel, the wear decreases as the frequency increases from 0 to 30 hertz. At frequencies over 30 hertz oxides no longer affect the wear rate. In the case of coaxial splines, the minimum frequency at which the oxides are effective may increase due to the extended time that the teeth surfaces are not in contact. Thirty hertz, 1800 rpm, is the speed of the most motors. This suggests that the frequency produced in the majority of the direct motor drive applications, as well as those with a speed reducer, is of significance.

J. Testing

The rules typically used for gear design are based on test results for lubricated gear sets. These results are not necessarily applicable to dry coaxial splines. Love [28] performed actual testing of splined axle shafts that produced a varicty of results. He attributes the mixed results to possible variations in the test. If variations are eliminated, more consistent test results would be expected. During the testing of the splines, the control parameters would include pressure, slip amplitude, frequency, temperature, humidity, residual stresses as well as others. This could present a challenge as the amplitude of the slip and load at the joint are some of the most difficult quantities to measure in a test.

Once adequate testing capability is established, testing of specific materials and conditions can be performed. The results can then be plotted on fretting maps and compared to the evaluations made with the coaxial spline model. Improvements can then be predicted.

K. Clutches and Couplings

Chapters 8 and 9 outline the findings of the coaxial spline model for clutches and couplings, respectively. Each of these power transmission components were evaluated in light of various geometry, material and application parameters. Computed results included the contact stress, pressure velocity product, and sliding amplitude. In the clutch, the largest reduction in contact stresses was obtained by reducing the Young's modulus. Increasing the pitch diameter, however, was the most effective means of reducing the maximum PV value. In the coupling, the greatest reduction in the contact stress was also achieved through the reduction of the Young's modulus. And in both the clutch and the coupling, the sliding distance was a direct function of the offset, and the sliding speed was proportional to the speed of rotation.

For the coupling, it was the offset of the splines that had the greatest impact, in that once a limit was exceeded, the loads increased exponentially. For the clutch, the radial slip force influenced the loads the most. In both cases, the best method of reducing the

contact stress and maximum PV value is by increasing the number of teeth in contact. Whenever this happens, the loads decrease. The coaxial spline model can be used to predict how many teeth will make contact, their contact stresses, maximum PV valuc, and sliding distance. These are the key elements which are then used to predict fretting and wear.

XI. Conclusions

Gear design is an old art centered on empirical information, and its standards are typically written for gear reducers with external teeth on both gears. These standards generally assume the use of a lubricant and cite lubricant temperature as a key factor in wear resistance.

The wear which takes place when the teeth make contact is either fretting wear, fretting corrosion, fretting fatigue, or reciprocating wear. For sliding amplitudes less than about 70 micrometers, fretting corrosion occurs. Displacements between about 70 to 300 micrometers produce fretting wear, fretting corrosion, and fretting fatigue. Reciprocating wear best describes the wear if displacements are over 300 micrometers. The model of the PV limit, in wear predictions, is nearly identical to the gear design scoring factor. Both are products of the pressure and velocity. Both are also temperature-limited, one of oil, the other plastic.

A coaxial spline model was developed to predict the interaction and key engineering properties of the gear teeth when loads, offsets, manufacturing tolerances, and wear are imposed. The model was used to calculate contact stresses, maximum PV values, and sliding amplitudes. Evaluations were made for both a clutch and a coupling. It is the radial force limit in the clutch that has the greatest impact on the teeth contact stresses, while in the coupling it is the amount of radial offset. In both cases, the greatest improvement was seen when additional teeth were brought into contact. This is most easily accomplished by reducing the Young's modulus of the material.

It has been found that key variables in many of the models presented in this paper are contact stress and PV values. These properties, when obtained from the coaxial spline model, can be evaluated in terms of the applicable fretting and wear theories to better understand and improve the design of coaxial splines.

Appendix

A. TK Solver™ Program for Calculation of Gear Tooth Deflection

Sta	Input	Name	Output	Unit	Comment
					Coaxial spline tooth deflections
					1/1998, Frank Bohm
					Version 1.0
L	25	N			Number of teeth
L	10	Pd		1/in	Pitch
L	30	ϕ		deg	Pressure angle
L	.4	b		in	Tooth Width
L	100	F		lbs	Force on tooth
					ANALYSIS PARAMETERS
	100	n			Number of incriments
	.001	T_Aspect			Tooth display aspect ratio
					INTERNAL TOOTH
L	2.701	IntMajDia		in	Major diameter
L	3E7	IntE		psi	Young's Modulus
					EXTERNAL TOOTH
		ExtA	.233166987183		Constant
L	.15708	Ext_tp		in	Circular tooth space at pitch diameter
L	2.299	ExtMinDia		in	Minor diameter
L	3E7	ExtE		psi	Young's Modulus
		Rp	1.25	in	Pitch Radius
		BaseDia	2.16506350946	in	Spline Base Diameter
		ψ	7.2	deg	Angle between teeth
		L	.201	in	Tooth Length
L		IntR	.506813828042	in	Internal tooth radius
L		ExtR	.506776545207	in	External tooth radius
L		Movement_angle	.000284643507	deg	Angle of movement due to deflection
L		Spring_rate	15,798,324	lbs/in	Spring rate of tooth
					FORCE BALANCE - Adjust rF to equal rC
L	1.2725	rF		in	Radius where force is applied
L		rC	1.27412	in	Radius where contact is made
		nC	38		Node where contact is made
		nF	38		Nearest node where the force is placed
		error	.00162	in	Error in force location to contact location
		nextrF	1.272824		

Variable Sheet T_BENDPR.TKW

St	Rule	
	Rp=N/2/Pd;	Pitch Radius
	L=(IntMajDia-ExtMinDia)/2;	Tooth Length - Assuming longer tooth
	ψ=360/N/2;	Angle between teeth
	BaseDia=Rp*2*cos(ϕ)	
	ExtA=2*(Ext_tp/2/Rp+tan(ϕ)-ϕ);	Constant
	CALL INTEG_FOR_Ext(L,n,ExtA,BaseDia/2,b,F,rF); External tooth	
	CALL INTEG_FOR_Int(L,n,ExtA,BaseDia/2,b,F,rF;nC,Movement_angle); Internal tooth	
	;********* Curvature of teeth surfaces	
	call Radius_of_curve(rC-L/n,rC,rC+L/n,elt('Ext_edge_1_angle,nC-1,0)*elt('r,nC-1,0),elt('Ext_edge_1_angle,nC,0)*elt('r,nC,0),	
	;	elt('Ext_edge_1_angle,nC+1,0)*elt('r,nC+1,0),1;ExtR)
	call Radius_of_curve(rC-L/n,rC,rC+L/n,elt('Int_edge_1_angle,nC-1,0)*elt('r,nC-1,0),elt('Int_edge_1_angle,nC,0)*elt('r,nC,0),	
	;	elt('Int_edge_1_angle,nC+1,0)*elt('r,nC+1,0),7;IntR)
	rC='r[nC]	
	nF=INT(n-(rF-ExtMinDia/2)/(L/n))	
	error=abs(rC-rF)	
	Spring_rate=F/Movement_angle/rC	
	nextrF=rF+.2*(rC-rF)	

Rule Sheet T_BENDPR.TKW

Comment:
Parameter Variables: IntE,ExtMinDia,T_Aspect,ψ
Input Variables: l,n,A,Rb,b,F,rF
Output Variables: contact,Movement_angle

St	Statement
	C1=0
	FOR i=1 to n
	x=l-i*l/n
	r=x+ExtMinDia/2
	'Int_x[i]=x
	'Int_m[i]=(SGN(rF-r)-1)/2*(rF-r)*F
	sum=x*(x^3+4*x^2*Rb+5*x*Rb^2+2*Rb^3)
	'Int_h2_arc[i]=2*ψ*pi()/180*r-(A*(x+Rb)+2*(x+Rb)*acos(Rb/(x+Rb)))
	IF sum>0 THEN 'Int_h2_arc[i]=2*ψ*pi()/180*r-(A*(x+Rb)-2/Rb*sqrt(x*(x^3+4*x^2*Rb+5*x*Rb^2+2*Rb^3))+2*(x+Rb)*acos(Rb/(x+Rb)))
	'Int_h_dx[i]=r*(1-cos('Int_h2_arc[i]/2/r))
	x=x+'Int_h_dx[i]; Adjust x for curvature in tooth
	IF x>l THEN x=l
	sum=x*(x^3+4*x^2*Rb+5*x*Rb^2+2*Rb^3)
	'Int_h_arc[i]=2*ψ*pi()/180*r-(A*(x+Rb)+2*(x+Rb)*acos(Rb/(x+Rb)))
	IF sum>0 THEN 'Int_h_arc[i]=2*ψ*pi()/180*r-(A*(x+Rb)-2/Rb*sqrt(x*(x^3+4*x^2*Rb+5*x*Rb^2+2*Rb^3))+2*(x+Rb)*acos(Rb/(x+Rb)))
	'Int_h[i]=2^(ExtMinDia/2+x)^sin('Int_h_arc[i]/2/(ExtMinDia/2+x))
	'Int_I[i]=b/12*'Int_h[i]^3
	C1=C1-'Int_m[i]/'Int_I[i]*l/n; First Constant for defl=0 at x=L
	NEXT
	; Initial Conditions, i=n
	'Int_sum_integ_1[n]='Int_m[n]/'Int_I[n]*l/n
	'Int_mag_integ_2[n]='Int_sum_integ_1[n]+C1
	'Int_sum_integ_2[n]='Int_mag_integ_2[n]*l/n
	FOR i=n-1 to 1 STEP -1
	'Int_sum_integ_1[i]='Int_sum_integ_1[i+1]+'Int_m[i]/'Int_I[i]*l/n
	'Int_mag_integ_2[i]='Int_sum_integ_1[i]+C1
	'Int_sum_integ_2[i]='Int_sum_integ_2[i+1]+'Int_mag_integ_2[i]*l/n
	NEXT
	FOR i=1 to n
	'Int_y[i]=-'Int_sum_integ_2[i]/IntE+'Int_sum_integ_2[1]/IntE
	'Int_h2_angle[i]='Int_h2_arc[i]/'r[i]
	'Int_y_angle[i]=atan('Int_y[i]/'r[i]); Edge deflection
	'Int_edge_1_angle[i]='Int_y_angle[i]+'Int_h2_angle[i]/2
	'Int_edge_1_angle_display[i]='Int_y_angle[i]+'Int_h2_angle[i]/2*T_Aspect
	NEXT
	; Find point of contact
	For i=1 to n
	'Delta_y[i]='Ext_edge_1_angle[i]-'Int_edge_1_angle[i]
	'Delta_y_display[i]='Ext_edge_1_angle_display[i]-'Int_edge_1_angle_display[i]
	NEXT
	minimum=MIN('Delta_y)
	minimum_display=MIN('Delta_y_display)
	contact=1

PROCEDURE: INTEG_FOR_Int T_BENDPR.TKW

St	Statement
	For i=1 to n
	'Int_edge_1_angle[i]='Int_edge_1_angle[i]+minimum
	'Int_edge_1_angle_display[i]='Int_edge_1_angle_display[i]+minimum_display
	'Int_edge_2_angle[i]='Int_edge_1_angle[i]-'Int_h2_angle[i]
	'Int_edge_2_angle_display[i]='Int_edge_1_angle_display[i]-'Int_h2_angle[i]*T_Aspect
	'Int_y_angle_display[i]='Int_edge_1_angle_display[i]/2+'Int_edge_2_angle_display[i]/2
	'Delta_y_angle[i]='Ext_edge_1_angle[i]-'Int_edge_1_angle[i]
	If 'Delta_y_angle[i]<=MIN('Delta_y_angle) then contact=i
	'Delta_y[i]='Delta_y_angle[i]*r[i]*1000000
	NEXT
	Movement_angle=-'Int_y_angle[contact]+'Ext_y_angle[contact]
	RETURN

PROCEDURE: INTEG_FOR_Int T_BENDPR.TKW

Comment:
Parameter Variables: ExtE,ExtMinDia,T_Aspect
Input Variables: l,n,A,Rb,b,F,rF
Output Variables:

```
St  Statement
    C1=0
    FOR i=1 to n
      x=l/n*i
      'r[i]=ExtMinDia/2+l-x
      'Ext_x[i]=x
      'Ext_m[i]=(SGN(rF-'r[i])+1)/2*(rF-'r[i])*F
      'Ext_h2_arc[i]=A*(l-x+Rb)-2/Rb*sqrt((l-x)*((l-x)^3+4*(l-x)^2*Rb+5*(l-x)*Rb^2+2*Rb^3))+2*(l-x+Rb)*acos(Rb/(l-x+Rb))
      'Ext_h_dx[i]='r[i]*(1-cos('Ext_h2_arc[i]/2/'r[i]));   fixed
      x=x-'Ext_h_dx[i];                                    Adjust x for curvature in tooth
      'Ext_h_arc[i]=(A*(l-x+Rb)-2/Rb*sqrt((l-x)*((l-x)^3+4*(l-x)^2*Rb+5*(l-x)*Rb^2+2*Rb^3))+2*(l-x+Rb)*acos(Rb/(l-x+Rb)))
      'Ext_h[i]=2*(ExtMinDia/2+l-x)*sin('Ext_h_arc[i]/2/(ExtMinDia/2+l-x));   fixed
      'Ext_I[i]=b/12*'Ext_h[i]^3;                          Area moment of inertia
      C1=C1-'Ext_m[i]/'Ext_I[i]*l/n;                       First constant for defl = 0 at x = L
    NEXT

    ;  Initial Conditions,  i=1
     'Ext_sum_integ_1[1]='Ext_m[1]/'Ext_I[1]*l/n
     'Ext_mag_integ_2[1]='Ext_sum_integ_1[1]+C1
     'Ext_sum_integ_2[1]='Ext_mag_integ_2[1]*l/n

    FOR i=2 to n
     'Ext_sum_integ_1[i]='Ext_sum_integ_1[i-1]+'Ext_m[i]/'Ext_I[i]*l/n
     'Ext_mag_integ_2[i]='Ext_sum_integ_1[i]+C1
     'Ext_sum_integ_2[i]='Ext_sum_integ_2[i-1]+'Ext_mag_integ_2[i]*l/n
    NEXT

    For i=1to n
     'Ext_y[i]='Ext_sum_integ_2[i]/FxtE-'Ext_sum_integ_2[n]/ExtE;   Centerline deflection
     'Ext_h2_angle[i]='Ext_h2_arc[i]/'r[i]
     'Ext_y_angle[i]=atan('Ext_y[i]/'r[i]);                        Edge deflection
     'Ext_edge_1_angle[i]='Ext_y_angle[i]-'Ext_h2_angle[i]/2
     'Ext_edge_2_angle[i]='Ext_h2_angle[i]+'Ext_edge_1_angle[i]
     'Ext_edge_1_angle_display[i]='Ext_y_angle[i]-'Ext_h2_angle[i]*T_Aspect/2
     'Ext_edge_2_angle_display[i]='Ext_h2_angle[i]*T_Aspect+'Ext_edge_1_angle_display[i]
    NEXT
    RETURN
```

PROCEDURE: INTEG_FOR_Ext T_BENDPR.TKW

Comment:
Parameter Variables:
Input Variables: x1,x2,x3,y1,y2,y3,n
Output Variables: R

St	Statement
	m12=(y2-y1)/(x2-x1); slope between first two points
	m23=(y3-y2)/(x3-x2); slope between second two points
	b12=y2-m12*x2; intercept of first two points
	b23=y2-m23*x2; intercept of second two points
	x12=(x1+x2)/2; midpoint between first two points
	y12=(y1+y2)/2; midpoint between first two points
	x23=(x3+x2)/2; midpoint between second two points
	y23=(y3+y2)/2; midpoint between second two points
	IF m12<>0 THEN mp12=-1/m12 ELSE mp12=1e50; slope of first two point's radius
	IF m23<>0 THEN mp23=-1/m23 ELSE mp23=1e50; slope of second two point's radius
	bp12=y12-mp12*x12; intercept of first two point's radius
	bp23=y23-mp23*x23; intercept of second two point's radius
	if mp12-mp23<>0 then xc=(bp23-bp12)/(mp12-mp23) else xc=99999999999; center of curve
	yc=mp12*xc+bp12; center of curve
	R=sqrt((x1-xc)^2+(y1-yc)^2)
	place('xr,n)=x1
	place('xr,n+1)=x2
	place('xr,n+2)=x3
	place('xr,n+3)=x23
	place('xr,n+4)=xc
	place('xr,n+5)=x12
	place('yr,n)=y1
	place('yr,n+1)=y2
	place('yr,n+2)=y3
	place('yr,n+3)=y23
	place('yr,n+4)=yc
	place('yr,n+5)=y12

PROCEDURE: Radius_of_curve T_BENDPR.TKW

List of References

1. Lee, J. R., "Fretting in Helicopters", *AGARG Conference Proceedings, No 161, Specialist Meeting on Fretting in Aircraft Systems,* AGARG, 1975, p. 3-1 to 3-10.
2. Calistrat, M. M., "Gear Coupling Lockup: Causes and Cures," *Power Transmission Design*, October, 1991, p. 31-32.
3. Fisher, M. J., and Wilson, W. E., "Vibration-Proof Coupling," *Patent number 5,006,007*, United States Patent and Trademark Office, Washington, DC, 1991.
4. Ying, S. C., "Sliding Support For a Superconduction Generator Rotor", *Patent number 4,178,777*, United States Patent and Trademark Office, Washington, DC, 1979.
5. American Gear Manufacturers Associations, *Standard Nomenclature of Gear-Tooth Wear and Failure, AGMA 210.02*, AGMA, Arlington, Va,1965.
6. Dudley, D. W., *Handbook of Practical Gear Design*, McGraw-Hill, New York, 1984.
7. Teeter, F. J. & Berger, M., "Wear Protection for Gears," *Gear Technology*, March, 1996, p. 27-29.
8. Grosberg, J., "A Critical Review of Gear Scoring Criteria," *Wear*, 43, 1977, p. 1-7.
9. Ku, P. M., "Gear Failure Modes - Importance of Lubrication and Mechanics," *Source Book on Gear Design, Technology and Performance*, American Society For Metals, Metals Park, OH, 1980, p. 292-299.
10. Lynwander, P., *Gear Drive Systems, Design and Application*, Marcel Dekker, New York, 1983.
11. Almen, J.O., and Boergehold, A.C. "Rear Axle Gears: Factors Which Influence Their Life," *Proc. ASTM*, 35, 1935, p. 99-146.
12. Lispon, C., "Wear, Considerations in Design," *Machine Design*, Dec. 1963, p. 140-144.
13. Wilde, R. A., "Failure in Gears and Related Machine Components" *Source Book on Gear Design, Technology and Performance*, American Society For Metals, Metals Park, OH, 1981, p. 300-311.
14. Bartz, W. J. and Kruger, V., "Pitting Fatigue of Gears - Some Ideas on Appearance, Mechanism and Lubrication Influence," *Source Book on Gear Design, Technology and Performance*, American Society For Metals, Metals Park, OH, 1982, p. 220-224.
15. Gay, C. E., 1970, "How to Design For Minimum Wear in Gears," *Machine Design*, 42, 29, Nov. 26, 1970 p. 92-97.
16. Yoshida, A., Ohue, Y., Karasuno, I., "Comparison of Surface Durability & Dynamic Performance of Powder Metal & Steel Gears," *Gear Technology*, September, 1995, p. 18-23 .

17. Bartz, W. J. and Kruger, V., "Influence of Lubricants On The Pitting Fatigue of Gears," *Wear*, 35 1975, p. 315-329.

18. Fowle, T. I., "Gear Lubrication: Relating Theory to Practice," *Lubrication Engineering*, 32, 1, Jan. 1976, p. 205-219.

19. ASTM G98-91, "Standard Test Method for Galling Resistance of Materials," *1994 Annual Book of ASTM Standards*, 03.02, ASTM, Philadelphia, PA, 1994, p. 396-398.

20. Shturtz, G., "The Beginner's Guide to Powder Metal Gears," *Gear Technology*, September, 1995, p. 26-28.

21. Bowen, C. W., "Review of Gear Testing Methods," *Source Book on Gear Design, Technology and Performance*, American Society For Metals, Metals Park, OH, 1983, p. 343-365.

22. Walker,, H. "Gear Tooth Deflection and Profile Modification, I," *The Engineer*, 166, 1938, p. 409-412.

23. Walker, H., "Gear Tooth Deflection and Profile Modification, 11," *The Engineer*, 166, 1938, p. 434-436.

24. Bartz, W.J., "The Influence of Lubricants on Failures of Bearings and Gears," *Source Book and Gear Design, Technology and Performance*, American Society for Metals, Metals Park, OH, 1980, p. 172-183.

25. Khol, R. (ed), *Machine Design, Basics of Design Engineering*, Penton Publishing, Cleveland, OH, 63, 13, June, 1991, p. 160.

26. Stoew, St. N., "The Laws of Abrasive Gear Wear, " *Maschinenbautechnik*, March 1973, p.98-102.

27. Hurricks, P.L., "The Mechanism of Fretting - A Review," *Wear*, 15, 1970, p. 389.

28. Love, R.J. (1956), "Fatigue In Automobiles," *Proceedings of the International Conference on Fatigue of Metals*, Institution of Mechanical Engineers, London, September, 1956, p 570-580.

29. Buckley, D. H., "Oxygen and Sulfer Interactions with a Clean Iron Surface and the Effect of Rubbing Contact on these Interactions," *NASA TN D-7283*, May 1973.

30. Tomlinson, G. A., "The Rusting of Steel Surfaces in Contact," *Proc. Roy. Soc.*, 115a, 1927, p. 472.

31. Uhlig, H. H., "Mechanism of Fretting Corrosion," *Journal of Applied Mechanics*, 21, 4, Dec., 1954, p. 401.

32. Uhlig, H. H., Feng, I. M., Tierney, W. D., and McCellan, A., "Fundamental Investigation of Fretting Corrosion," *NACA Technical Note 3029*, Dec., 1953.

33. Halliday, J. S., and Hirst, W., "The Fretting Corrosion of Mild Steel," *Proc. Roy. Soc.*, London, 236A, August 2, 1956, p. 411-425.

34. Godfrey, D., "Investigation of Fretting Corrosion by Microscopic Observation," *NACA Technical Note 2039*, February, 1950.

35. Godfrey, D., "A Study of Fretting Wear in Mineral Oil," *Lubrication Engineering*, 12, January-February, 1956, p. 37-42.

36. Godfrey, D., and Bailey, J. M., "Coefficient of Friction and Damage to Contact Area During the Early Stages of Fretting - I. Glass, Copper of Steel Against Copper," *NACA Technical Note* 3011, September, 1953.

37. Godfrey, D., and Bailey, J. M., "Early Stages of Fretting of Copper, Iron, and Steel," *Lubrication Engineering*, 10, May-June, 1954, p. 155-159.

38. Godfrey, D., and Bisson, E. E., "NACA Studies of Mechanism of Fretting (Fretting Corrosion) and Principles of Mitigation," *Lubrication Engineering*, 8, October, 1952, p.241-243.

39. Feng, I. M., "Fundamental Study of the Mechanism of Fretting," *Final Report AD59089*, M. I. T., Lubrication Lab, Cambridge, Mass., February 28, 1955.

40. Feng, I. M., and Rightmire, B. G., "The Mechanism of Fretting," M. I. T., Cambridge, Mass, AD 4463, 1952.

41. Feng, I. M., and Rightmire, "The Mechanics of Fretting," *Lubrication Engineering*, 9, p. 134.

42. Feng, I. M., and Rightmire, B. G., "An Experimental Study of Fretting Fatigue," *Proc. Inst. Mech. Engrs.*, London, 170, 1965, p. 1055-1060.

43. Waterhouse, R. B., "Fretting Corrosion," *Proc. Inst. Mech. Engrs.*, 169, 1955, p. 1159-1172.

44. Stowere, I. F. and Rabinowicz, E., "The Mechanism of Fretting Wear," *Trans. ASME*, Ser. F, 95, 1, 1973, p. 65.

45. Bailey, J. M., and Godfrey, D., "Coefficient of Friction and Damage to Contact Area During the Early Stages of Fretting. II-Steel, Iron, Iron Oxide, and Glass Combinations," *NACA Technical Note 3144*, April 1954.

46. Wright, K. H., "An Investigation of Fretting Corrosion," *Proceedings, Institute of Mechanical Engineers*, Vol. 18, 1952-53, p. 556.

47. Sikorskii, M. E., "Correlation of the Coefficients of Adhesion with Various Physical and Mechanical Properties of Metals," *J. Basic Eng.*, 85, 1963, p. 279.

48. Rabinowicz, E., *Friction and Wear of Materials*, Wiley, New York, 1965.

49. Vingsbo, O., and Soderberg, S., "On Fretting Maps," *Wear*, 126, 1988, p. 131-147.

50. Mindlin, R. D., "Compliance of Elastic Bodies in Contact," *Journal of Applied Mechanics*, 16, 1949, p. 259-268.

51. Ohmae, N., and Tsukizoe, T., "The Effect of Slip Amplitude on Fretting," *Wear*, 27, 1974, p. 281.

52. Bill, R. C., "Review of Factors That Influence Fretting Wear," *Materials Evaluation Under Fretting Conditions, ASTM STP 780*, American Society for Testing and Materials, 1982, p. 165-182.

53. K. Nishioka and K. Kirakawa, "Fundamental Investigations of Fretting Fatigue: Part 5. The Effect of Relative Slip Amplitude," *Bull. JSME*, 12, 52, 1969, p. 692 - 697.

54. Mason, W. P., and White, S. D., "New Techniques For Measuring Forces and Wear in Telephone Switching Apparatus," *Bell Systems Technical Journal*, 31, 1952, p. 469.

55. Basile, S., "Plastic Gear Design: Doing It Right," *Power Transmission Design*, March, 1993, p. 33-35.

56. American Gear Manufacturers Associations, *Standard Nomenclature of Gear-Tooth Wear and Failure, AGMA 110.03*, AGMA, Arlington, Va,1962.

57. Hoeppner, D.W. and Gates, F. L., "Fretting Fatigue Considerations in Engineering Design," *Wear*, 70, 1981, p 115-164.

58. Waterhouse, R. B., *Fretting Corrosion*, Pergamon, Toronto, 1972.

59. Waterhouse, R. B., "The Role of Adhesions and Delaminations in the Fretting Wear of Metallic Material," *Wear*, 45, 1977, p. 355-364.

60. Bowden, F. P., and Tabor, D., *The Friction and Lubrication of Solids*, Oxford Univ. Press, Oxford, 1, 1953.

61. Bethune, B., and Waterhouse, R. B., "Adhesion of Metal Surfaces Under Fretting Conditions, pts. 1, 2," *Wear*, 12,1968 p. 289-369.

62. Campbell, W. E., "The Current Status of Fretting Corrosion," *Symposium on Fretting Corrosion; Presented at the Fifty-Fifth Annual Meeting (Fiftieth Anniversary Meeting)*, American Society For Testing Materials, New York, N. Y., June 25, 1952, Philadelphia.

63. Hurricks, P. L., "The Mechanism of Fretting - A Review," *Wear*, 15, 1970, p. 389.

64. Bethune, B., and Waterhouse, R. B., "Adhesion Between Fretting Steel Surfaces," *Wear*, 8, 1965, p. 22.

65. Archard, J. F., "Wear," *In Interdisciplinary Approach to Frictional Wear*, NASA, Washington D. C., 1968, p 267-304.

66. Waterhouse, R. B., M. Helmi Atti and R. B. Waterhouse, (eds), "The Problems of Fretting Fatigue Testing," *Standardization of Fretting Fatigue Test Methods and Equipment, ASTM STP 1159*, American Society for Testing and Materials, Philadelphia, 1992, p. 13-19.

67. Hoeppner, D.W., "Material/Structure Degradation Due to Fretting-Initiated Fatigue," *Canadian Aeronautics and Space Journal*, 27, 3, 1981, p. 221-231.

68. Waterhouse, R. B., "Introduction to Fatigue," *Fretting Fatigue*, Applied Science, London, 1981, p. 14-21.

69. Endo, K., and Goto, H., "Initiation and Propagation of Fretting Fatigue Cracks," *Wear*, 38, 1976, p. 311-324.

70. Forsyth, P.J. E., "Occurrence of Fretting Fatigue Failures in Practice," *Fretting Fatigue*, Applied Science, London, 1983, pp 100-101.

71. Hoeppner, D.W., "Mechanisms of Fretting Fatigue and Their Impact on Test Methods Development," *Standardization of Fretting Fatigue Test Methods and Equiptment, ASTM STP 1559,* ASTM, Philadelphia, PA., 1992, p. 23-31.

72. Stepanov, V. N., "Specific Features of the Fretting Curves Under Fretting Corrosion Conditions," *Soviet Materials Science*, 3, 3, 1967, p 203-205.

73. Filimonov, G. N., "The Selection of a Base Number of Loading Cycles When Testing for Fatigue Under Fretting Conditions," *Soviet Engineering Research*, 1, 5, 1981, p 27-28.

74. Waterhouse, R. & Taylor, D., "The Initiation of Fatigue Cracks in a 0.7% Carbon Steel by Fretting", *Wear* 17, 1971, p. 139-137.

75. Sato, K., "Damage Formation During Fretting Fatigue," *Wear*, 125, 1988, p163-174.

76. Dobromirski, J. M.,M., Helmi Atti and R. B. Waterhouse, (ed) "Variables of Fretting Process: Are There 50 of Them?" *Standardization of Fretting Fatigue Test Methods and Equipment, ASTM STP 1159*, American Society for Testing and Materials, Philadelphia, 1992, p. 60-66.

77. Nishioka, K., Nishimura, S. and Hirakawa, K., "Fundamental Investigations of Fretting Fatigue, Part 3," *Bulletin of JSME*, 12, 51, 1969, p. 397-407.

78. Nishioka, K., and Hirakawa, K., "Fundamental Investigations of Fretting Fatigue, Part 2" *Bulletin of JSME,* 12, 50,1969, p. 180-187.

79. Dorn, E., *Mechanical Behavior of Metals at Elevated Temperature*, McGraw Hill, 1961.

80. Venkatesh, V. C. and Krishnamurthy, R., "On Some Aspects of Metallurgical Changes During Gear Pitting," *Source Book on Gear Design, Technology and Performance*, American Society For Metals, Metals Park, OH, 1983, p. 224-228.

81. Nowell, D. and Hills, D. A., "Crack Initiation Criteria in Fretting Fatigue," *Wear*, 136, 1990, p. 329-343.

82. Szolwinski, M. P., Harish, Farris, T.N., Sakagami, T., "The Use of Thermal Imiging for In-Situ Characterization of Frictional Behavior in Mixed-Mode Fretting Contact," *World Wide Web (Internet), http://aae.www.ecn.purdue.edu/ szolwins/Presentations/JSME-1997/paper.html.*

83. Nakazawa, K., Sumita, M. and Maruyama, N., "A New Information in Fretting Fatigue Failure in Metallic Structural Materials," *World Wide Web (Internet), http://.www.ecn.purdue.edu/ sozolwins/Presentations/JSME-1997/paper.html.*

84. Adibnazari, E., and Hoeppner, D.W., "Characteristics of the Fretting Fatigue Damage Threshold," *Wear*, 159, 1992, p. 43-56.

85. Wharton, M. H., Taylor, D. E., and Waterhouse, R. B., "Metallurgical Factors in the Freting-Fatigue Behavior of 70/30 Brass and .7% Carbon Steel," *Wear*, 27, 1973, p. 61.

86. Adibnazari, E., and Hoeppner, D.W., "A Fretting Fatigue Normal Pressure Threshold Concept," *Wear*, 160, 1993, p. 33-35.

87. Ruiz, C., Boddington, P. H. B., and Chen, K. C., "An Investigation of Fatigue and Fretting in a Dovetail Joint," *Exp. Mech.*, 24, 3,1984, p. 208-217.

88. Nix, K. J., and Lindley, T. C., "The Influence of Relative Slip Range and Contact Materials on the Fretting Fatigue Properties of 3.5 NiCrMoV Rotor Steel," *Wear*, 125, 1988, p 147-162.

89. O'Connor, J. J., "The Role of Elastic Stress Analysis in the Interpretation of Fretting Fatigue," *Fretting Fatigue*, Applied Science, London, 1982, p.23-31.

90. Marsh, K. J., *Industrie Anzeiger*, 88, 31, 1966, p. 640.

91. Johnson, K. L., "Surface Interaction Between Elastically Loaded Bodies Under Tangential Forces," *Proc. Roy. Soc. Lond. A*, 230, 1955, p. 531.

92. *Annual Book of ASTM Standards, Sect. 00, Vol, 00.01, Index,* American Society of Testing and Materials, Philadelphia, PA, 1994.

93. Vingsbo, O. B.,M., Helmi Atti and R. B. Waterhouse (eds), "Fretting and Contact Fatigue Studied with the Aid of Fretting Maps," *Standardization of Fretting Fatigue Test Methods and Equipment, ASTM STP 1159,* American Society for Testing and Materials, Philadelphia, PA.

94. Bayer, R. G., *Mechanical Wear Prediction and Prevention*, Marcel Dekker, New York, 1994.

95. Archard, J. F., "Contact and Rubbing of Flat Surfaces," *J. Appl. Phys.*, 24, 8, 1953, p. 981-988.

96. Archard, J. F., and Hirst, W., "The Wear of Metals Under Unlubricated Conditions," *Proc. Roy. Soc. Lond., Series A*, 236, 1956, p. 397.

97. Feng, I. M., and Uhlig, H. H., "Fretting Corrosion of Mild Steel in Air and Nitrogen," *Journal of Appl. Mech.*, 21, 1954, p. 395-400.

98. Charney, H., "Fundamentals of Interfacial Slip Damping," *M.S. Thesis*, Department of Mechanical Engineering, M. I. T., June, 1970.

99. McDowell, J. R., "Fretting of Hardened Steel in Oil," *Trans. American Society of Lubrication Engineers*, 1, 2, 1958, p.287-295.

100. Rabinowicz, E., "Friction and Wear of Metals," *Metals Engineering Quarterly*, 1, 2, 1967, p. 4-8.

101. Rabinowicz, E., "Advances in Wear-Resistant Materials," *ASME Paper 72-DE-28.*

102. Farrell, R. F. and Eyre, T. S., "The Relationship Between Load and Sliding Distance in the Initiation of Mild Wear in Steels," *Wear*,1970, p. 359-372.